

# Emergence of tissue polarization from synergy of intracellular and extracellular auxin signaling

Krzysztof Wabnik<sup>1,2,3,6</sup>, Jürgen Kleine-Vehn<sup>1,2,6,\*</sup>, Jozef Balla<sup>4</sup>, Michael Sauer<sup>1,2,7</sup>, Satoshi Naramoto<sup>1,2</sup>, Vilém Reinöhl<sup>4</sup>, Roeland MH Merks<sup>1,2,8</sup>, Willy Govaerts<sup>3</sup> and Jiří Friml<sup>1,2,5,\*</sup>

<sup>1</sup> Department of Plant Systems Biology, VIB, Ghent University, Ghent, Belgium, <sup>2</sup> Department of Plant Biotechnology and Genetics, Ghent University, Ghent, Belgium, <sup>3</sup> Department of Applied Mathematics and Computer Science, Ghent University, Ghent, Belgium, <sup>4</sup> Department of Plant Biology, Mendel University, Brno, Czech Republic and <sup>5</sup> Department of Experimental Biology, Masaryk University, Brno, Czech Republic

<sup>6</sup> These authors contributed equally to this work

<sup>7</sup> Present address: Departamento de Genética Molecular de Plantas, Centro Nacional de Biotecnología, Consejo Superior de Investigaciones Científicas, Madrid 28049, Spain

<sup>8</sup> Present address: Centrum Wiskunde & Informatica, 1098 XG Amsterdam, and Netherlands Consortium for Systems Biology, 1098 XG Amsterdam, The Netherlands

\* Corresponding authors. J Friml or J Kleine-Vehn, Department of Plant Systems Biology, VIB, Ghent University, Technologiepark 927, B-9052 Ghent, Belgium.

Tel.: + 32 9 3313913; Fax: + 32 9 3313809; E-mail: jiri.friml@psb.vib-ugent.be or Tel.: + 32 9 3313946; Fax: + 32 9 3313809; E-mail: jurgen.kleine-vehn@psb.vib-ugent.be

Received 25.5.10; accepted 2.11.10

**Plant development is exceptionally flexible as manifested by its potential for organogenesis and regeneration, which are processes involving rearrangements of tissue polarities. Fundamental questions concern how individual cells can polarize in a coordinated manner to integrate into the multicellular context. In canalization models, the signaling molecule auxin acts as a polarizing cue, and feedback on the intercellular auxin flow is key for synchronized polarity rearrangements. We provide a novel mechanistic framework for canalization, based on up-to-date experimental data and minimal, biologically plausible assumptions. Our model combines the intracellular auxin signaling for expression of PINFORMED (PIN) auxin transporters and the theoretical postulation of extracellular auxin signaling for modulation of PIN subcellular dynamics. Computer simulations faithfully and robustly recapitulated the experimentally observed patterns of tissue polarity and asymmetric auxin distribution during formation and regeneration of vascular systems and during the competitive regulation of shoot branching by apical dominance. Additionally, our model generated new predictions that could be experimentally validated, highlighting a mechanistically conceivable explanation for the PIN polarization and canalization of the auxin flow in plants.**

*Molecular Systems Biology* 6: 447; published online 21 December 2010; doi:10.1038/msb.2010.103

*Subject Categories:* simulation and data analysis; plant biology

*Keywords:* auxin; canalization; cell polarity; PIN proteins

This is an open-access article distributed under the terms of the Creative Commons Attribution Noncommercial No Derivative Works 3.0 Unported License, which permits distribution and reproduction in any medium, provided the original author and source are credited. This license does not permit commercial exploitation or the creation of derivative works without specific permission.

## Introduction

A key question in developmental biology relates to the fundamental issue of how an individual cell in a polarized tissue senses the polarities of its neighbors and its position within the tissue. In plant development, this issue is of pronounced importance, because plants have the remarkable ability to redefine cell and tissue polarities in different developmental programs, such as embryogenesis, postembryonic organogenesis, vascular tissue formation, and tissue regeneration (Kleine-Vehn and Friml, 2008).

In 1880, Charles Darwin predicted that a growth-stimulating molecule directionally moves within plant tissues (Darwin and Darwin, 1880). This growth regulator was later on termed auxin and represents the first isolated phytohormone. Intercellular auxin transport, in conjunction with local auxin

biosynthesis, is postulated to define auxin gradients during embryonic and postembryonic development, giving positional cues for primordium formation, organ patterning, and tropistic growth (Friml *et al.*, 2002; Benková *et al.*, 2003; Reinhardt *et al.*, 2003; Heisler *et al.*, 2005; Scarpella *et al.*, 2006; Dubrovsky *et al.*, 2008). The direction of the auxin transport depends largely on the polar subcellular localization of PINFORMED (PIN) proteins at the plasma membrane (Petrášek *et al.*, 2006; Wiśniewska *et al.*, 2006). As the molecular basis of the PIN polarization in plants remains unexplored, theoretical and experimental insights into mechanisms that regulate the PIN polarity are of outstanding interest to plant biologists.

PIN proteins recycle between the plasma membrane and the intracellular endosomal compartments (Geldner *et al.*, 2001; Dhonukshe *et al.*, 2007). This recycling modulates PIN-dependent auxin efflux rates and enables rapid changes in

PIN polarity (Dhonukshe *et al*, 2008; Kleine-Vehn *et al*, 2008a). Additionally, auxin interferes with the PIN recycling by inhibiting the PIN protein internalization (Paciorek *et al*, 2005).

At the tissue level, polarization of PIN proteins in individual cells has been suggested to be coordinated in the surrounding cells by a positive feedback between auxin and its directional transport (Mitchison, 1980; Sauer *et al*, 2006). As the molecular mechanism for PIN polarization still needs to be unraveled, numerous theoretical studies have been applied to test various hypotheses. In the canalization hypothesis (Sachs, 1981), an underlying positive feedback loop exists between the auxin-flux and auxin-transport capacity of cells, ultimately canalizing auxin progressively into discrete channels. It incorporates a hypothetical flux sensor component as an essential part of the auxin feedback mechanism for PIN polarization (Mitchison, 1980) and is widely exploited in so-called flux-based models to study PIN-dependent developmental processes, such as venation patterning in leaves (Rolland-Lagan and Prusinkiewicz, 2005; Sauer *et al*, 2006; Scarpella *et al*, 2006). On the basis of the experimental observation of adverse PIN polarization during phyllotactic patterning in vegetative shoot apical meristems (Reinhardt *et al*, 2003), PIN proteins have been proposed to orient to the side of the cell that faces the neighboring cell with the highest auxin concentration (Jönsson *et al*, 2006; Smith *et al*, 2006). This alternative hypothesis integrates an unknown short-range intercellular signal, transmitting the auxin concentration of its direct neighbors (Sahlin *et al*, 2009). Concentration-based models can reproduce various phyllotactic patterns occurring in planta (Reinhardt *et al*, 2003; Jönsson *et al*, 2006; Smith *et al*, 2006) and initiation of the primary leaf vein (Merks *et al*, 2007).

The flux-based (Mitchison, 1980; Rolland-Lagan and Prusinkiewicz, 2005) and concentration-based models (Merks *et al*, 2007) provide conceptually different frameworks for PIN polarization during venation patterning in plants. Unless additional assumptions are included (Feugier *et al*, 2005), these models predict the low auxin concentration in vein precursors, which contradicts the experimental observations of high auxin signaling in developing veins (Scarpella *et al*, 2006).

To assess this issue, flux-based and concentration-based models were combined into a dual polarization model, in which the dominating mechanism depends on the actual auxin content of the cells (Bayer *et al*, 2009). This model generates the simultaneous appearance of high auxin concentration in emerging veins and recapitulates PIN polarization and auxin transport during early midvein formation and phyllotaxis.

Nevertheless, biological evidence for a hypothetical flux sensor (Mitchison, 1980; Rolland-Lagan and Prusinkiewicz, 2005; Bayer *et al*, 2009) and/or a short-range signal (Jönsson *et al*, 2006; Smith *et al*, 2006; Merks *et al*, 2007; Bayer *et al*, 2009) for PIN polarization remains difficult to identify. To overcome this problem, individual cells have been suggested to read out hypothetical intracellular auxin gradients to polarize PIN proteins by a yet to be clarified perception mechanism (Kramer, 2009). Based solely on the steepness of this internal auxin gradient (independently of the overall auxin concentrations), PIN proteins would polarize toward the side

of the cell with the lowest intracellular auxin concentration (Kramer, 2009). This model predicts that a conductive auxin channel originates from an auxin sink instead of an auxin source, whereas experimental observations suggest the opposite (Sauer *et al*, 2006).

Here, we propose a novel, biologically plausible model for PIN polarization that combines intracellular and extracellular auxin signaling as a unifying approach for tissue polarization in plants. The model integrates experimental data, such as auxin feedback on PIN transcription (Peer *et al*, 2004; Heisler *et al*, 2005) via a nuclear auxin signaling pathway (Chapman and Estelle, 2009) and auxin feedback on PIN endocytosis (Paciorek *et al*, 2005) via the hypothetical, yet conceivable assumption of extracellular auxin perception. The extracellular receptor-based polarization (ERP) model faithfully reproduces PIN polarization and auxin distribution patterns during vascularization, tissue regeneration, vein connection, generation of leaf vein loops, and competitive auxin canalization for axillary bud outgrowth. The detailed analysis of our model revealed new mechanistic insights into initiation, maintenance, and robustness of PIN polarization during venation patterning and tissue regeneration. Remarkably, the ERP model generated new predictions that were experimentally validated. The versatility and accuracy of model predictions highlight the importance and plausibility of dual auxin perception for PIN polarization and auxin-driven plant development.

## Results

### Assumptions of the ERP model

Tissue polarization requires cell-to-cell communication, but, in plants, a biologically conceivable mechanism for PIN polarization was elusive. Therefore, we assumed that the extracellular space (apoplast) provides a relatively easy mean for a direct and simple cell-to-cell communication by the competitive utilization of one or more signaling components (receptors). Notably, the first isolated auxin-binding protein (ABP1) has been proposed to be secreted and to be active in the apoplast (for review see Napier *et al*, 2002; Tromas *et al*, 2009), indicating the possibility for extracellular auxin signaling.

Auxin exerts its action to a large extent by modulating gene expression via binding to the well-characterized nuclear auxin receptor TIR1 (reviewed in Chapman and Estelle, 2009). Here, we explored the simplest, yet biologically plausible, scenario in which auxin would act both intracellularly on PIN expression and extracellularly on the subcellular dynamics of PIN proteins via receptor-mediated signaling pathways.

The computational approach to model the PIN polarization integrated available molecular and cell biological data. Biological data (I) and hypothetical assumptions (II) were incorporated into a computer model for auxin transport and PIN polarization (for model details see Supplementary information and Supplementary Tables 1–3).

(I) The auxin fluxes were modeled between discrete cells and cell wall compartments by using the chemiosmotic hypothesis (Goldsmith *et al*, 1981; Figure 1A). Accordingly, auxin slowly diffused and was actively transported by the

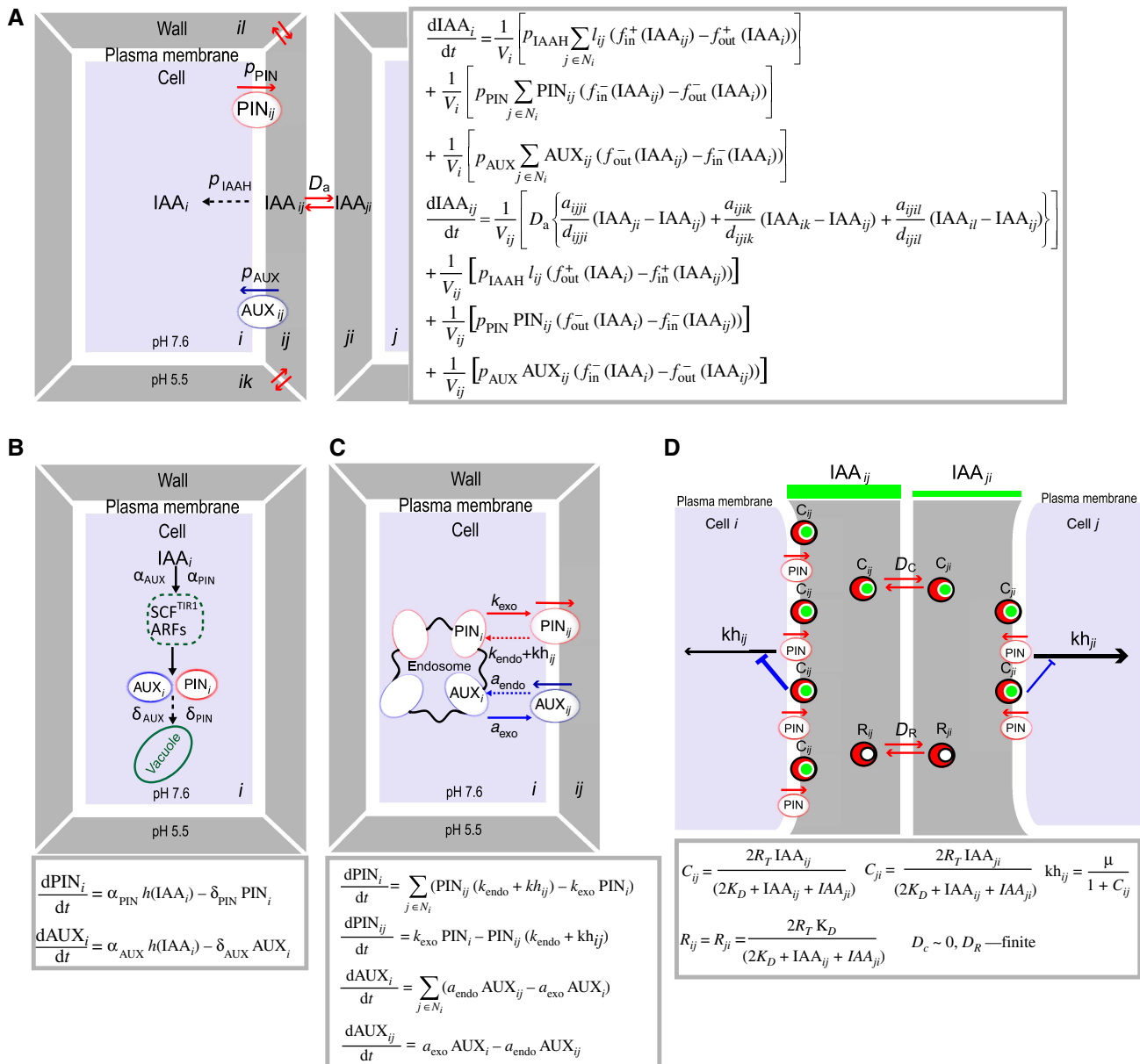


**Figure 1** Schematic and mathematical representations of the main model assumptions. **(A)** Schematic and mathematical representations of auxin transport between cells ( $i, j$ ) and cell wall interfaces ( $ij, ji, ik$ , and  $il$ ).  $IAA_i$  describes the mean auxin concentration in the  $i$ th cell; whereas  $IAA_{ij}$  and  $IAA_{ji}$  determine the auxin concentrations in discrete wall compartments ( $ij$  and  $ji$ ). The functions  $f_{in}^+/f_{in}^-$  and  $f_{out}^+/f_{out}^-$  are used to evaluate the fractions of auxin in the cell and in the cell wall. Dashed arrows indicate the rate of passive auxin diffusion into the cell and  $p_{IAAH}$  describes the membrane permeability for protonated auxin.  $D_a$  is the diffusion coefficient of auxin between neighboring wall compartments.  $p_{PIN}$  and  $p_{AUX}$  are parameters that determine PIN- and AUX/LAX-dependent efflux and influx of auxin across the plasma membrane, respectively.  $PIN_{ij}/PIN_{ji}$  and  $AUX_{ij}/AUX_{ji}$  are PIN (red) and AUX/LAX (blue) levels, respectively, in neighboring plasma membranes. **(B)** Schematic and mathematical representations of intracellular auxin perception: auxin-induced carrier synthesis (solid black arrows) and basic carrier degradation (dashed black arrows). The  $\alpha_{PIN}$  and  $\alpha_{AUX}$  are the rates of auxin-dependent PIN and AUX/LAX expression, respectively. The degradation rates of PIN and AUX/LAX proteins are given by parameters  $\delta_{PIN}$  and  $\delta_{AUX}$ . **(C)** Schematic and mathematical representations of auxin carrier trafficking. The rates of endo- and exocytosis affect carrier abundance at the plasma membrane. PIN<sub>i</sub> corresponds to the PIN level at the plasma membrane of the  $i$ th cell (red arrows) and AUX<sub>i</sub> determines the AUX/LAX level (blue arrows) in the  $i$ th cells. The base rates for PIN exocytosis and PIN endocytosis are  $k_{exo}$  and  $k_{endo}$ , whereas  $a_{endo}$  and  $a_{exo}$  similarly correspond to AUX/LAX recycling rates. The component  $kh_{ij}$  determines the inhibitory effect of auxin on the PIN internalization at a given cell side. **(D)** Schematic and mathematical representations of extracellular receptor-based auxin signaling pathway for modulation of PIN trafficking. Two adjacent cells share a common pool of extracellular auxin receptors denoted as  $2R_T = C_{ij} + C_{ji} + R_{ij} + R_{ji}$ , where  $C_{ij}$  and  $C_{ji}$  represent the levels of the auxin-bound receptor in the discrete wall compartments facing the surfaces of the adjacent cells  $i$  and  $j$ .  $R_{ij}$  and  $R_{ji}$  correspond to the levels of free receptors that undergo diffusion between common wall compartments ( $D_R$ ). The auxin receptors are activated by auxin via direct binding at the cell surface and transfer an inhibitory signal to regulate PIN internalization rates ( $kh_{ij}$  and  $kh_{ji}$ ) that is linked with their temporal immobilization at a given side of the cells ( $D_C \sim 0$ ). The green bars represent auxin concentrations in the discrete cell wall compartments.

AUX/LAX family of auxin influx carriers into the cell (Swarup *et al*, 2005; Figure 1A). To exit the cell, auxin required an active transport mediated by the PIN auxin efflux carriers (Petrášek

*et al*, 2006; Figure 1A). The auxin diffusion between discrete wall compartments was also taken into account, because of its importance for auxin transport (Swarup *et al*, 2005; Kramer

*et al*, 2007). Moreover, we considered that the diffusion of auxin was significantly reduced in the apoplast (Kramer *et al*, 2007). On the single-cell level, the ERP model incorporated an auxin-dependent carrier expression (Peer *et al*, 2004; Heisler *et al*, 2005; Vieten *et al*, 2005) that is mediated intracellularly (Figure 1B) by the nuclear TIR1-dependent pathway (Kepinski and Leyser, 2005; Dharmasiri *et al*, 2005). In the model, auxin carriers undergo constitutive degradation in lytic vacuoles (Abas *et al*, 2006; Kleine-Vehn *et al*, 2008b; Figure 1B). The auxin influx carriers (AUX/LAX) were assumed to be uniformly distributed at the plasma membranes, and their targeting mechanisms are considered to be distinct from the PIN proteins (Kleine-Vehn *et al*, 2006; Figure 1C). The dynamics of PIN recycling allowed the translocation of proteins between different cell sides and rapid changes in PIN polarity, as well as in response to various external and internal signals (Benková *et al*, 2003; Friml *et al*, 2002, 2003; Heisler *et al*, 2005; Dhonushe *et al*, 2008; Kleine-Vehn *et al*, 2008a). Similarly to most recent models (Ibañes *et al*, 2009; Sahlin *et al*, 2009), we included this dynamics of PIN recycling and assumed the auxin-dependent regulation of PIN internalization (Paciorek *et al*, 2005; Figure 1C).

(II) In our model, the concentration-dependent effect of auxin on PIN internalization (Paciorek *et al*, 2005) involved the extracellular receptor-based signaling pathway at the cell surface (Figure 1D), the extracellular pools of hypothetical auxin receptors were shared by each pair of neighboring cells, and the competitive utilization of these auxin receptors allowed direct cell-to-cell communication (Figure 1D). We assumed that auxin binding to the receptor induced signals to inhibit PIN internalization, leading to differential PIN protein retention at different cell sides. Although the direct mode of the signal transfer is unknown, we speculated that bound receptors might be recruited and, hence, temporarily immobilized, to the plasma membrane (or alternatively to cell wall components) for signal transfer, which is modeled by the reduced diffusion of receptors involved in the auxin signaling (Figure 1D). Simultaneously, free receptors from the intercellular pools underwent free diffusion (Figure 1D). To reduce the model complexity, auxin binding to the receptors immediately imposed an inhibitory signal to the nearest cell (Figure 1D). To model the spatial proximity of receptor-based signal transfer to the nearest cell side, we divided the apoplast into two discrete compartments suitable for computational reasons (Figure 1D). The strength of auxin signaling was determined by the amount of auxin-bound receptors present in these discrete wall compartments (Figure 1D).

Analysis of our model revealed that differences in diffusion rates of bound auxin and free receptors are crucial for the model performance. This competitive utilization mechanism enabled cell-to-cell communication in the model, leading to receptor enrichment at the site of increased auxin concentration (Supplementary Figure 1).

We propose that the implementation of these biological data (I) and hypothetical assumptions (II) are sufficient to generate PIN polarity in a given tissue. The model generates initially a weak, diffusion-driven auxin gradient in the apoplast, with asymmetric PIN retention at neighboring cell sides as a consequence (Figure 2A). The competitive utilization of the auxin signaling components would lead to a coordinated

asymmetry in PIN internalization rate in the neighboring cells and finally to the alignment of PIN polarity.

Indeed, the synergy of the local auxin signaling between each pair of competing cells promoted tissue polarization (Figure 2B). Intriguingly, this feedback regulation of polar auxin transport contributed to formation of steeper extracellular auxin gradient (Figure 2A and B). In conclusion, the PIN polarization and polar auxin transport both depended on and contributed to the establishment of a differential auxin signaling (Figure 2C and D). Such feedback loop led ultimately to the alignment of PIN polarization within a tissue (Figure 2B).

### The ERP model robustly reproduces PIN1 polarity during vascular development

To test whether the ERP model could reproduce the PIN1 polarity patterns observed *in vivo* during vein formation, we used a tissue grid layout and applied minimal assumptions, such as the presence of an auxin source and a distal sink (Figure 3). After auxin application, the simulation revealed that PIN1 polarized away from an auxin source, confirming our theoretical expectations (see above). PIN1 expression was initially broad (Figure 3A and C), but converged over time to a single cell file with strong PIN1 expression and polarization (Figure 3B). This simulation recapitulated the experimental observations during vein formation that PIN1 expression was initially broad with poorly defined polarity (Figure 3E). The addition of an auxin sink was not essential to polarize the PIN proteins (data not shown), but imposed directionality on the developing vein that ultimately linked the auxin source and sink by a PIN-dependent conductive auxin channel.

To analyze behavior, sensitivity, and robustness of the ERP model, we tested the contribution of model components for predicted PIN polarity and auxin distribution patterns. These components include extracellular receptor-based auxin perception and competitive utilization of receptors by neighboring cells (Supplementary Figures 1–3), auxin-mediated carrier expression (Supplementary Figures 4 and 5), PIN- and AUX/LAX-dependent polar transport (Supplementary Figures 6 and 7), and auxin diffusion (Supplementary Figures 8 and 9).

Our model predictions were robust with respect to altered source or sink locations (Supplementary Figure 10) or intracellular auxin gradients (Supplementary Figure 11). The ERP model provided a robust mechanism for canalization of auxin flow (Supplementary Figure 10). Additionally, this model is able to capture conflicting PIN behaviors including PIN polarization with or against the auxin gradient (Supplementary Figures 12–16). During midvein formation, neighboring cells at the advancing edge of the forming vein display transient PIN polarization toward each other (Bayer *et al*, 2009). Intriguingly, the ERP model reproduced this PIN polarization pattern: cells at the growing edge of the forming conductive channel polarized the PIN proteins toward the auxin channel (Figure 3C). In the simulations, the initially weak apoplastic auxin gradient between these cells led to relatively high auxin-dependent inhibition of the PIN endocytosis at the plasma membrane of both cells and, consequently, PIN proteins in neighboring cells became polarized toward

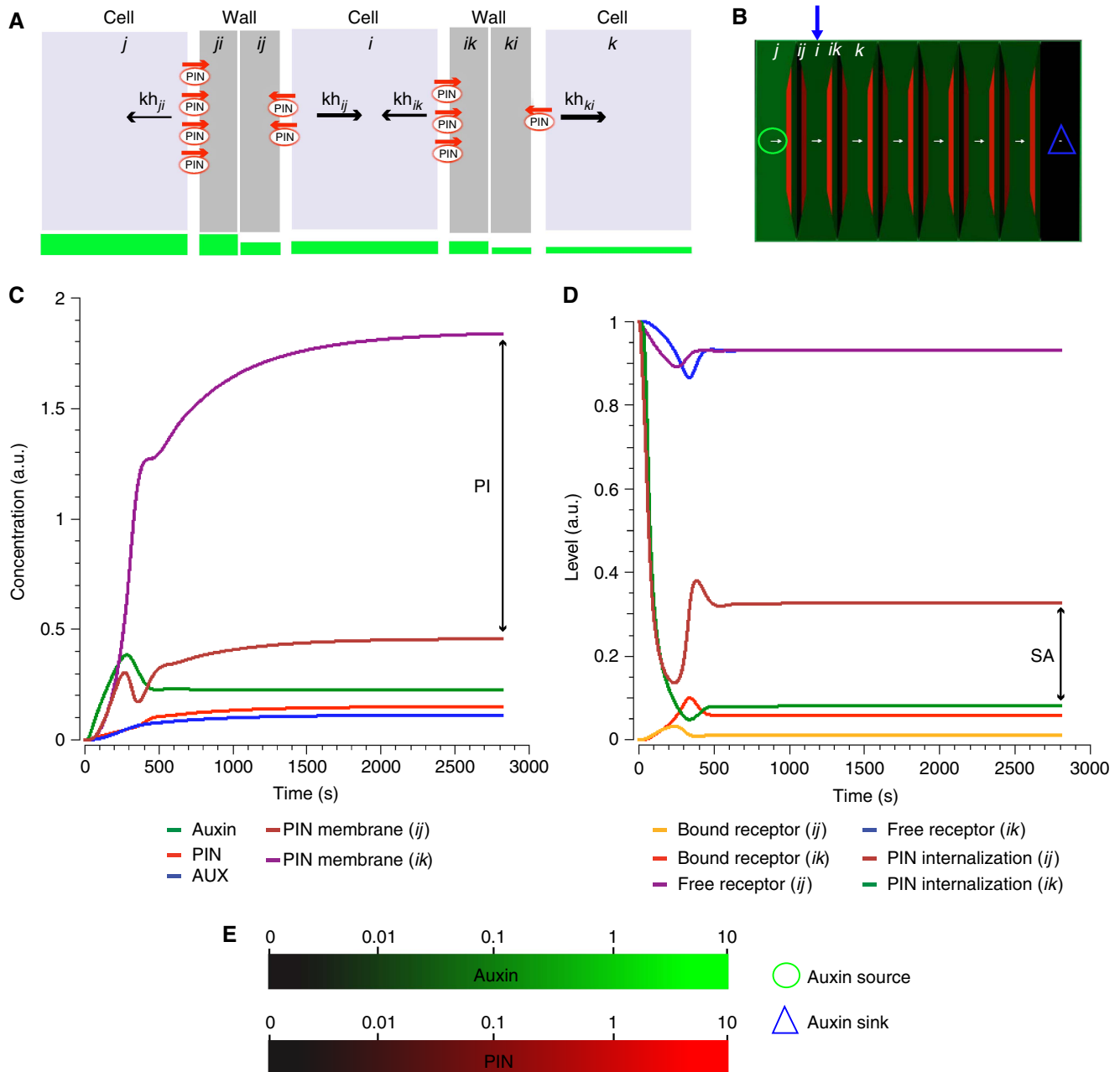


**Figure 2** Global polar signal in the cell file produced by the synergy of the local extracellular auxin signaling. **(A)** Schematic representation of a cell file separated by discrete cell wall compartments. Indexes *i*, *j*, and *k* correspond to the three depicted cells. The wall compartments between adjacent pairs of cells are represented by indexes *ij*/*ij* (between cells *i* and *j*) and *ik*/*ki* (between cells *i* and *k*). The component *kh* with the corresponding index determines the effective rate of the PIN internalization at the given cell side, as described in Figure 1D. PIN (red) abundance at the plasma membrane presumably correlates with the profile of the auxin gradient (green bars). **(B)** *In silico* model simulation on the cell file predicting PIN polarization and canalization of auxin flow. Red and green depict PIN proteins and auxin distribution, respectively. The blue arrow marks the position of the monitored cell in the cell file. **(C)** Time-course profiles of auxin concentration, intracellular PIN and AUX/LAX levels (PIN<sub>*i*</sub> and AUX<sub>*i*</sub>), and PIN membrane levels (PIN<sub>*ij*</sub> and PIN<sub>*ik*</sub>). **(D)** Time-course profiles of bound ( $C_j$  and  $C_{ik}$ ) and free receptor ( $R_j$  and  $R_{ik}$ ). The levels are normalized by total amount of receptors in the pool ( $R_T$ );  $kh_{ij}$  and  $kh_{ik}$  are the corresponding PIN internalization rates. The polarization index (PI) indicates asymmetry and represents the ratio between PIN levels at the *ik*th plasma membrane and those of the *ij*th membrane (C). The signaling asymmetry (SA) depicts difference in extracellular auxin signaling between *ik*th and *ij*th sides of the cell *i* (D). PI and SA are associated with different states of the cell polarization: no polarization (PI ~ 0, SA ~ 0), initiation of polarization (PI and SA increased), and maintenance of polarization (PI and SA saturated). **(E)** Color coding schemes for auxin concentrations and PIN levels used in all model simulations. Auxin concentrations can vary from 0 (black) to 10 (bright green). PIN levels at the plasma membrane may change from 0 (black) to 10 (bright red). White arrows point in the direction of preferential PIN polarity and the arrow size indicates the relative strength of the PIN expression in the cell. Green circle (source) and blue triangle (sink) illustrate the positions of auxin source and auxin sink on the tissue template.

each other. However, because differences in the auxin transport rates of these neighboring cells (derived from auxin-dependent regulation of auxin carrier expression and

polarity) progressively enhanced the extracellular auxin gradient, an enhanced asymmetry in the local auxin signaling was created. The competitive utilization of auxin receptors in

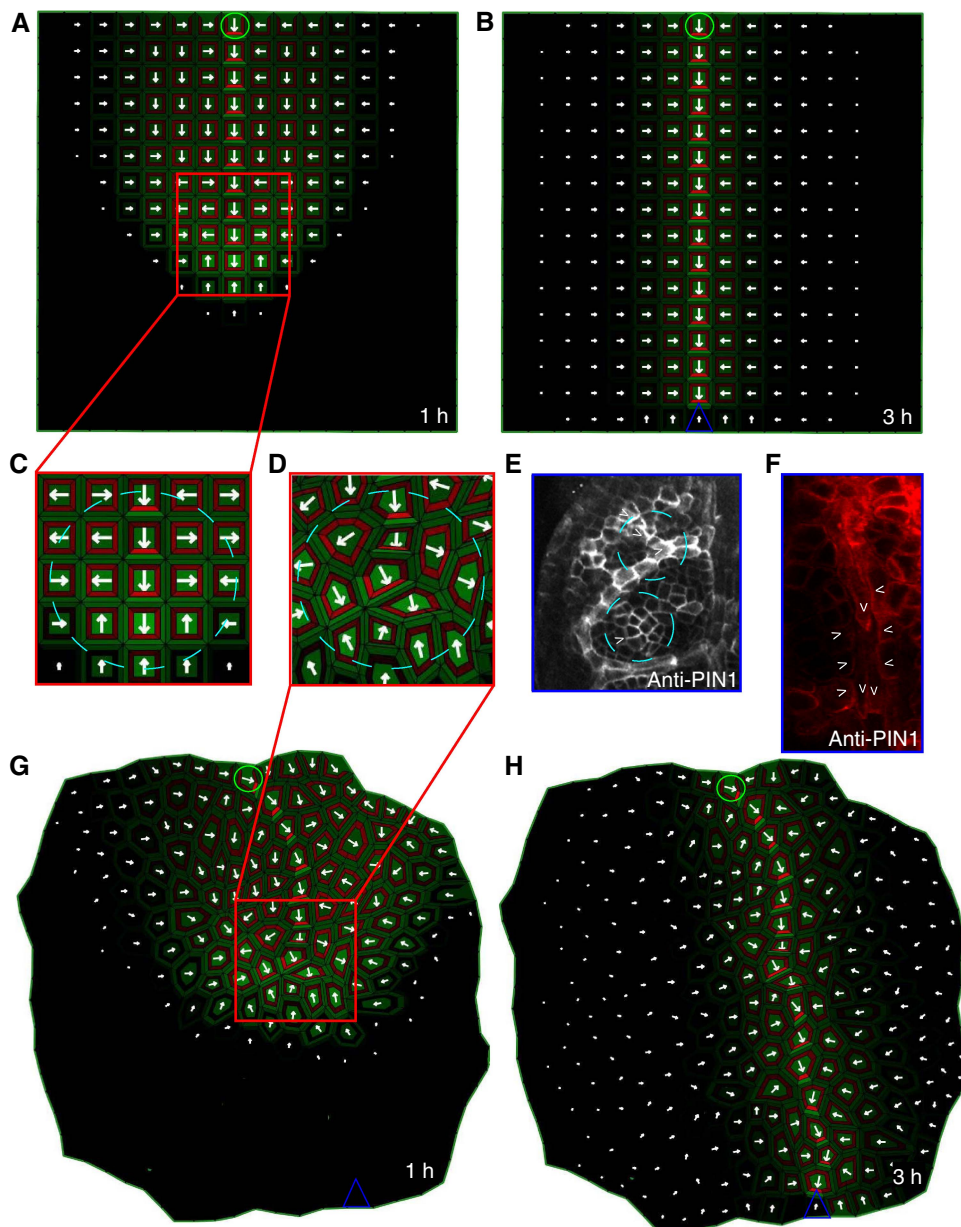


**Figure 3** Experimental and simulated PIN-dependent auxin canalization. **(A–C)** Simulations of the ERP model on a grid tissue layout. Initially, a broad PIN1 expression domain was predicted (A, C), originating from the site of auxin application (green circle). Subsequently, this expression domain became narrowed to a single cell file, and, finally, produced a conductive auxin channel that connected the auxin source to the distal auxin sink (blue triangle) (B). **(D, E)** The broad PIN1 expression domain predicted by the model simulation using the cellular layout (D) and reported *in vivo* in *Arabidopsis* during leaf venation patterning with PIN1 immunolocalization (E). **(F)** PIN polarization during primary vein initiation in young leaves as reported by the PIN1 antibody. Provascular cells show basal PIN1 polarization while the surrounding cells are polarized toward them. **(G, H)** ERP model simulation using the cellular tissue layout. The initial, broad PIN1 expression domain (G) becomes reduced to a narrow domain of strong PIN expression (H). The cells adjacent to the vascular strand are polarized toward it (H), as observed *in planta* (F). In the simulations, the PIN proteins are indicated in red and the auxin distribution in green. Green circle (source) and blue triangle (sink) illustrate the positions of auxin source and auxin sink on the tissue template. Arrowheads in panels E and F highlight preferential PIN1 polarization.

the apoplast was necessary for the propagation of differential extracellular auxin signaling and the coordination of PIN polarity within the tissue (Supplementary Figures 1–3). Interestingly, the complete removal of auxin-induced carrier expression from the ERP model did not cause the loss of PIN polarity and auxin canalization in the model simulations (although polarization patterns were less realistic), but only when either the high amount of carriers in the

initial pool (Supplementary Figures 4A–L) or high auxin-independent carrier expression (Supplementary Figures 5A–L) were integrated in the model. Next, we tested the ERP model on a more natural tissue layout in which cell shape varied (Figure 3D and G). The model accurately predicted the PIN1 polarization in the natural tissue layout (Figure 3H), recapitulating primary vein formation as observed in leaves (Figure 3F).

For both virtual tissues, the model reproduced the basal PIN1 polarization in provascular cells and lateral PIN1 polarization, pointing toward the conductive auxin channel, in adjacent cells (Figure 3B and G). Interestingly, this observation of lateral PIN1 polarization was absent from the predictions of flux-based models (Mitchison, 1980; Feugier *et al*, 2005; Rolland-Lagan and Prusinkiewicz, 2005). In our model, owing to the high auxin concentrations, the auxin carrier expression is stronger in the conductive channel compared with the adjacent tissues. Furthermore, the PIN-driven efflux is strongly oriented toward the basal cell side of provascular cells while auxin influx remains uniform. This leads to stronger auxin influx compared with auxin efflux at the lateral side of the provascular cell, ultimately triggering the carrier-driven formation of a weak horizontal auxin gradient. In response to this gradient, PIN1 in the neighboring tissues polarized toward the conductive channel. Surprisingly, we found that the activity of the AUX/LAX proteins buffered the motility of auxin in the wall and largely contributed to the maintenance of PIN polarization and auxin gradients in the tissues (Supplementary Figure 7). This finding is consistent with a role of AUX/LAX proteins in phyllotactic patterning (Bainbridge *et al*, 2008).

### The ERP simulations suggest the appearance of high auxin concentration in veins

Simulations with the ERP model on tissue layouts predicted PIN1 polarization during the formation of the conductive auxin channel (vein precursor). Other single mechanism-based models, such as flux-based (Mitchison, 1980; Rolland-Lagan and Prusinkiewicz, 2005) and concentration-based models (Merks *et al*, 2007), anticipate low auxin concentrations in the developing veins, which is in contradiction with experimental observations (Scarpella *et al*, 2006). However, several solutions for this problem have been suggested, such as enhanced AUX/LAX-dependent auxin uptake (Kramer, 2004; Swarup *et al*, 2005) or constant total carrier protein abundance (Feugier *et al*, 2005). On the other hand, the ERP model reproduces auxin canalization patterns, involving the dynamic changes in auxin-dependent carrier expression. The auxin concentrations in our model simulations were higher in the emerging veins than in those of surrounding tissues (Figure 4A). An elevation of auxin concentration was observed in provascular cells, whereas neighboring cells showed a steep decrease in auxin concentrations (Figure 4B). This observation might be conceptualized as the balance between PIN1-dependent auxin export from adjacent cells toward the vein precursors and the active drainage of auxin from lateral tissues by AUX/LAX-dependent influx into the provascular cells.

The *in silico* predictions of our model illustrate that high auxin concentrations and high auxin fluxes can simultaneously guide venation patterning, as suggested experimentally (Scarpella *et al*, 2006). Importantly, the ERP model predicted PIN1 polarization not only away from the auxin source but also toward provascular cells with high auxin levels; thus, through a single mechanism, the model recapitulates cell polarization events both away from and toward an auxin maximum.

### The ERP model is robust with respect to tissue growth

We successfully utilized the ERP model to reproduce PIN1 polarity in a tissue grid and a more natural tissue layout. To investigate the flexibility and robustness of the model, we additionally imposed a dynamic growth simulation onto the natural tissue layout by assuming that the tissue consecutively expanded and subdivided as the cells changed their size and gave rise to daughter cells (Figure 4C). For more details on modeling growth, we refer to Supplementary information. The growth simulations of the ERP model revealed that (following auxin source and sink application) discrete PIN-dependent auxin channels were maintained within growing cells (cell expansion) and, moreover, were unaffected due to cell division in surrounding tissues (Figure 4D and E). Under these assumptions, the dynamic interplay of intracellular and extracellular auxin signaling might explain the robust adaptation of vascular patterning to tissue growth.

### The ERP model reproduces vein connections

The ERP model simulations faithfully reproduced vein formation and progression. Beside single-vein formations, plants have evolved a complex network of connected vasculature. Classical experiments had revealed that preexisting vasculature attracts *de novo* established veins, allowing vein connections to be made (Sachs, 1981), but the underlying mechanism of these inspiring observations remained to be solved.

To study whether the ERP model could provide a theoretical framework to assess the mechanisms underlying these classical experiments, the ERP model was simulated on grid tissue layout and, initially, a single-vein pattern was induced by introducing an auxin source and a distal sink. Next, secondary auxin sources were introduced adjacent to the primary vein (Figure 5A). The simulation showed that a new conductive auxin channel was formed, which originated from the lateral auxin source and ultimately connected to the preexisting vein (Figure 5B). Both *in planta* and *in silico*, it was observed that PIN proteins in the cells that surrounded a conductive auxin channel were polarized toward that channel (Figure 3). In our simulations, it is this preferential lateral polarization toward the auxin-containing channels that leads to the attraction of secondary veins.

### The ERP model recapitulates vein loop patterns

Although complex vein networks in leaves are not fully understood, PIN-dependent auxin transport at the leaf margin and auxin biosynthesis appear to initiate vein loop formation (Scarpella *et al*, 2006). To test whether these complex vascular patterns could emerge by using the ERP model, the cellular tissue layout was simulated with an auxin-induced single-vein pattern (Figure 5C–H). As a bipolar PIN1 localization at the side of the vein loop initiation had been observed experimentally (Scarpella *et al*, 2006), we tested whether a bipolar PIN1 signal would be triggered by the sequential introduction of lateral auxin sources in pairs of neighboring cells within the tissue surrounding the main vasculature. Within these pairs of cells, a bipolar PIN1 localization occurred that led to an auxin flow in two

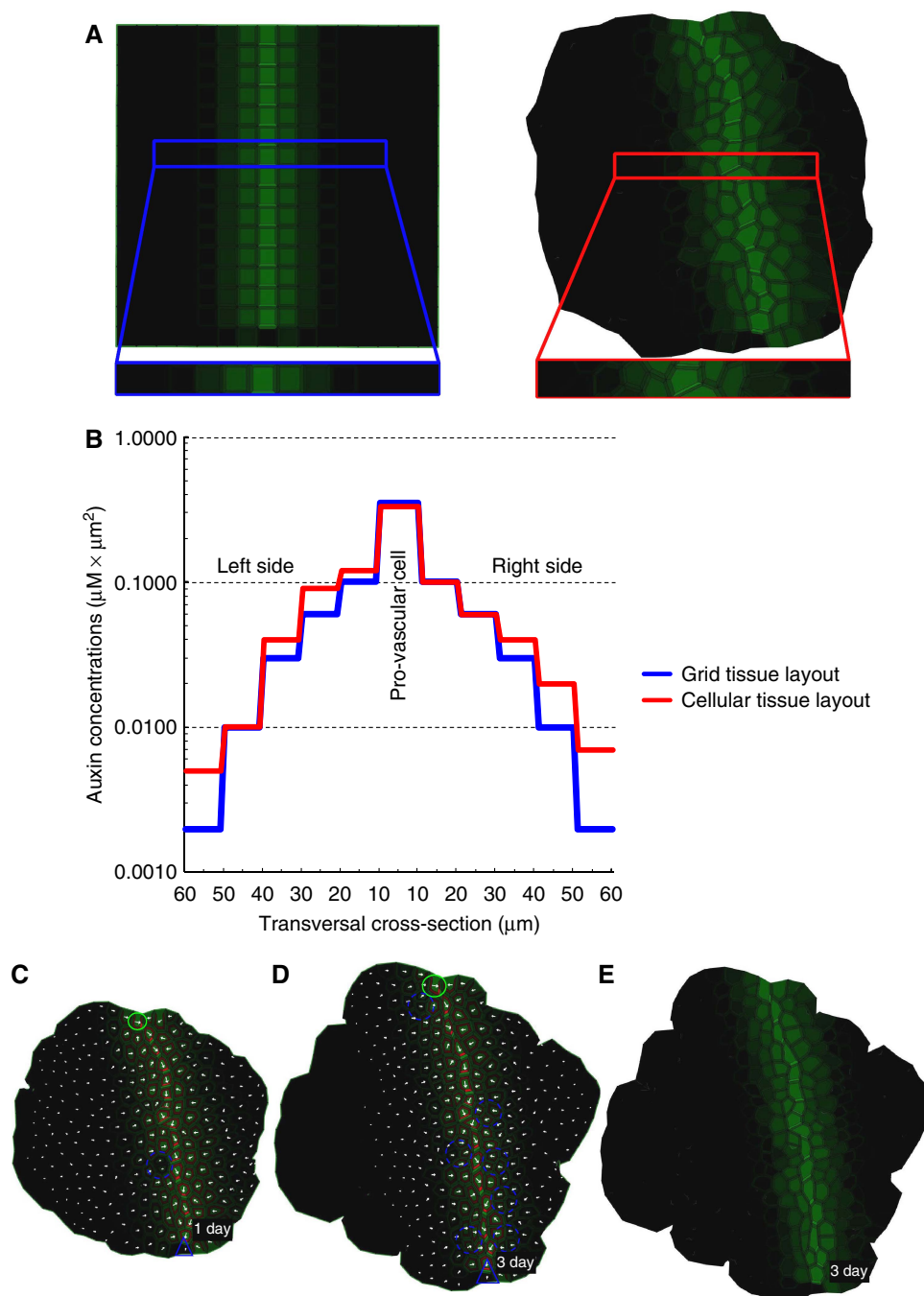


**Figure 4** Steady-state auxin distribution patterns during vein propagation and robustness of vein pattern toward tissue growth. **(A)** Steady-state auxin distribution patterns for grid and cellular tissue layouts. **(B)** Examination of the auxin concentrations in cross sections of the tissue layouts showing that the auxin concentration is 10-fold higher in the provascular cells than in the surrounding tissues. **(C, D)** Simulation of auxin canalization during dynamic tissue growth. The vein pattern is not altered due to tissue growth. The model predicts PIN1 polarity pattern **(C)** as observed *in vivo* in *Arabidopsis* (Figure 3E and F). The auxin distribution pattern during tissue growth **(E)** corresponds to that in the non-growing tissue **(A)**. Green circle (source) and blue triangle (sink) illustrate the positions of auxin source and auxin sink on the tissue template. Blue dashed circles highlight the exemplary regions of cell division.

directions from the auxin sources, leaving a trace of polarized cells. Over time, the emerging veins were attracted by the main vein and, finally, formed closed vascular strands (vein loop precursors; Figure 5C–F). The leaf vein loop precursors produced by the simulation contained high auxin concentrations (Figure 5H) and displayed a narrow PIN1 expression

domain (Figure 5C–F). These predicted patterns were consistent with the PIN and auxin distribution patterns observed in developing leaves (Figure 5G and H). Additionally, we found that the distance of the lateral auxin sources from the main vasculature might determine the shape, radius, and length of the secondary vein (data not shown).

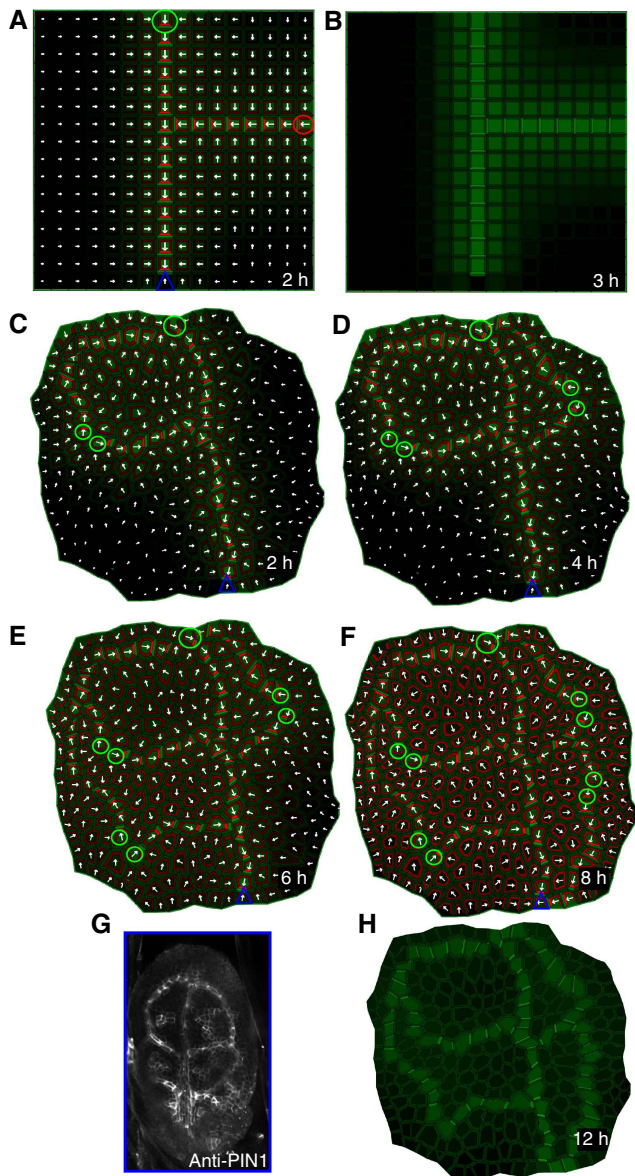


**Figure 5** Experimental and simulated auxin distributions and PIN polarization patterns during vein attraction and vein loop formation. **(A, B)** *In silico* experiment with the induction of a strong lateral auxin source (red). The main vein attracts the secondary vein, leading to a vascular connection **(A)**. **(B)** Corresponding steady-state auxin distribution pattern. **(C–F)** Simulation of sequential application of lateral auxin sources **(C–F)**. Sequential addition of lateral auxin sources resulting in a complex vein loop pattern **(D)**, with a predicted PIN1 distribution pattern that is similar to that detected by PIN1 immunolocalization in *Arabidopsis* leaves **(G)**. **(H)** Corresponding steady-state auxin concentration pattern revealing high auxin concentration accumulation in vein loops, as observed *in planta* (Scarpella *et al*, 2006). Green circle (source) and blue triangle (sink) illustrate the positions of auxin source and auxin sink on the tissue template.

### The ERP model predicts competitive canalization during shoot branching

The ERP model simulations predict that vein connections occur when the lateral auxin source is either comparable with

or stronger than the primary auxin source (data not shown). This finding suggests that the interconnection of vascular systems might depend on the actual auxin concentration ratio between competing auxin sources, a relation reminiscent to a process proposed to regulate shoot branching. Auxin production and auxin flow in the primary shoot impose an apical dominance over lateral buds and inhibit their outgrowth (Thimann and Skoog, 1933). The removal of the apical auxin source, for instance by decapitation, leads to bud outgrowth. A competitive auxin transport mechanism between the dormant bud and stem vasculature has been proposed to regulate bud outgrowth (Prusinkiewicz *et al*, 2009; Balla *et al*, 2010). Accordingly, dormant buds fail to polarize PIN proteins and establish a PIN-dependent auxin flow and vein connection to the main vein in the stem, limiting their developmental progression.

To investigate whether the temporal supremacy of the primary auxin source in the system might be the actual reason for the inhibition of vein connection, we simulated the ERP model on grid tissue layout (stem representation), with a dominant apical auxin source and a distal auxin sink to induce a primary vein. Subsequently, we reduced the strength of the primary auxin source, which could correspond to virtual stem decapitation (Figure 6A). Afterward, we introduced a secondary lateral auxin source (Figure 6B). Over time, vein connection was observed from the lateral auxin source, following PIN1 polarization toward the primary vein (Figure 6C–E). To verify the model outcome experimentally, we studied the PIN1 localization by immunolocalization with a PIN1 antibody in pea (*Pisum sativum*) stems. After stem decapitation (Figure 6F), exogenous application of auxin to the lateral site of the stem resulted in PIN1 expression at the site of application and polarization of PIN1 toward the preexisting vasculature (Figure 6G and H). To substantiate this finding, we reactivated the primary auxin source after stem decapitation (Figure 6I and J), before the virtual application of the secondary auxin source (Figure 6K). Under this condition, the lateral auxin source failed to connect to the primary vasculature (Figure 6L and M), which could be validated by performing PIN1 immunolocalizations on pea stems to which an apical auxin source had been applied after decapitation (Figure 6N–P).

The observations from the model simulations and experiments imply that the temporal supremacy of primary over secondary auxin sources is presumably determined by the relative strength of the sources. To support this conclusion, we analyzed the behavior of the ERP model under the variable strength of auxin input in the system (Supplementary Figure 12). The dynamic instabilities characterized by periodic oscillations of PIN polarization in the presence of a weak auxin source corresponded to the absence of vein connection (vein repulsion) (Supplementary Figures 12M–P). In contrast, an increase of the overall auxin concentrations in the tissue caused by the presence of an enhanced auxin source led to the stable formation of vein patterns (Supplementary Figures 12E–L). These findings are in agreement with experimental and theoretical observations based on PIN-dependent auxin transport (Prusinkiewicz *et al*, 2009).

The ERP simulations revealed simple, yet important, mechanistic insights into this type of competitive inhibition

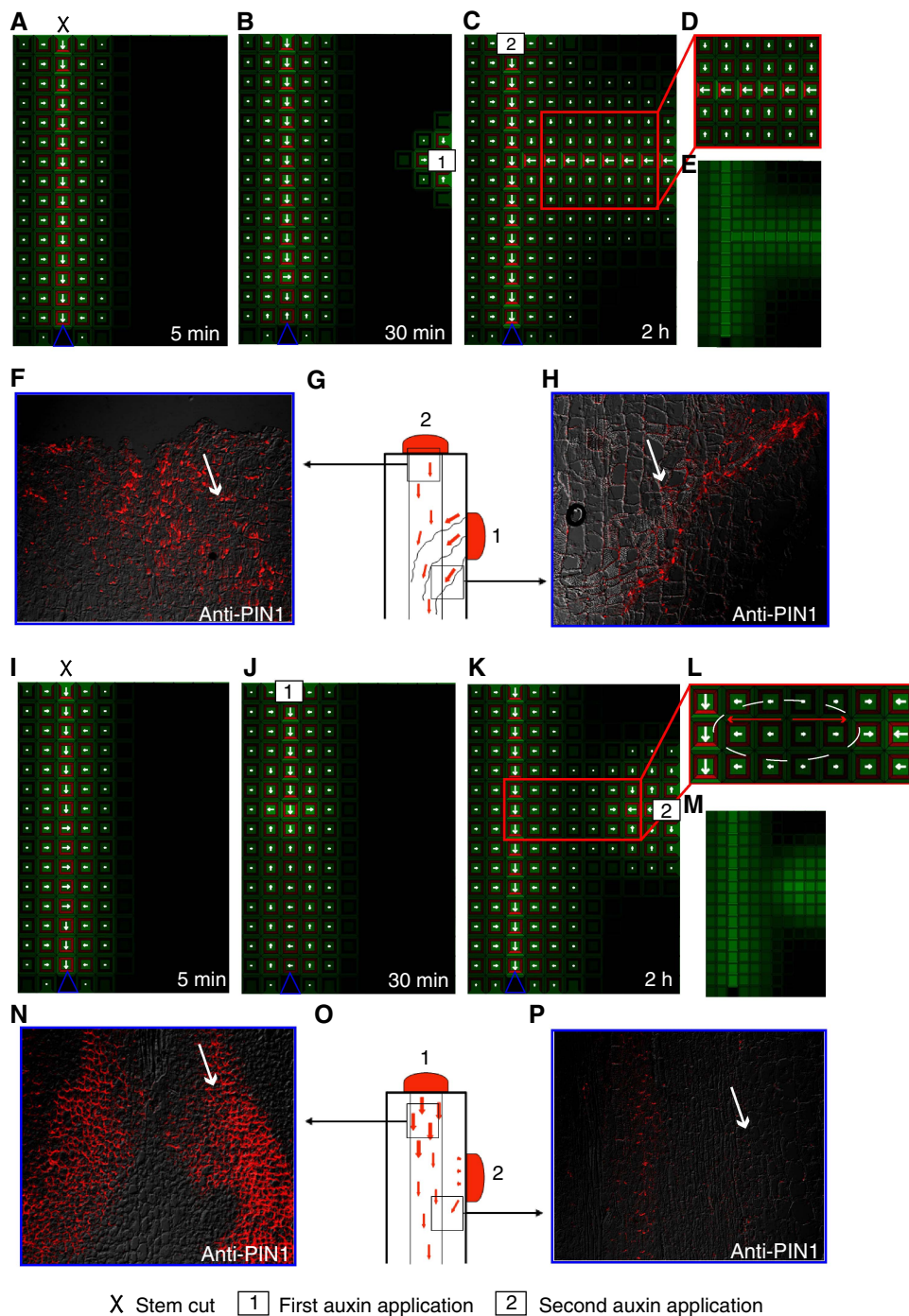


**Figure 6** Experimental and simulated auxin distributions and PIN polarization patterns during branching activation and inhibition. **(A–E)** Simulation of a virtual stem cut (A) and subsequent virtual auxin applications, first to the lateral site (B) and second to the apical site (C). (D) Unilateral PIN1 polarity in the proximity of the main vein and canalization from the lateral auxin source, as predicted by ERP model (E). **(F–H)** PIN1 immunolocalization in pea stems after decapitation (F, H) (Balla *et al*, 2010). Auxin was applied first laterally and then apically (G). Canalization from the lateral source occurs analogously to that from a secondary auxin source (F, H). **(I–M)** Simulations of a virtual stem cut (I) and subsequent virtual auxin application, first to the apical site (J) and second to the lateral side of the tissue (K). (L) Bipolar PIN1 polarity in the cells between the main vein and the lateral source, resulting in the lack of vein connection (M). **(N–P)** PIN1 immunolocalization in pea stems after decapitation and subsequent auxin application (N, P) (Balla *et al*, 2010). Auxin was applied first to the apical site and then to the lateral site (O). Canalization from the lateral source did not occur (P). Blue triangle (sink) illustrate the positions of auxin sink on the tissue template. Arrows in panels F, H, N and P highlight preferential PIN1 polarization.

that had initially been proposed to explain branching patterns in plants (Prusinkiewicz *et al*, 2009). Our simulations faithfully reproduced PIN polarization toward the existing

conductive auxin channel and preferential PIN polarization toward the newly forming auxin channel. However, the pattern of PIN polarization at the growing tip of the channel led to

adverse PIN polarization in the proximity of the main vein (Figure 6L). Accordingly, the auxin concentration in the emerging lateral vein precursor needed to be comparable with or higher than that in the main vein to break this adverse polarization and to establish a vein connection (Figure 6C and Supplementary Figure 12). Thus, our modeling and experimental results provide a strong support for the hypothesis of competitive auxin canalization (Prusinkiewicz *et al*, 2009) proposed for shoot branching in plants.

### Self-organization and dynamics of the ERP model explain PIN polarity rearrangements during vascular regeneration

The ERP model accounted for vascular patterning processes, such as vein formation and propagation, competitive vein attraction/repulsion, and vein loop formation. Next, we studied another interesting aspect of vascular patterning linked to the regeneration of plant vasculature after local tissue wounding. Local wounding during tissue regeneration stimulates rearrangements in the polar localization of PIN proteins, thus providing plants with a flexible developmental adaptation (Benková *et al*, 2003; Sauer *et al*, 2006). We tested the ERP model for changes in PIN polarity and auxin distribution associated with the regeneration of vasculature after wounding. First, we simulated an apical auxin source and distal auxin sink to establish an initial steady-state vein pattern. Subsequently, we disrupted this pattern by introducing virtual wounding (cell ablation; Figure 7A–C). A few minutes after wounding, auxin accumulated above the wound (Figure 7D), after which the PIN1 proteins were re-polarized. These flexible polarity rearrangements led to the regeneration of a conductive auxin channel circumventing the ablated cells (Figure 7E; Sauer *et al*, 2006). Additionally, the model simulation suggested a transient downregulation of the *PIN1* expression below the ablated cells (Figure 7F) that had not been reported previously.

To test these observations experimentally, we used a PIN1 antibody to study PIN1 distribution after wounding in pea stems. Tissue ablation resulted in a reduction in PIN1 expression just below the wound (Figure 7G). The PIN polarity pattern observed after *de novo* vascular regeneration (Figure 7G) was very similar to that predicted by the ERP model (Figure 7H and I).

The whole sequence of events predicted by the model, including auxin accumulation above the wound and PIN polarization around the wound, are consistent with previous experimental findings (Sauer *et al*, 2006). The model forecasts that the ectopic accumulation of auxin (new sources) above the wound and the decrease in auxin content below the wound (new sinks) is the actual trigger for vein regeneration. Accordingly, high auxin above the wound functions as a new auxin source that leads to PIN polarization toward the tissues with low auxin concentration below the wound. Concomitantly, the auxin-induced carrier expression integrated in the ERP model was necessary to facilitate this PIN re-polarization during vein regeneration (Supplementary Figures 4M–P and 5M–P), suggesting a temporal downregulation of PIN expression in the surroundings of the ablated region, ectopic auxin accumulation above the wound, and *de novo* PIN synthesis

facilitating rearrangement of PIN polarity and guiding the regeneration of tissues.

## Discussion

A unique feature of auxin among the plant hormones is its tightly regulated, cell-to-cell polar transport that allows auxin to convey positional and directional signals between cells and to contribute to tissue polarization and patterning. Here, we validate a conceptually novel mechanism for polarization of auxin transport in plant tissues. Our computer model integrates up-to-date cell biological data and a minimal theoretical framework for an auto-regulatory positive feedback loop between auxin and its polar redistribution of PIN auxin transporters. The subcellular dynamics of auxin carriers and auxin feedback on carrier expression that have been reported experimentally are both integrated into our model. Additionally, the model provides a mechanistically plausible framework for extracellular receptor-based auxin regulation for spatiotemporal synchronization and coordination of cell polarity, which, to our knowledge, had never been exploited in previous theoretical or experimental studies.

We propose that plant cells compete for extracellular auxin receptors to establish their polarities within tissues. Neither the auxin gradients in the cell wall nor the competitive utilization of receptors in the extracellular space had been so far considered for spatial-temporal regulation of the PIN abundance at the plasma membrane (Sahlin *et al*, 2009).

We demonstrated the plausibility of the ERP model for various processes, including *de novo* vascularization, venation patterning, and tissue regeneration in computer simulations performed with only minimal initial assumptions, namely a discrete auxin source and a distal sink. Moreover, these simulations were robust with respect to variable conditions, such as tissue growth, membrane permeability, auxin diffusion and auxin carrier expression levels, and position of auxin sources/sinks.

The ERP model reproduces the very detailed PIN polarization events that occur during primary vein initiation (Scarpella *et al*, 2006), such as basal PIN polarity in provascular cells, transient adverse PIN polarization in neighboring cells during the alignment of tissue polarization, and inner-lateral polarity displayed by the tissues surrounding a conductive auxin channel. Additionally, the ERP model generates high auxin concentration and high auxin flux simultaneously in emerging veins, revising the classical canalization models (Mitchison, 1980; Rolland-Lagan and Prusinkiewicz, 2005). Importantly, all the simulations support the claim that the ERP model represents the first single approach that faithfully reproduces the PIN polarization, both with the auxin gradient (basal PIN1 polarity in provascular cells) and against the auxin gradient (transient adverse PIN1 polarization in neighboring cells surrounding the provascular bundle), as well as producing the corresponding auxin distribution patterns during auxin canalization.

Interestingly, the ERP model predicts that minimal assumptions, such as the regulated position and strength of auxin sources, are sufficient to explain (i) the source-to-sink guided organization of complex venation patterns (loops) at the base

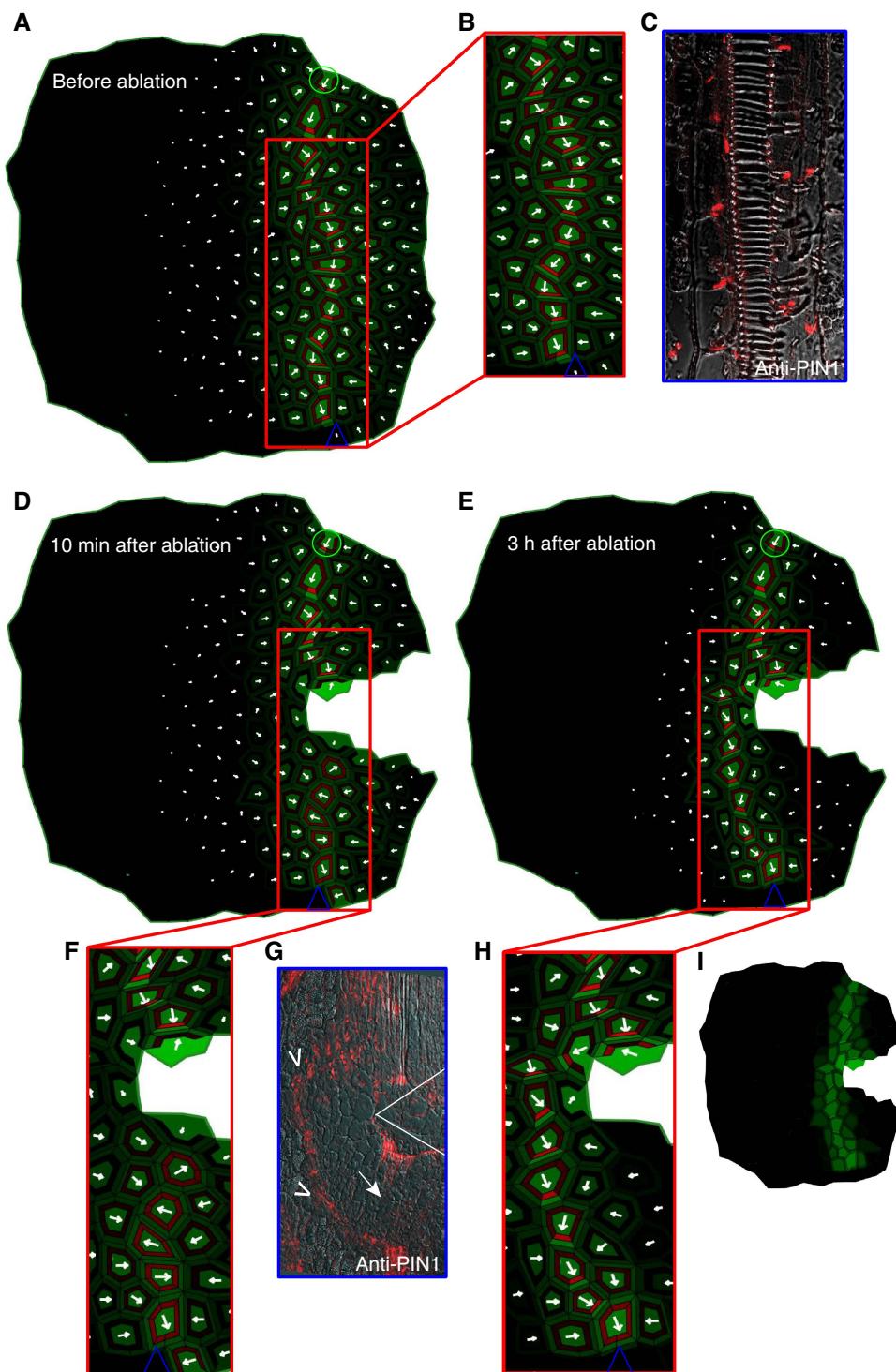


**Figure 7** Experimental and simulated rearrangement of PIN polarity after wounding. **(A–C)** PIN1 polarization pattern in the model simulation (A and B) and in a *pea* stem (C) before tissue ablation. **(D)** Downregulation of PIN1 expression below the wound apparent immediately after wounding. **(E)** Restoration of the vascular pattern by circumvention of the ablated cells. **(F–H)** Enlarged views of the wound site. PIN1 downregulation in response to wounding in the model simulation (F), and in the *pea* wounding experiment (G), as reported with the PIN1 antibody (white arrow). The predicted PIN polarization pattern after vein regeneration (H) is similar to that observed in the *pea* stem (G) as indicated by the white arrowheads. **(I)** Auxin distribution pattern revealing the auxin accumulation site just above the ablated cells. Green circle (source) and blue triangle (sink) illustrate the positions of auxin source and auxin sink on the tissue template.

of a leaf solely by the read out of localized auxin concentration spots (Scarpella *et al*, 2006) and (ii) the actual magnitude of auxin sources as a self-reliant signal to control mutual auxin

source competition for vascular connection, for instance during the auxin transport regulation of shoot branching. The model simulations revealed that the generation of these

complex and often transient PIN polarities is a self-emerging property of the ERP model. Importantly, the stability of these complex polarities is regulated by auxin in a concentration-dependent manner that provides a new explanation for vein attraction and repulsion phenomena.

Finally, we have demonstrated that the self-organizing dynamics of the ERP model produce a system that is able to adapt to external disruptions and provide a mechanistic framework for processes such as vascular tissue regeneration (Sauer *et al.*, 2006). By guiding a switch in PIN polarization and creating the associated temporal changes in auxin accumulation, a flexible pattern was created that allows the plant to adapt. The model analysis revealed the necessity of tight regulation of carrier expression by auxin for vascular patterning and regeneration after wounding. The ERP model simulations also illustrate how macroscopically different developmental processes, such as vascular tissue formation and apical dominance-controlled shoot branching, can be unified by a single mechanism derived through the combination of intracellular auxin feedback on carrier expression and extracellular perception-based regulation of the auxin carrier trafficking.

Here, we propose that extracellular auxin signaling facilitated by high-affinity binding of auxin to its extracellular receptor is essential to account for coordinated polarization of PIN proteins and auxin canalization during vascular development. The putative candidate for extracellular auxin receptor is ABP1 that resides in the lumen of the endoplasmic reticulum and is secreted to the cell wall (Napier *et al.*, 2002) where it is physiologically active (Leblanc *et al.*, 1999; Steffens *et al.*, 2001). Auxin inhibits clathrin-dependent PIN internalization via binding to ABP1 (Robert *et al.*, 2010). However, ABP1 and its contribution to coordinated tissue polarity still needs to be experimentally investigated (Tromas *et al.*, 2009). Such extracellular fraction of ABP1 (or yet to be identified ABPs) could correspond to the intercellular pools of extracellular auxin receptors in the ERP model. It still remains to be tested whether the ERP model could account for complex PIN polarity and auxin distribution patterns associated with embryogenesis, root system maintenance, and *de novo* organ formation.

## Materials and methods

### Computational methods

For model description, parameters, sensitivity analysis, and simulation insets, we refer to Supplementary information. The model was based on a version of *VirtualLeaf* (Merks *et al.*, 2007; Merks *et al.*, 2010), a cell-based simulation tool for modeling plant development. All simulations were run until steady-state patterns emerged. All figures were processed in Adobe Illustrator. Figures 3–7 and Supplementary movies 1–7 are screenshots from the model simulations. The *VirtualLeaf* binaries with the ERP model definitions (pseudo C++ source) are available on the public website <http://users.UGent.be/~kwabnick>.

### Experimental methods

Whole-mount immunolocalizations in *Arabidopsis thaliana* (L.) *Heyhn* leaves were carried out as described (Friml *et al.*, 2003) and in pea (*Pisum sativum*) on 5-mm longitudinal epicotyl sections according

to the method established and described for *Arabidopsis* stems (Friml *et al.*, 2003). The anti-*Arabidopsis* PIN1 antibody also recognized a polarly localized homologous PIN protein in pea (Sauer *et al.*, 2006). The following antibodies and dilutions were used: anti-PIN1 (1:500), FITC- and CY3-conjugated anti-rabbit (1:500), or anti-mouse (1:500). For wounding experiments, pea seedlings were used 5 days after germination. Incisions to 70–80% of the stem diameter were made on epicotyls between the cotyledons and the first axillary bud. Wounded tissue was separated with plastic film. At least 20 epicotyls from two independent experiments were analyzed. After the treatments, epicotyl sections were fixed, embedded in paraffin, and processed for anti-PIN1 immunocytochemistry as described (Friml *et al.*, 2003).

Specimens were viewed under a confocal laser-scanning microscope TCS SP2 AOBS (Leica; <http://www.leica-microsystems.com>) with a  $\times 10/0.4$ ,  $\times 20/0.7$ , or  $\times 63/1.4$  objective at room temperature or with Fluoview 200 (Olympus; <http://www.olympusfluoview.com>) and a  $\times 20/0.50$  objective at room temperature. Images were acquired with the Leica confocal software 2.00 or Fluoview 5.1 software, saved as TIF files, processed with Adobe Photoshop 7.0 (<http://www.adobe.com>), and adjusted for brightness and contrast.

### Supplementary information

Supplementary information is available at the *Molecular Systems Biology* website ([www.nature.com/msb](http://www.nature.com/msb)).

## Acknowledgements

We thank Angharad Jones for critical reading of the paper, Przemyslaw Prusinkiewicz for fruitful discussions and comments, and Martine De Cock for help in preparing it. This work was supported by grants from the Research Foundation-Flanders (Odysseus) and Grant Agency of the Academy of Sciences of the Czech Republic Grant IAA601630703 to JF, the Research Foundation-Flanders (project no. 3G006507) to WG, Marie Curie European Reintegration Grant 230974 to RMHM, and Czech Ministry of Education LC06034 to JB This work was co-financed by the Netherlands Consortium for Systems Biology (NCSB), which is part of the Netherlands Genomics Initiative/Netherlands Organization for Scientific Research. JF, JK-V, KW, RMHM, WG designed the experiments; KW, JK-V, MS, JB, SN performed the experiments; KW, JK-V and JF wrote the paper.

## Conflict of interest

The authors declare that they have no conflict of interest.

## References

- Abas L, Benjamins R, Malenica N, Paciorek T, Wiśniewska J, Moulinier-Anzola JC, Sieberer T, Friml J, Luschnig C (2006) Intracellular trafficking and proteolysis of the *Arabidopsis* auxin-efflux facilitator PIN2 are involved in root gravitropism. *Nat Cell Biol* **8**: 249–256
- Bainbridge K, Guyomarç'h S, Bayer E, Swarup R, Bennett M, Mandel T, Kuhlemeier C (2008) Auxin influx carriers stabilize phyllotactic patterning. *Genes Dev* **22**: 810–823
- Balla J, Kalousek P, Reinöhl V, Friml J, Procházka S (2010) Competitive canalization of PIN-dependent auxin flow from axillary buds controls pea bud outgrowth. *Plant J* (in press)
- Bayer EM, Smith RS, Mandel T, Nakayama N, Sauer M, Prusinkiewicz P, Kuhlemeier C (2009) Integration of transport-based models for phyllotaxis and midvein formation. *Genes Dev* **23**: 373–384
- Benková E, Michniewicz M, Sauer M, Teichmann T, Seifertová D, Jürgens G, Friml J (2003) Local, efflux-dependent auxin gradients as a common module for plant organ formation. *Cell* **115**: 591–602

- Chapman EJ, Estelle M (2009) Mechanism of auxin-regulated gene expression in plants. *Annu Rev Genet* **43**: 265–285
- Darwin C, Darwin F (1880) *The Power of Movement in Plants*. London, John Murray, pp 592
- Dharmasiri N, Dharmasiri S, Estelle M (2005) The F-box protein TIR1 is an auxin receptor. *Nature* **435**: 441–445
- Dhonukshe P, Aniento F, Hwang I, Robinson DG, Mravec J, Stierhof Y-D, Friml J (2007) Clathrin-mediated constitutive endocytosis of PIN auxin efflux carriers in *Arabidopsis*. *Curr Biol* **17**: 520–527
- Dhonukshe P, Tanaka H, Goh T, Ebine K, Mähönen AP, Prasad K, Blilou I, Geldner N, Xu J, Uemura T, Chory J, Ueda T, Nakano A, Scheres B, Friml J (2008) Generation of cell polarity in plants links endocytosis, auxin distribution and cell fate decisions. *Nature* **456**: 962–966
- Dubrovsky JG, Sauer M, Napsucially-Mendivil S, Ivanchenko MG, Friml J, Shishkova S, Celenza J, Benková E (2008) Auxin acts as a local morphogenetic trigger to specify lateral root founder cells. *Proc Natl Acad Sci USA* **105**: 8790–8794
- Feugier FG, Mochizuki A, Iwasa Y (2005) Self-organization of the vascular system in plant leaves: inter-dependent dynamics of auxin flux and carrier proteins. *J Theor Biol* **236**: 366–375
- Friml J, Vieten A, Sauer M, Weijers D, Schwarz H, Hamann T, Offringa R, Jürgens G (2003) Efflux-dependent auxin gradients establish the apical–basal axis of *Arabidopsis*. *Nature* **426**: 147–153
- Friml J, Wiśniewska J, Benková E, Mendgen K, Palme K (2002) Lateral relocation of auxin efflux regulator PIN3 mediates tropism in *Arabidopsis*. *Nature* **415**: 806–809
- Geldner N, Friml J, Stierhof Y-D, Jürgens G, Palme K (2001) Auxin transport inhibitors block PIN1 cycling and vesicle trafficking. *Nature* **413**: 425–428
- Goldsmith MHM, Goldsmith TH, Martin MH (1981) Mathematical analysis of the chemosmotic polar diffusion of auxin through plant tissues. *Proc Natl Acad Sci USA* **78**: 976–980
- Heisler MG, Ohno C, Das P, Sieber P, Reddy GV, Long JA, Meyerowitz EM (2005) Patterns of auxin transport and gene expression during primordium development revealed by live imaging of the *Arabidopsis* inflorescence meristem. *Curr Biol* **15**: 1899–1911
- Ibañes M, Fàbregas N, Chory J, Caño-Delgado AI (2009) Brassinosteroid signaling and auxin transport are required to establish the periodic pattern of *Arabidopsis* shoot vascular bundles. *Proc Natl Acad Sci USA* **106**: 13630–13635
- Jönsson H, Heisler MG, Shapiro BE, Meyerowitz EM, Mjolsness E (2006) An auxin-driven polarized transport model for phyllotaxis. *Proc Natl Acad Sci USA* **103**: 1633–1638
- Kepinski S, Leyser O (2005) The *Arabidopsis* F-box protein TIR1 is an auxin receptor. *Nature* **435**: 446–451
- Kleine-Vehn J, Friml J (2008) Polar targeting and endocytic recycling in auxin-dependent plant development. *Annu Rev Cell Dev Biol* **24**: 447–473
- Kleine-Vehn J, Dhonukshe P, Sauer M, Brewer P, Wiśniewska J, Paciorek T, Benková E, Friml J (2008a) ARF GEF-dependent transcytosis and polar delivery of PIN auxin carriers in *Arabidopsis*. *Curr Biol* **18**: 526–531
- Kleine-Vehn J, Dhonukshe P, Swarup R, Bennett M, Friml J (2006) Subcellular trafficking of the *Arabidopsis* auxin influx carrier AUX1 uses a novel pathway distinct from PIN1. *Plant Cell* **18**: 3171–3181
- Kleine-Vehn J, Leitner J, Zwiewka M, Sauer M, Abas L, Luschnig C, Friml J (2008b) Differential degradation of PIN2 auxin efflux carrier by retromer-dependent vacuolar targeting. *Proc Natl Acad Sci USA* **105**: 17812–17817
- Kramer EM (2004) PIN and AUX/LAX proteins: their role in auxin accumulation. *Trends Plant Sci* **9**: 578–582
- Kramer EM (2009) Auxin-regulated cell polarity: an inside job? *Trends Plant Sci* **14**: 242–247
- Kramer EM, Frazer NL, Baskin TI (2007) Measurement of diffusion within the cell wall in living roots of *Arabidopsis thaliana*. *J Exp Bot* **58**: 3005–3015
- Leblanc N, David K, Grosclaude J, Pradier J-M, Barbier-Brygoo H, Labiau S, Perrot-Rechenmann C (1999) A novel immunological approach establishes that the auxin-binding protein, Nt-abp1, is an element involved in auxin signaling at the plasma membrane. *J Biol Chem* **274**: 28314–28320
- Merks RMH, Guravage M, Inzé D, Beemster GTS (2010) VirtualLeaf: an Open Source framework for cell-based modeling of plant tissue growth and development. *Plant Physiol* (in press)
- Merks RMH, Van de Peer Y, Inzé D, Beemster GTS (2007) Canalization without flux sensors: a traveling-wave hypothesis. *Trends Plant Sci* **12**: 384–390
- Mitchison GJ (1980) The dynamics of auxin transport. *Proc R Soc Lond B* **209**: 489–511
- Napier RM, David KM, Perrot-Rechenmann C (2002) A short history of auxin-binding proteins. *Plant Mol Biol* **49**: 339–348
- Paciorek T, Zažímalová E, Ruthardt N, Petrášek J, Stierhof Y-D, Kleine-Vehn J, Morris DA, Emans N, Jürgens G, Geldner N, Friml J (2005) Auxin inhibits endocytosis and promotes its own efflux from cells. *Nature* **435**: 1251–1256
- Peer WA, Bandyopadhyay A, Blakeslee JJ, Makam SN, Chen RJ, Masson PH, Murphy AS (2004) Variation in expression and protein localization of the PIN family of auxin efflux facilitator proteins in flavonoid mutants with altered auxin transport in *Arabidopsis thaliana*. *Plant Cell* **16**: 1898–1911
- Petrášek J, Mravec J, Bouchard R, Blakeslee JJ, Abas M, Seifertová D, Wiśniewska J, Tadele Z, Kubeš M, Ovanová M, Dhonukshe P, Skůpa P, Benková E, Perry L, Křeček P, Lee OR, Fink GR, Geisler M, Murphy AS, Luschnig C *et al* (2006) PIN proteins perform a rate-limiting function in cellular auxin efflux. *Science* **312**: 914–918
- Prusinkiewicz P, Crawford S, Smith RS, Ljung K, Bennett T, Ongaro V, Leyser O (2009) Control of bud activation by an auxin transport switch. *Proc Natl Acad Sci USA* **106**: 17431–17436
- Reinhardt D, Pesce E-R, Stieger P, Mandel T, Baltensperger K, Bennett M, Traas J, Friml J, Kuhlemeier C (2003) Regulation of phyllotaxis by polar auxin transport. *Nature* **426**: 255–260
- Robert S, Kleine-Vehn J, Barbez E, Sauer M, Paciorek T, Baster P, Vanneste S, Zhang J, Simon S, Hayashi K, Dhonukshe P, Yang Z, Bednarek SY, Jones AM, Aniento F, Zažímalová E, Friml J (2010) ABP1 mediates auxin inhibition of clathrin-dependent endocytosis in *Arabidopsis*. *Cell* **143**: 111–121
- Rolland-Lagan A-G, Prusinkiewicz P (2005) Reviewing models of auxin canalization in the context of leaf vein pattern formation in *Arabidopsis*. *Plant J* **44**: 854–865
- Sachs T (1981) The control of the patterned differentiation of vascular tissues. *Adv Bot Res* **9**: 151–262
- Sahlin P, Söderberg B, Jönsson H (2009) Regulated transport as a mechanism for pattern generation: capabilities for phyllotaxis and beyond. *J Theor Biol* **258**: 60–70
- Sauer M, Balla J, Luschnig C, Wiśniewska J, Reinöhl V, Friml J, Benková E (2006) Canalization of auxin flow by Aux/IAA-ARF-dependent feed-back regulation of PIN polarity. *Genes Dev* **20**: 2902–2911
- Scarpella E, Marcos D, Friml J, Berleth T (2006) Control of leaf vascular patterning by polar auxin transport. *Genes Dev* **20**: 1015–1027
- Smith RS, Guyomarç’h S, Mandel T, Reinhardt D, Kuhlemeier C, Prusinkiewicz P (2006) A plausible model of phyllotaxis. *Proc Natl Acad Sci USA* **103**: 1301–1306
- Steffens B, Feckler C, Palme K, Christian M, Böttger M, Lüthen H (2001) The auxin signal for protoplast swelling is perceived by extracellular ABP1. *Plant J* **27**: 591–599
- Swarup R, Kramer EM, Perry P, Knox K, Leyser HMO, Haseloff J, Beemster GTS, Bhalerao R, Bennett MJ (2005) Root gravitropism requires lateral root cap and epidermal cells for transport and response to a mobile auxin signal. *Nat Cell Biol* **7**: 1057–1065
- Thimann KV, Skoog F (1933) Studies on the growth hormone of plants. III. The inhibiting action of the growth substance on bud development. *Proc Natl Acad Sci USA* **19**: 714–716
- Tromas A, Braun N, Muller P, Khodus T, Paponov IA, Palme K, Ljung K, Lee J-Y, Benfey P, Murray JAH, Scheres B, Perrot-Rechenmann C

(2009) The AUXIN BINDING PROTEIN 1 is required for differential auxin responses mediating root growth. *PLoS One* **4**: e6648

Vieten A, Vanneste S, Wiśniewska J, Benková E, Benjamins R, Beeckman T, Luschig C, Friml J (2005) Functional redundancy of PIN proteins is accompanied by auxin-dependent cross-regulation of PIN expression. *Development* **132**: 4521–4531

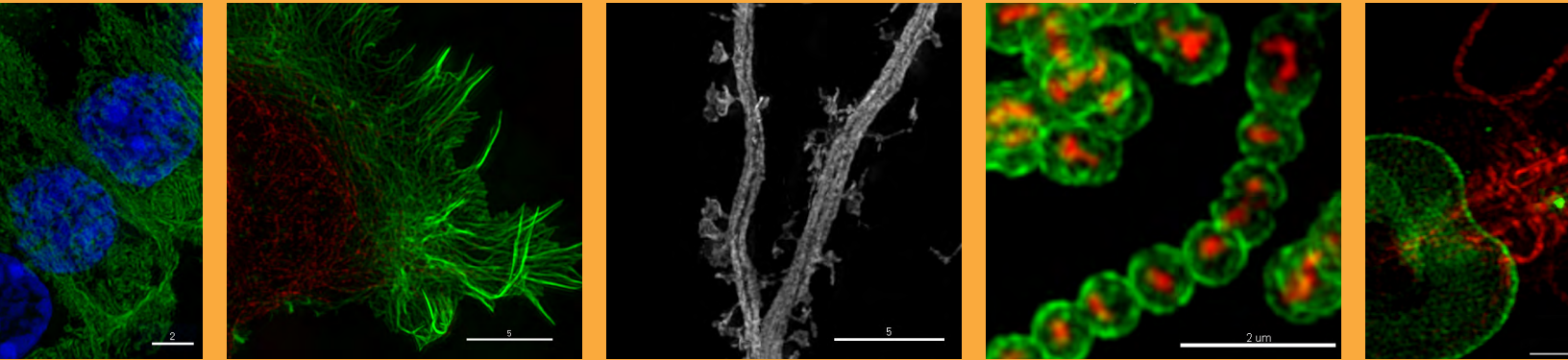
Wiśniewska J, Xu J, Seifertová D, Brewer PB, Růžička K, Blilou I, Rouquié D, Benková E, Scheres B, Friml J (2006)

Polar PIN localization directs auxin flow in plants. *Science* **312**: 883



*Molecular Systems Biology* is an open-access journal published by *European Molecular Biology Organization* and *Nature Publishing Group*. This work is licensed under a Creative Commons Attribution-Noncommercial-No Derivative Works 3.0 Unported License.

Real data.  
Real installations.  
Real super-resolution imaging.



Learn more about the DeltaVision OMX super-resolution imaging system at [www.superresolution.com](http://www.superresolution.com).

# SUPPLEMENTAL MATERIAL

## **Emergence of tissue polarization from synergy of intracellular and extracellular auxin signaling**

**Krzysztof Wabnik<sup>1,2,3,8</sup>, Jürgen Kleine-Vehn<sup>1,2,8,\*</sup>, Jozef Balla<sup>4</sup>, Michael Sauer<sup>1,2,6</sup>, Satoshi Naramoto<sup>1,2</sup>, Vilém Reinöhl<sup>4</sup>, Roeland M.H. Merks<sup>1,2,7</sup>, Willy Govaerts<sup>3</sup> and Jiří Friml<sup>1,2,5,\*</sup>**

<sup>1</sup> Department of Plant Systems Biology, VIB, 9052 Gent, Belgium, <sup>2</sup> Department of Plant Biotechnology and Genetics, Ghent University, 9052 Gent, Belgium, <sup>3</sup> Department of Applied Mathematics and Computer Science, Ghent University, 9000 Gent, Belgium, <sup>4</sup> Department of Plant Biology, Mendel University, 613 00 Brno, Czech Republic, <sup>5</sup> Department of Experimental Biology, Masaryk University, 601 77 Brno, Czech Republic

<sup>6</sup> Present address: Departamento de Genética Molecular de Plantas, Centro Nacional de Biotecnología, Consejo Superior de Investigaciones Científicas, 28049 Madrid, Spain.

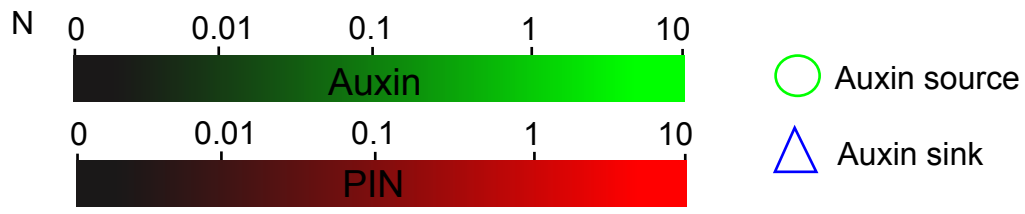
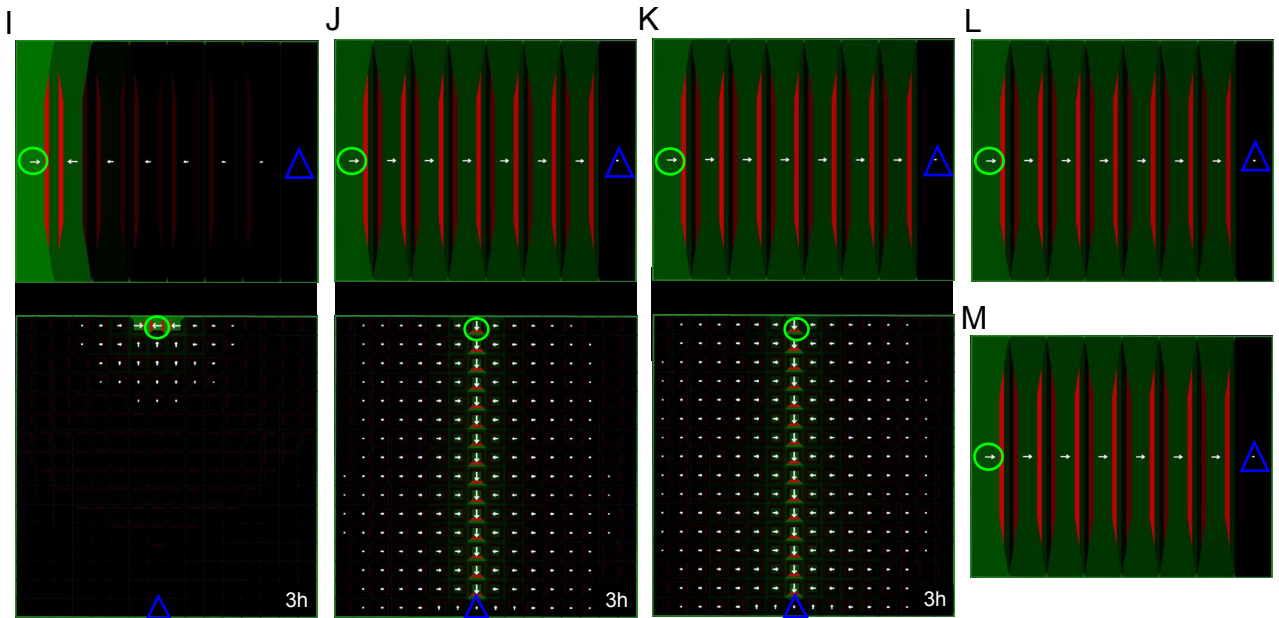
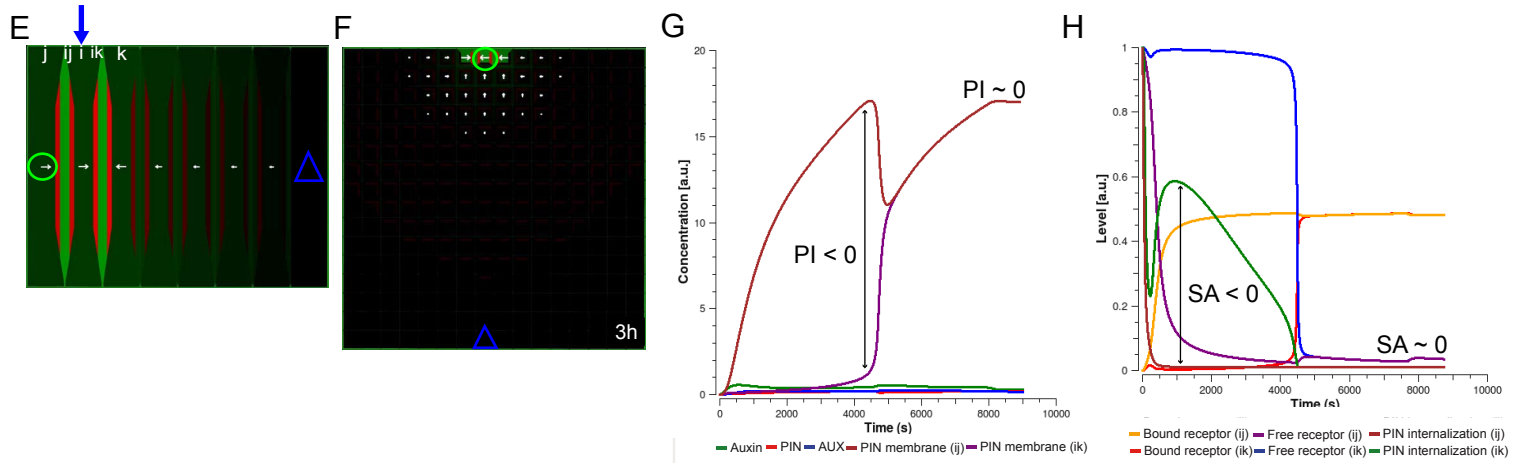
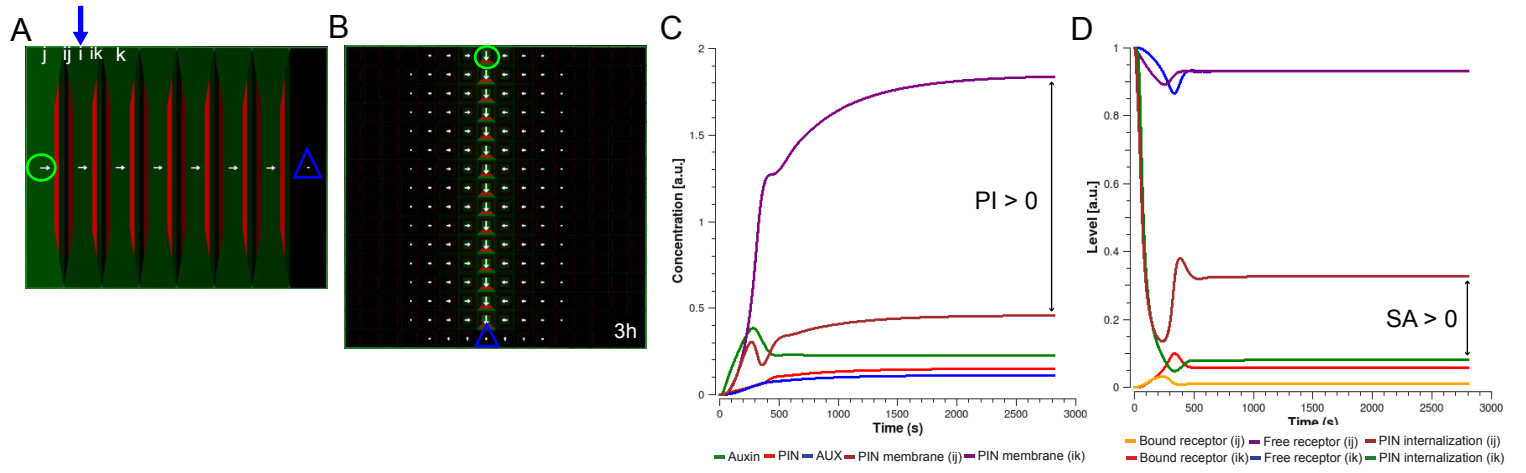
<sup>7</sup> Present address: The Netherlands Centrum Wiskunde & Informatica, 1098 XG Amsterdam, The Netherlands.

<sup>8</sup> These authors contributed equally to this work.

\* Corresponding authors. Department of Plant Systems Biology, VIB, Ghent University, Technologiepark 927, B-9052 Gent, Belgium. Tel.: +32 9 3313800; Fax: +32 9 3313809; E-mail: jiri.friml@psb.vib-ugent.be and jurgen.kleine-vehn@psb.vib-ugent.be

# TABLE OF CONTENTS

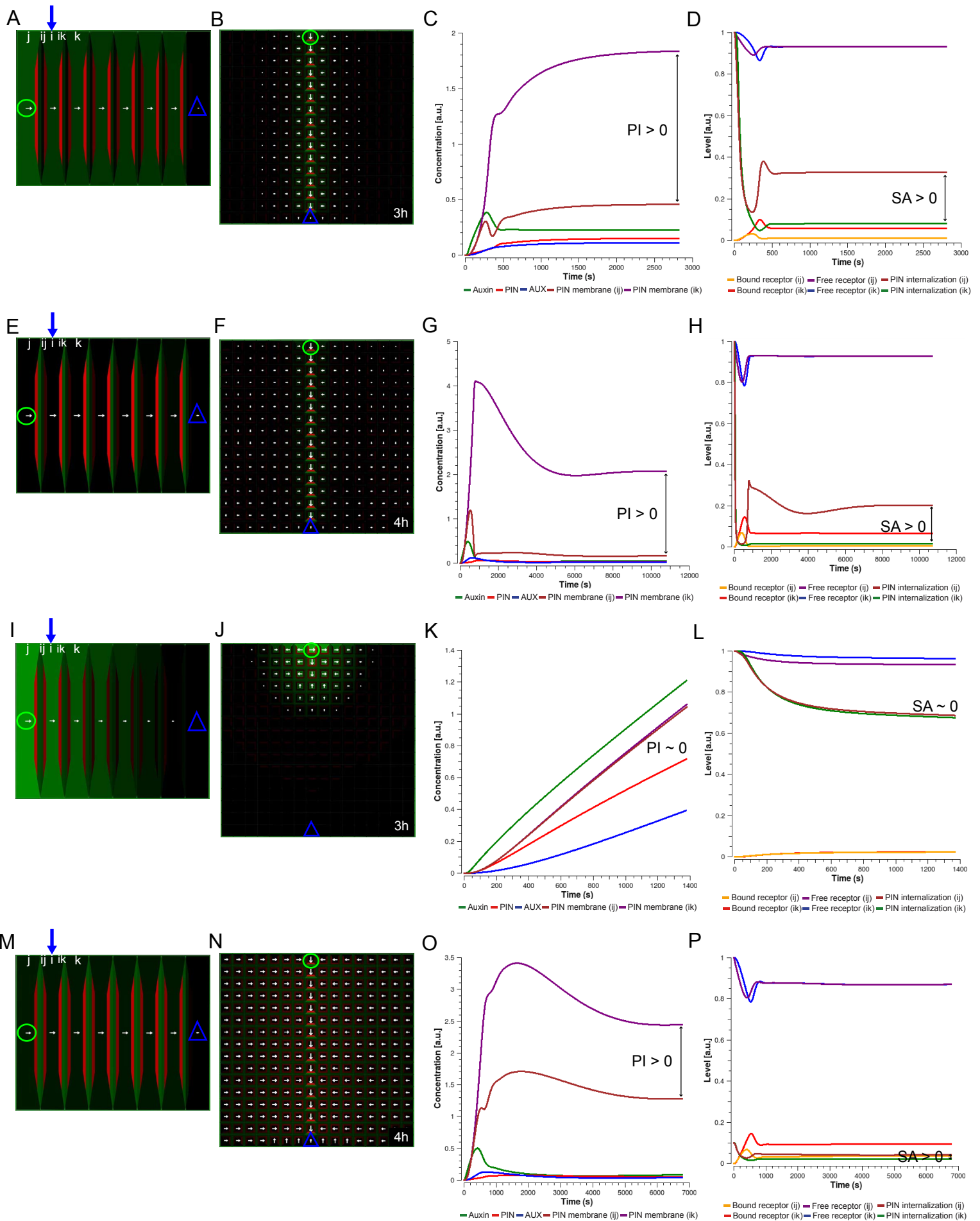
<b>Supplementary Figures .....</b>	<b>3-34</b>
1. Supplementary Figure 1 .....	3-4
2. Supplementary Figure 2 .....	5-6
3. Supplementary Figure 3 .....	7-8
4. Supplementary Figure 4 .....	9-10
5. Supplementary Figure 5 .....	11-12
6. Supplementary Figure 6 .....	13-14
7. Supplementary Figure 7 .....	15-16
8. Supplementary Figure 8 .....	17-18
9. Supplementary Figure 9.....	19-20
10. Supplementary Figure 10 .....	21-22
11. Supplementary Figure 11 .....	23-24
12. Supplementary Figure 12 .....	25-26
13. Supplementary Figure 13 .....	27-28
14. Supplementary Figure 14 .....	29-30
15. Supplementary Figure 15 .....	31-32
16. Supplementary Figure 16 .....	33-34
<b>Model .....</b>	<b>35-45</b>
<b>Supplementary Tables .....</b>	<b>46-48</b>
<b>Supplementary Movies .....</b>	<b>49-51</b>
<b>Additional references .....</b>	<b>52-53</b>
<b>Pseudo c++ code for the ERP model .....</b>	<b>54-65</b>



**Supplementary Figure 1. Model sensitivity with respect to diffusion rates of free and bound auxin receptor.**

**(A-D)** *In silico* ‘WT’ control simulation - Model simulations on the file of cells (A) and on the cellular grid (B) showed PIN polarization and canalization of auxin flow from an auxin source towards a distal auxin sink. Diffusion rate of free receptor ( $D_R$ ) was set at  $1 \mu\text{m}^2\text{s}^{-1}$  and diffusion of bound auxin receptor ( $D_C$ ) was assumed negligible ( $\sim 0$ ). **(C)** Time-course profiles of auxin concentration, intracellular PIN and AUX/LAX levels ( $PIN_i$  and  $AUX_i$ ), and PIN membrane levels ( $PIN_{ij}$  and  $PIN_{ik}$ ). **(D)** Time-course profiles of bound ( $C_{ij}$  and  $C_{ik}$ ) and free receptor ( $R_{ij}$  and  $R_{ik}$ ) levels normalized by total amount of receptors in the pool ( $R_T$ ); and corresponding PIN internalization rates ( $kh_{ij}$  and  $kh_{ik}$ ). Polarization Index (PI) and Signaling Asymmetry (SA) are given to evaluate asymmetry (see also Figure legend 2 for description). **(E-H)** Model simulations on the file of cells (E) and on the cellular grid (F) are presented for diffusion rates of bound and unbound receptor that were equivalent ( $D_R=D_C=1 \mu\text{m}^2\text{s}^{-1}$ ). In this case, neither PIN polarization towards an auxin sink nor canalization of auxin flow were observed. This model simulation predicted that neighboring cells tend to pump auxin out to the common cell wall (E, F). Initially, PI and SA were negative, suggesting that more PINs and higher auxin signaling was present at  $ij$ -th side of the cell. In time they both approach zero which is reflected in non-polar cell behavior (G, H). **(I)** Model simulations on the file of cells and on the cellular grid are presented and diffusion rates of bound and unbound receptor were  $D_R=1 \mu\text{m}^2\text{s}^{-1}$ ,  $D_C=0.1 \mu\text{m}^2\text{s}^{-1}$ , **(J)**  $D_R=1 \mu\text{m}^2\text{s}^{-1}$ ,  $D_C=0.001 \mu\text{m}^2\text{s}^{-1}$ , **(K)**  $D_R=0.1 \mu\text{m}^2\text{s}^{-1}$ ,  $D_C=0 \mu\text{m}^2\text{s}^{-1}$ , **(L)**  $D_R=10 \mu\text{m}^2\text{s}^{-1}$ ,  $D_C=0 \mu\text{m}^2\text{s}^{-1}$ , **(M)**  $D_R=100 \mu\text{m}^2\text{s}^{-1}$ ,  $D_C=0 \mu\text{m}^2\text{s}^{-1}$ .

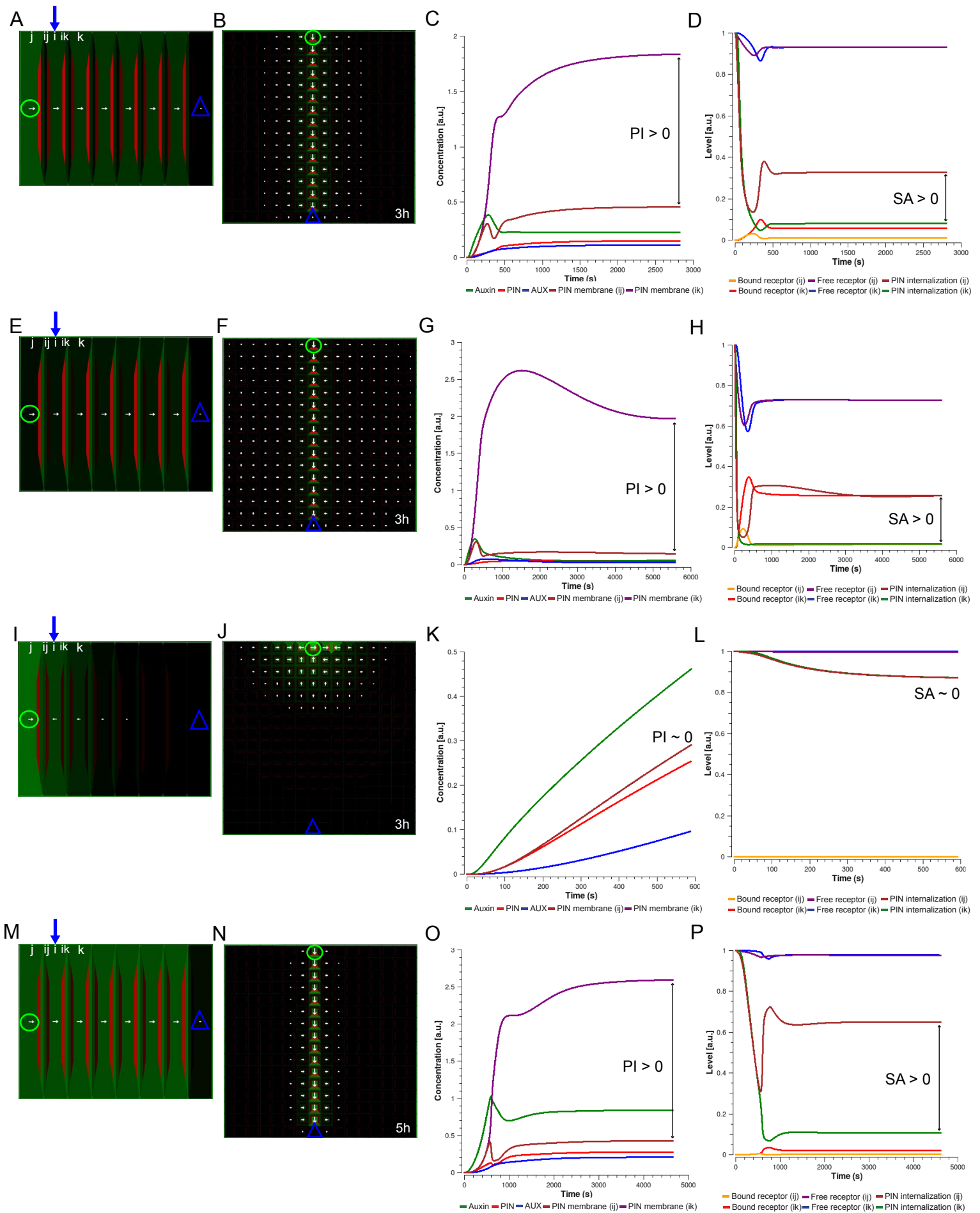
A ratio of bound/unbound receptor mobility, denoted as  $\alpha = D_C/D_R$  (equations 19-22) directly reflects the asymmetry of signaling on PIN internalization (SA). The lower this ratio is the higher SA becomes. Here, we demonstrated that our model predicts PIN polarization patterns if the diffusion rate of recruited receptors ( $D_C$ ) is assumed to be at least an order of magnitude lower than the diffusion rate of free soluble receptors ( $D_R$ ). **(N)** Color coding and symbols are as in Figure 2E and apply to all model simulations.



**Supplementary Figure 2. Model sensitivity with respect to abundance of extracellular auxin receptors.**

**(A-D)** *In silico* ‘WT’ control simulation - Model simulations on the file of cells (A) and on the cellular grid (B) showed PIN polarization and canalization of auxin flow from an auxin source towards a distal auxin sink. The amount of receptors in the intercellular pools was:  $R_T = 100$  (virtually the same as control simulation presented in Supplementary Figure 1A-D). **(E-H)** Model simulations on the file of cells (E) and on the cellular grid (F) are presented for  $R_T = 10000$ . The predicted vascular pattern by model simulation had dropped auxin concentrations (G) presumably due to high levels of extracellular auxin signaling (H), more PINs at the plasma membranes and thus more PIN-dependent auxin transport in the tissue (G). Note that steady-state values of PI and SA were slightly increased (G, H) compared to those in control simulation (C, D) **(I-L)** Model simulations on the file of cells (I) and on the cellular grid (J) are presented for  $R_T = 1$ . Here,  $R_T$  parameter was significantly reduced which was reflected in over-accumulation of auxin in the cell (K) and the high PIN internalization rates (L). Note that both PI and SA were practically 0. However, the reduction of effective rate of PIN internalization ( $\mu = 1 \text{ s}^{-1}$ ) by a 10-fold was sufficient to reestablish differential auxin signaling (increased SA) **(O, P)**, trigger PIN polarization (PI > 0) and reproduce vein pattern **(M, N)**. These findings indicate parameter  $\mu$  is limiting parameter for PIN recycling. Inset of parameter  $\mu$  allows in our model to increase or decrease PIN levels at the plasma membrane to modulate a sensitivity of feedback mechanism to the amount of extracellular receptors available in the intracellular pool.

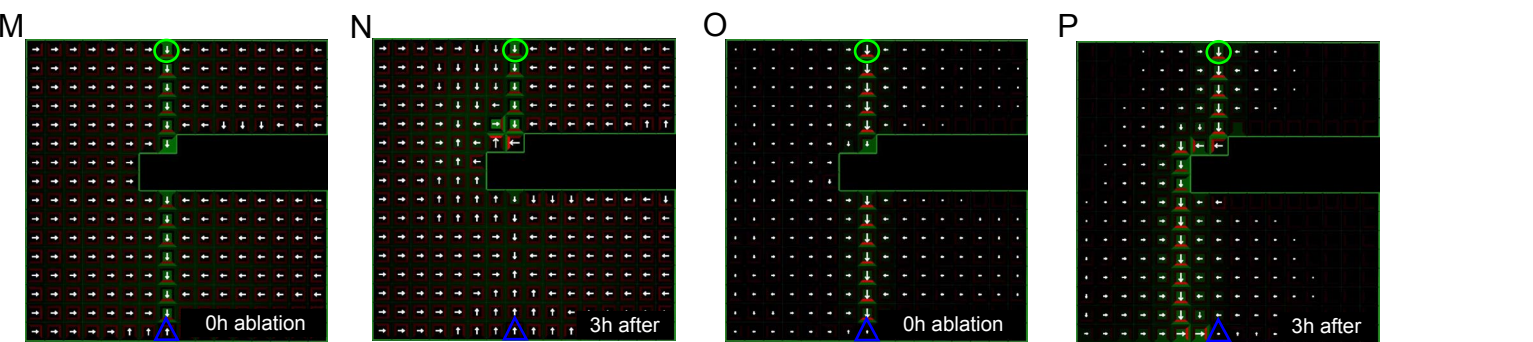
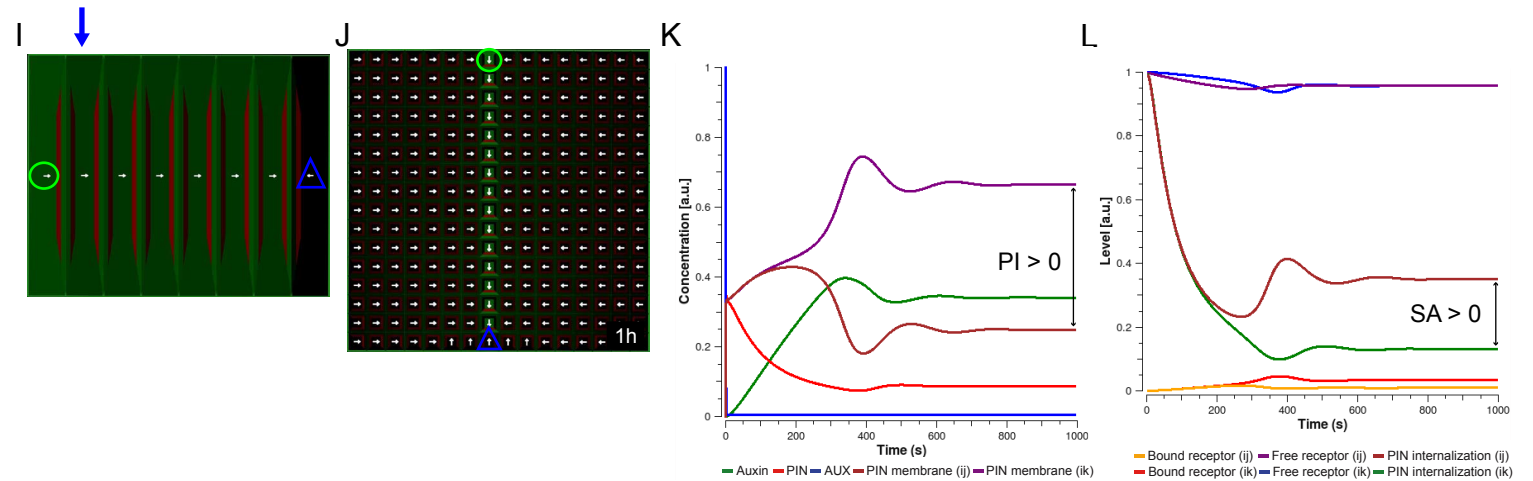
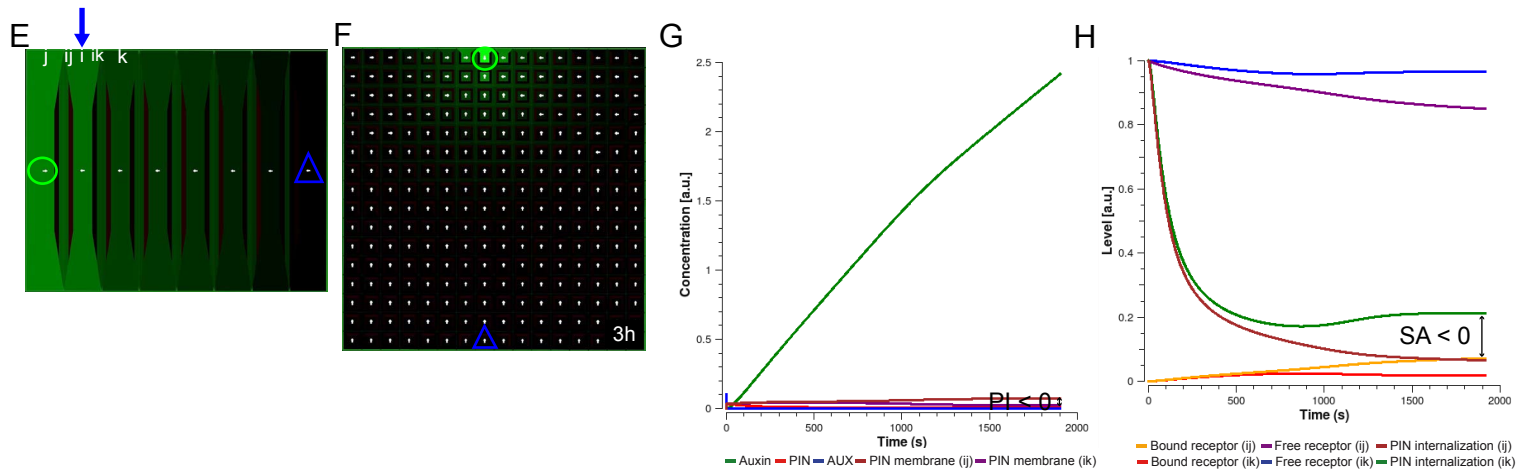
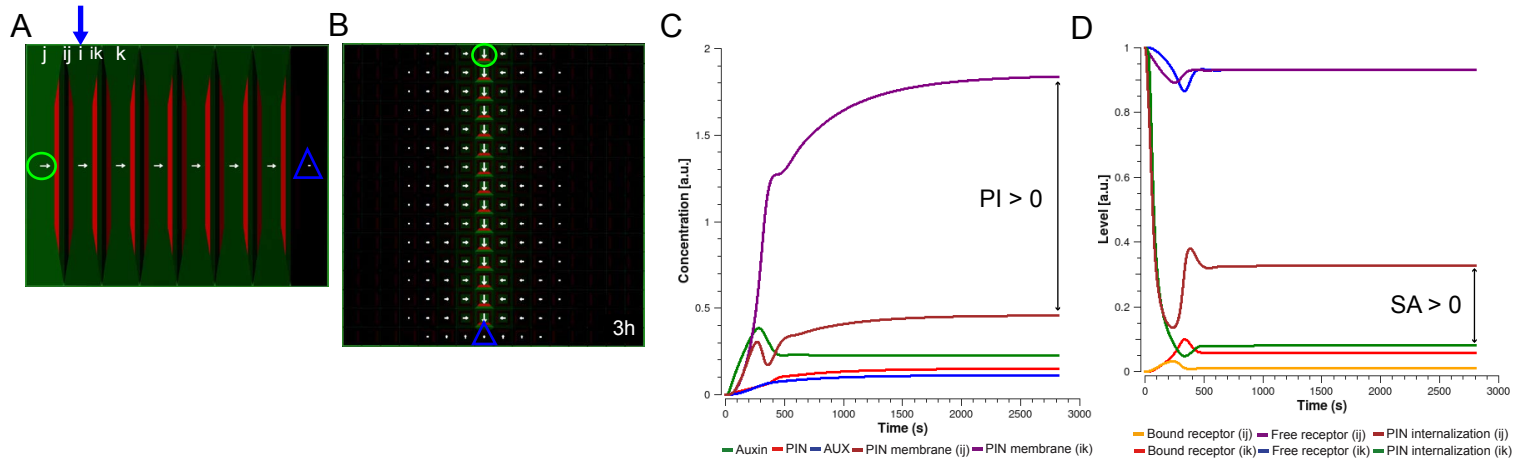
Polarization Index (PI) and Signaling Asymmetry (SA) are introduced in Figure 2. For symbols and color code, see Figures 2E and Supplementary Figure 1N.



**Supplementary Figure 3. Model sensitivity with respect to extracellular receptor recycling.**

**(A-D)** *In silico* ‘WT’ control simulation - Model simulations on the file of cells (A) and on the cellular grid (B) reproduced PIN polarization and canalization of auxin flow from an auxin source towards a distal auxin sink. The dissociation constant of extracellular receptor (represented by the ratio between forward and backward rates of receptor cycling, equation 14) was:  $K_D = 1 \mu\text{M}$  (virtually the same as control simulation presented in Supplementary Figure 1A-D). **(E-H)** Model simulations on the file of cells (E) and on the cellular grid (F) are presented for  $K_D = 0.1 \mu\text{M}$ . This model simulation predicted the vascular pattern with lower auxin concentrations in the channel due to appearance of more PINs at the plasma membrane and higher auxin transport in the cells (G). However, the appearance of low auxin concentrations in this model simulation resulted in saturated auxin signaling (higher SA (H) compared to control simulation (D)). Also a strong PIN polarity was observed (increased PI) (G). **(I-L)** Model simulations on the file of cells (I) and on the cellular grid (J) are presented for  $K_D = 10 \mu\text{M}$ . Due to low affinity rate (high  $K_D$ ) receptor-based auxin signaling was partially blocked (SA  $\sim 0$ ) (L) and no PIN polarization (PI  $\sim 0$ ) was predicted by the model (K). Interestingly, a 10-fold decrease of diffusion of auxin in the apoplast **(M-P)** resulted in increased SA (P) and strong PIN polarization (increased PI) yet enough to canalise auxin flow (M, N). Notably, the time point at the initiation of PIN polarization (for PI  $> 0$ ) was delayed ( $\sim 500\text{s}$ , O, P) compared to that in the control simulation ( $\sim 250\text{s}$ , C, D). This finding implicates that auxin binding to extracellular receptor should occur fast ( $K_D < 10 \mu\text{M}$ ) to balance the effect of free auxin diffusion in the cell wall. Interestingly, the putative auxin binding protein (ABP1) - a candidate for extracellular auxin receptor, has high affinity and specificity to auxin ( $K_D$  ranges from  $0.05 \mu\text{M}$  to  $5 \mu\text{M}$ ) for pH of 5.5 [17].

Polarization Index (PI) and Signaling Asymmetry (SA) are introduced in Figure 2. For symbols and color code, see Figures 2E and Supplementary Figure 1N.



**Supplementary Figure 4. The role of auxin-dependent carrier expression in vascular patterning and tissue regeneration.**

**(A-D)** *In silico* ‘WT’ control simulation - Model simulations on the file of cells (A) and on the cellular grid (B) predicted PIN polarization and canalization of auxin flow from an auxin source towards a distal auxin sink. The auxin-dependent carrier expression rates were:  $\alpha_{PIN}=0.1$ ,  $\alpha_{AUX}=0.1$ , and carrier degradation terms:  $\delta_{PIN}=0.003$ ,  $\delta_{AUX}=0.003$  (equations 5-7, virtually the same as control simulation presented in Supplementary Figure 1A-D). **(E-H)** Simulations on the file of cells (E) and on the cellular grid (F) are presented for the model conditions that do not include auxin-induced carrier expression. Initially, the fixed pool of auxin carriers was assigned to each cell and set at 0.1 a.u. (arbitrary units). Under this condition, auxin canalization could not be reproduced by the ERP model simulations (E, F). The observed values of PI and SA were negative which resulted in the adverse PIN polarization (towards auxin source) in our model simulations (G, H). **(I-L)** Model simulations on the file of cells (I) and on the cellular grid (J) are presented. The amount of auxin carriers in the pool was set at 1 (K, L). The positive values of both PI and SA were associated with PIN polarization from and an auxin source (I, J). Although, the steady-state patterns of PIN polarization were obtained after approx. 16 min (K, L) which was faster than in control simulation (~50 min) (C, D). This results clearly indicate that PIN proteins are important components of the model and thus the sufficient level of PINs ( $\geq 1$  a.u.) has to be associated with each cell when carrier expression is turned off. **(M-P)** Simulations of tissue regeneration on the regular cellular grid. (M, N) Fixed pool of carriers in each cell was set at 1 a.u. and no regeneration of vascular pattern was observed (N). (O, P) ‘WT’ control simulation – model with auxin-induced carrier expression and fixed carrier degradation predicts dynamic re-polarization of cells in direct surrounding of ablated region, down regulation of PINs below the wound and consequently vein regeneration (P).

These results of the model simulations suggest that both PIN degradation and a dynamic regulation of PIN expression by auxin are necessary to narrow down PIN expression domains below the ablated region, and subsequent for *de novo* polarization of PINs (P).

Polarization Index (PI) and Signaling Asymmetry (SA) are introduced in Figure 2. For symbols and color code, see Figures 2E and Supplementary Figure 1N.

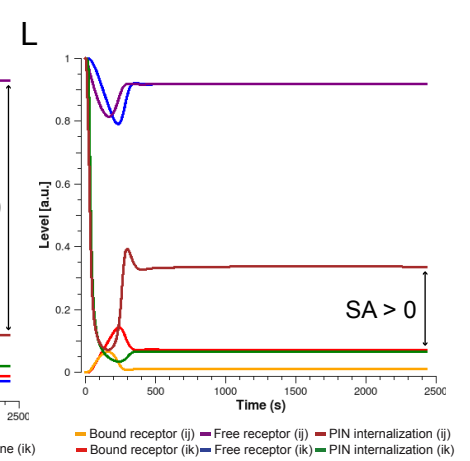
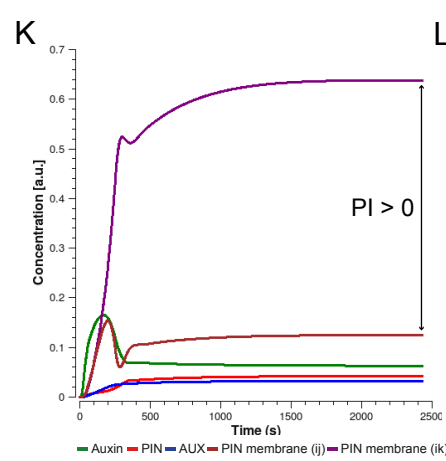
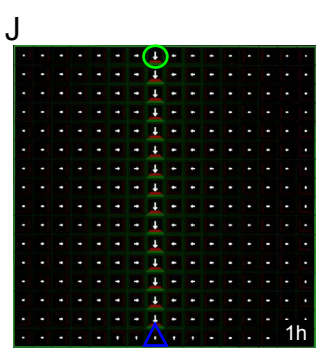
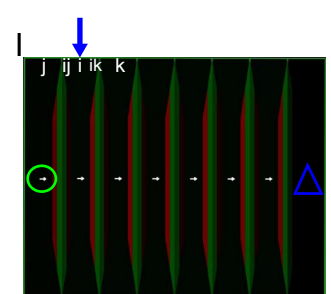
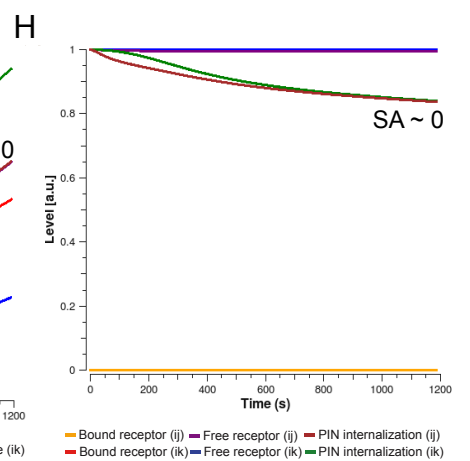
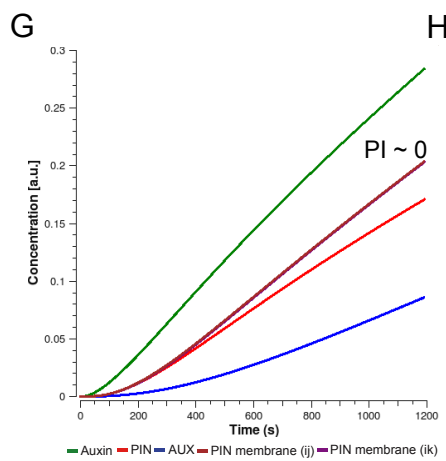
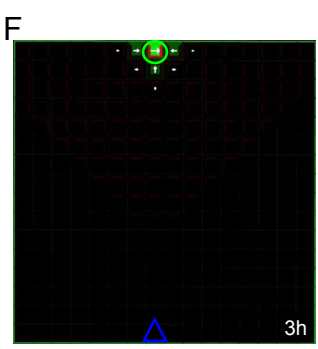
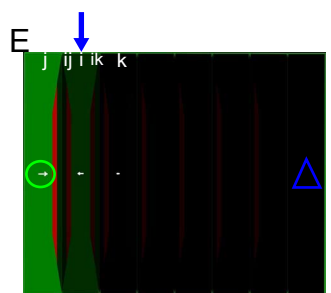
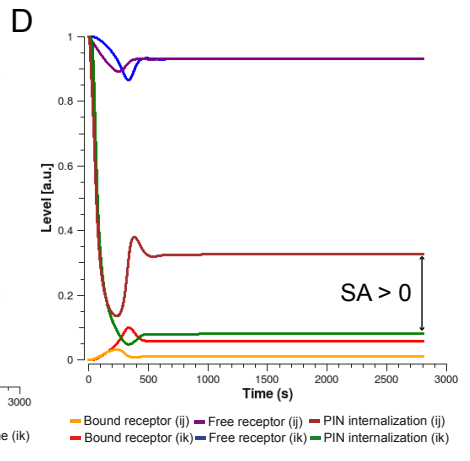
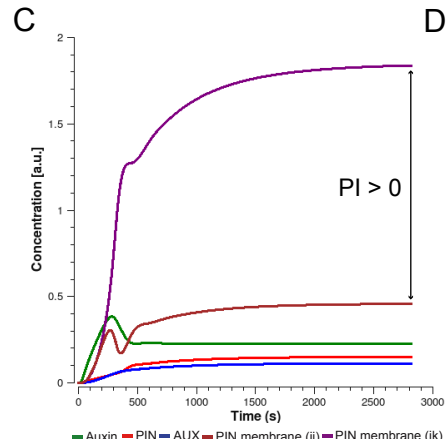
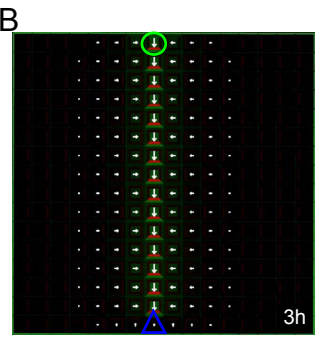
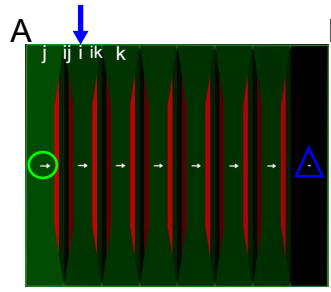


**Supplementary Figure 5. Auxin-dependent versus auxin-independent carrier expression in vascular patterning and tissue regeneration.**

**(A-D)** *In silico* ‘WT’ control simulation - Model simulations on the file of cells (A) and on the cellular grid (B) predicted PIN polarization and canalization of auxin flow from an auxin source towards a distal auxin sink. The auxin-dependent carrier expression rates were:  $\alpha_{PIN}=0.1$ ,  $\alpha_{AUX}=0.1$ , and carrier degradation terms:  $\delta_{PIN}=0.003$ ,  $\delta_{AUX}=0.003$  (equations 5-7, virtually the same as control simulation presented in Supplementary Figure 1A-D). **(E-H)** Model simulations on the file of cells (E) and on the cellular grid (F) are presented for the model with an auxin-independent carrier expression. The rates of fixed carrier expression were:  $\alpha_{PIN}=0.01$ ,  $\alpha_{AUX}=0.01$ , and carrier degradation terms:  $\delta_{PIN}=0.003$ ,  $\delta_{AUX}=0.003$ . The ERP model predicted the canalization of auxin flow and basal PIN polarization in pro-vascular cells (E, F). Note that PI and SA were slightly increased (G, H) compared to those in control simulation (C, D) presumably due to higher PIN signal at the plasma membrane of each cell. Notably, this model simulation predicted the adverse PIN polarization in the cells that surrounded pro-vascular channel, and only broad, uniform and strong PIN expression was observed in the whole tissue (F). **(I-J)** Simulations on the file of cells and on the cellular grid for the ERP model with auxin-dependent carrier expression rates that were:  $\alpha_{PIN}=1$ ,  $\alpha_{AUX}=1$  (I) and  $\alpha_{PIN}=0.01$ ,  $\alpha_{AUX}=0.01$  (J). **(K-L)** Model simulations on the file of cells and on the cellular grid with fixed carrier expression rates:  $\alpha_{PIN}=0.1$ ,  $\alpha_{AUX}=0.1$  (K) and  $\alpha_{PIN}=0.001$ ,  $\alpha_{AUX}=0.001$  (L) are presented. Note that low levels of carrier expression in the model resulted in patterning defects (L). **(M-P)** ‘WT’ control simulation – the model with an auxin-induced carrier expression allows for dynamic repolarization of cells in direct surrounding of ablated region, down regulation of PINs below the wound and consequently vein regeneration (M, N). The model with fixed carrier expression ( $\alpha_{PIN}=0.01$ ,  $\alpha_{AUX}=0.01$ ) was not able to reproduce PIN polarization during vein regeneration (O, P).

In agreement with results presented in Supplementary Figure 4, these model simulations demonstrated the importance of auxin-dependent regulation of PIN expression for generating realistic, narrowed and flexible PIN polarization patterns during auxin canalization and vascular regeneration.

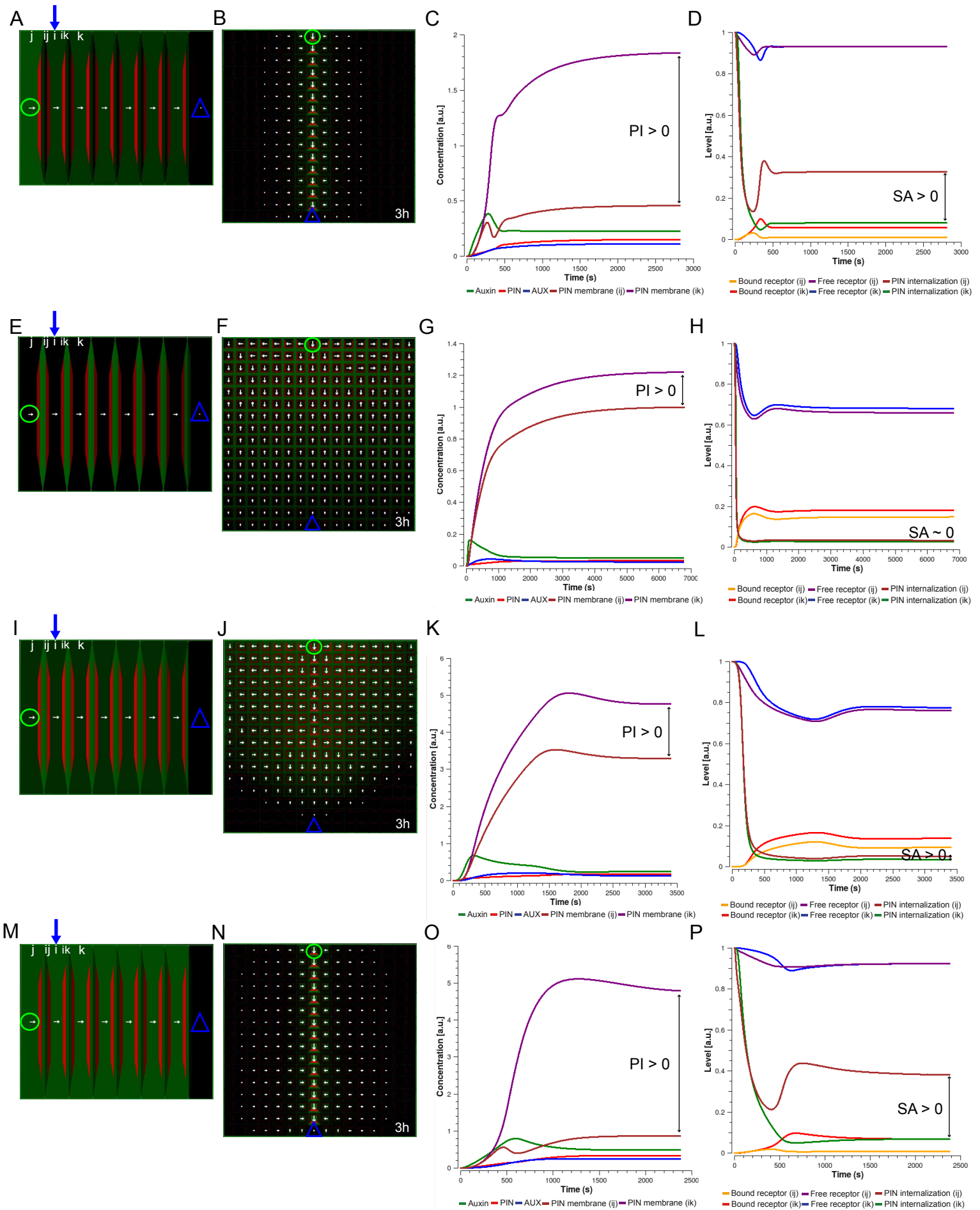
Polarization Index (PI) and Signaling Asymmetry (SA) are introduced in Figure 2. For symbols and color code, see Figures 2E and Supplementary Figure 1N.



**Supplementary Figure 6. Model robustness with respect to the efficiency of PIN-dependent auxin transport.**

(A-D) ‘WT’ control simulation - Model simulations on the file of cells (A) and on the cellular grid (B) showed PIN polarization and canalization of auxin flow from an auxin source towards a distal auxin sink. The permeability of PIN-dependent transport ( $p_{PIN}$ ) was set at  $30 \mu\text{ms}^{-1}$  (virtually the same as control simulation presented in Supplementary Figure 1A-D). (E-H) Model simulations on the file of cells (E) and on the cellular grid (F) are presented for parameter  $p_{PIN}=1 \mu\text{ms}^{-1}$  which mimic *pin* mutants (practically the lack of PIN-dependent transport). In this simulation, the canalization of auxin flow did not occur (E, F). Moreover, model predicted accumulation of auxin in the tracked cell (G) which resulted in the lack of PIN polarization ( $PI \sim 0$ ) (G) and no visible asymmetry in extracellular auxin signaling ( $SA \sim 0$ ) (H). (I-L). Model simulations on the file of cells (I) and on the cellular grid (J) are presented for parameter  $p_{PIN}=300$ . In this case the capacity of PIN-dependent auxin transport ( $p_{PIN}$ ) was set a 10-fold higher than that in control simulation (A-D). No qualitative change of model behavior was observed (K, L) compared to control simulation (C, D). Additionally, auxin concentrations were lower in the channel (I, J) than those reported in the control simulation (A, B). These model simulations suggest that the capacity of PIN-dependent auxin transport ( $p_{PIN}$ ) is crucial parameter for the model to reproduce venation patterning and its inset should be higher than the weak “background” permeability of  $1 \mu\text{ms}^{-1}$  (E, H).

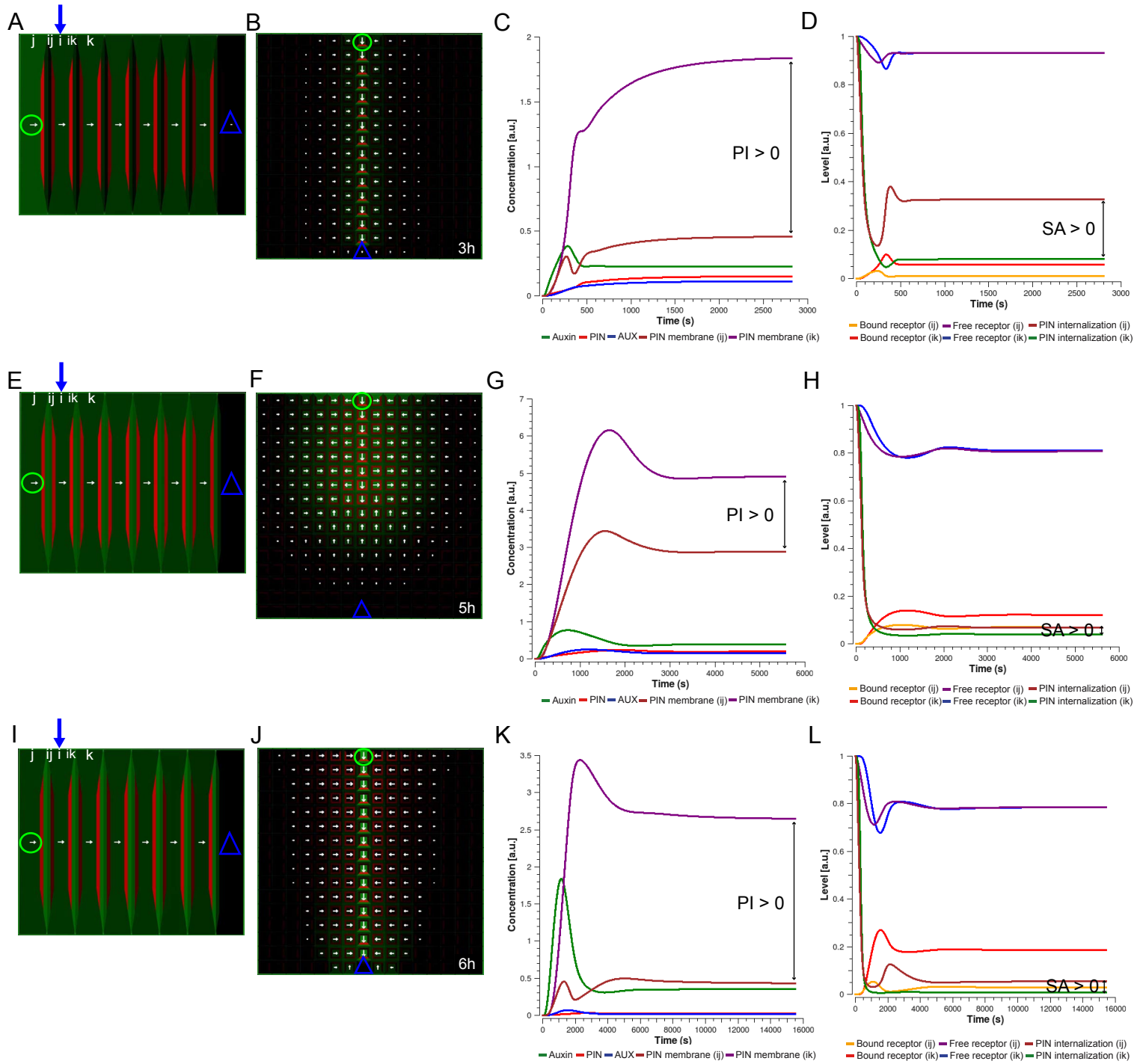
Polarization Index (PI) and Signaling Asymmetry (SA) are introduced in Figure 2. For symbols and color code, see Figures 2E and Supplementary Figure 1N.



**Supplementary Figure 7. Model sensitivity with respect to the efficiency of AUX/LAX-dependent auxin transport.**

(A-D) ‘WT’ control simulation - Model simulations on the file of cells (A) and on the cellular grid (B) showed PIN polarization and canalization of auxin flow from an auxin source towards a distal auxin sink. The permeability of AUX/LAX-dependent transport ( $p_{AUX}$ ) was set at  $30 \mu\text{ms}^{-1}$  (virtually the same as control simulation presented in Supplementary Figure 1A-D). (e-h) Model simulations on the file of cells (E) and on the cellular grid (F) are reported for parameter  $p_{AUX}=1 \mu\text{ms}^{-1}$ . Here, the canalization of auxin flow was not predicted by model simulations as well as strong basal PIN polarization in pro-vascular cells and lateral polarization of surrounding tissues (E, F). A very weak difference in PIN levels between  $ik$ -th and  $ij$ -th plasma membranes was established (small PI) (G). However, this weak PIN polarization did not get enhanced and maintained presumably due to a shallow difference in extracellular auxin signaling across the cell wall ( $SA \sim 0$ ) (H). (I-L) Model simulations on the file of cells (I) and on the cellular grid (J) are presented for parameter  $p_{AUX}$  set at  $1 \mu\text{ms}^{-1}$  and for a 10-fold higher inset of  $p_{IAAH}$ . Note that *in silico* AUX/LAX phenotype (E-H) was virtually rescued as predicted by model simulation (I, J). Nevertheless, the basal PIN polarization in the pro-vascular cells was not maintained (small PI) and thus an auxin source did not connect to a distal auxin sink (J). Interestingly, this model simulation predicted no delay in the initiation of PIN polarization (K, L) compared to control simulation (C, D). This suggests that a diffusion-based auxin influx into cell ( $p_{IAAH}$ ) tends to delay, but does not balance the auxin efflux from cell (K). Consequently, auxin was trapped in the extracellular space in high concentrations and thus no significant asymmetry in extracellular auxin signaling was generated ( $SA \sim 0$ ) (L). Our model simulations indicate that the contribution of AUX/LAX carriers to the dynamic drainage of auxin from the apoplast is central to the maintenance of basal PIN polarization in the pro-vascular cells and lateral PIN polarization of surrounding tissues (A, B). (M-P) Model simulations on the file of cells (M) and on the cellular grid (N) are presented for parameter  $p_{AUX}=300 \mu\text{ms}^{-1}$ . The capacity of AUX/LAX-dependent auxin transport was a 10-fold higher than that in control simulation (A-D). Model predicted that auxin efflux from the cell is balanced by active AUX/LAX influx resulting in increased PI (O) and increased SA (P).

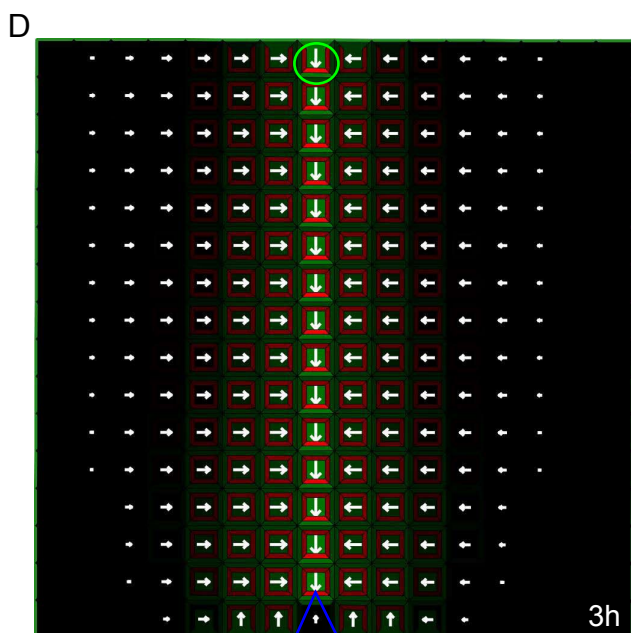
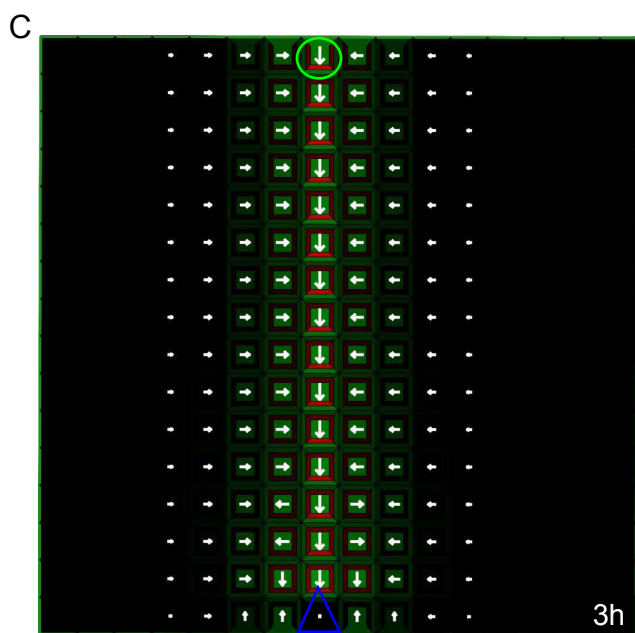
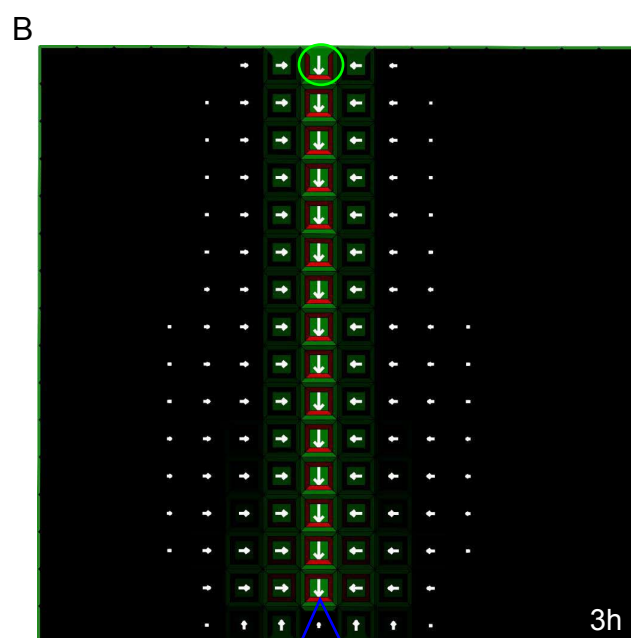
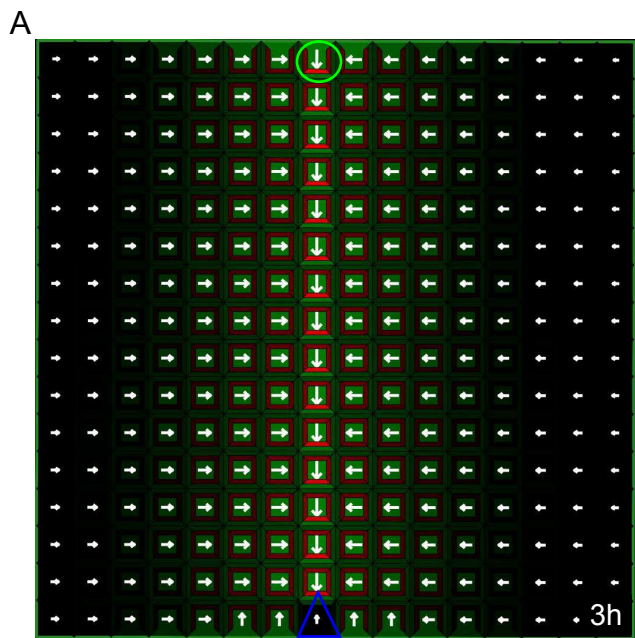
Polarization Index (PI) and Signaling Asymmetry (SA) are introduced in Figure 2. For symbols and color code, see Figures 2E and Supplementary Figure 1N.



**Supplementary Figure 8. Model sensitivity with respect to the speed of polar auxin transport.**

(A-D) ‘WT’ control simulation - Model simulations on the file of cells (A) and on the cellular grid (B) showed PIN polarization and canalization of auxin flow from an auxin source towards a distal auxin sink. The saturation of polar auxin transport ( $k_t$ ) was set at 1  $\mu\text{M}$  (virtually the same as control simulations presented in Supplementary Figure 1A-D). (E-H) Model simulations on the file of cells (E) and on the cellular grid (F) are presented for parameter  $k_t=10 \mu\text{M}$ . The initiation of PIN polarization was observed ( $\text{PI} > 0$ ) (G), however, no significant difference in extracellular auxin signaling was reported (low SA) (H). The model simulations predicted a transient basal PIN polarization in pro-vascular cells and no lateral polarization of surrounding tissues (E, F). In this case the low capacity of polar auxin transport provided no means to counteract apoplastic auxin diffusion and consequently, PIN polarization associated with the positive value of PI could not be sufficiently maintained (G, H). (I-L) Model simulations on the file of cells (I) and on the cellular grid (J) are presented for parameter  $k_t=10 \mu\text{M}$ , and a 10-fold decrease of auxin diffusion in the apoplast ( $D_a$ ) compared to that used in control simulations ( $D_a = 100 \mu\text{m}^2\text{s}^{-1}$ ). (I, J) Model predicted virtual rescue of *in silico* phenotype (E-H). Notably, the simulation demonstrated a transient maximum of PI associated with PIN polarization that was a 10-fold stronger (K) than that observed in control simulation (C). Similarly, this reduction in apoplastic diffusion ( $D_a$ ) in our model resulted in an increase of SA (L). This indicates that the speed of carrier-dependent auxin transport system has to be comparable or faster than passive movement of auxin within the cell wall.

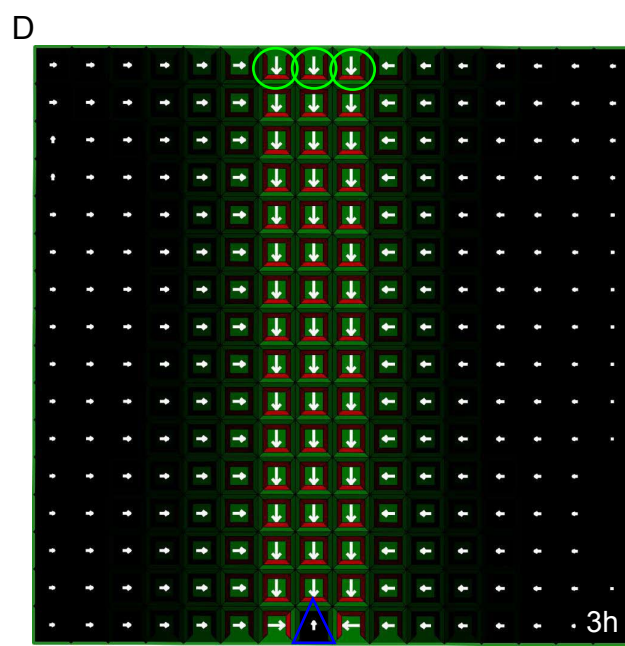
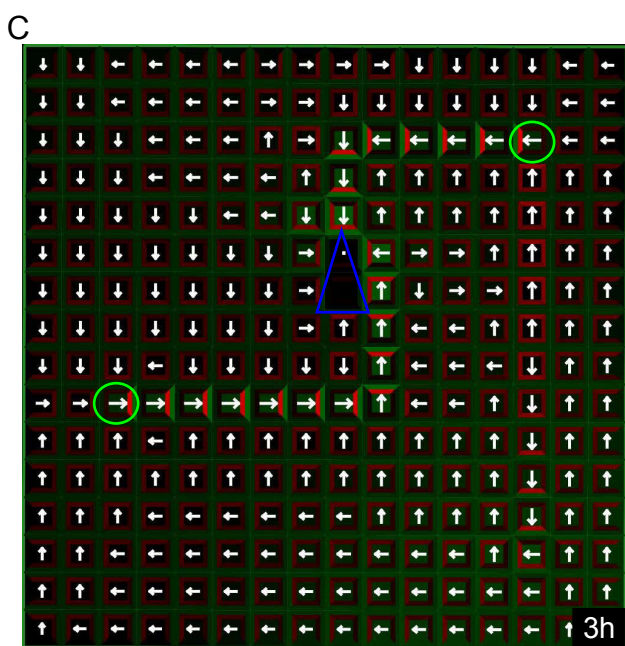
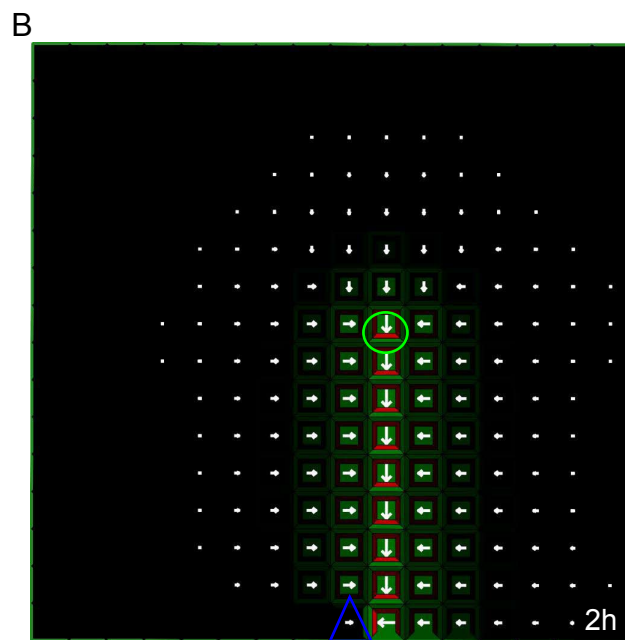
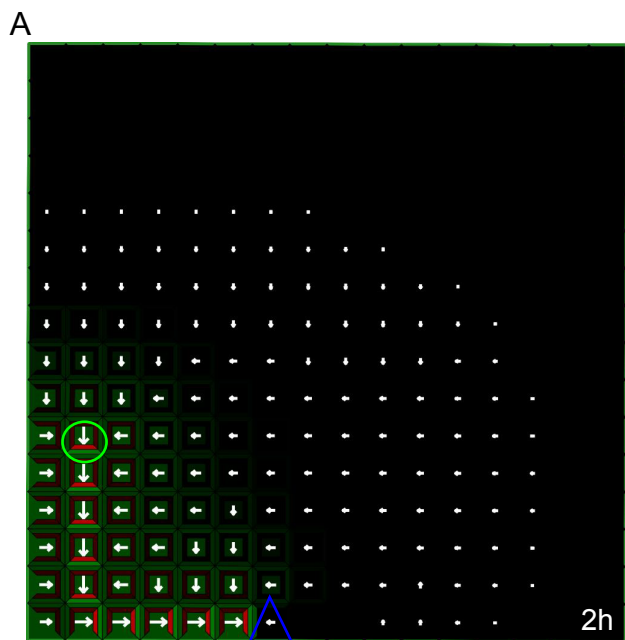
Polarization Index (PI) and Signaling Asymmetry (SA) are introduced in Figure 2. For symbols and color code, see Figures 2E and Supplementary Figure 1N.



**Supplementary Figure 9. Model robustness with respect to diffusion and permeability rates.**

**(A)** PIN polarity and auxin distribution patterns for a 5-fold increase of apoplastic auxin diffusion ( $D_a$ ) that was originally set at  $100 \mu\text{m}^2\text{s}^{-1}$ . **(B)** A sharp auxin distribution pattern was observed in the model simulation with a 5-fold decrease of  $D_a$ . The ERP model with the values of apoplastic auxin diffusion from range of  $10 \mu\text{m}^2\text{s}^{-1}$  up to  $500 \mu\text{m}^2\text{s}^{-1}$  which covers the variety of measurement of apoplastic auxin diffusion in plants [11]-[13]. **(C)** A 5-fold increase in the total membrane permeability values ( $p_{PIN}$  and  $p_{AUX}$ ) had no visible impact on PIN polarization and the canalization of auxin flow. **(D)** Cell polarity and auxin distribution patterns in model simulation with a 5-fold decrease in the total permeability values:  $p_{PIN}=p_{AUX}=6 \mu\text{ms}^{-1}$ .

For symbols and color code, see Figures 2E and Supplementary Figure 1N.

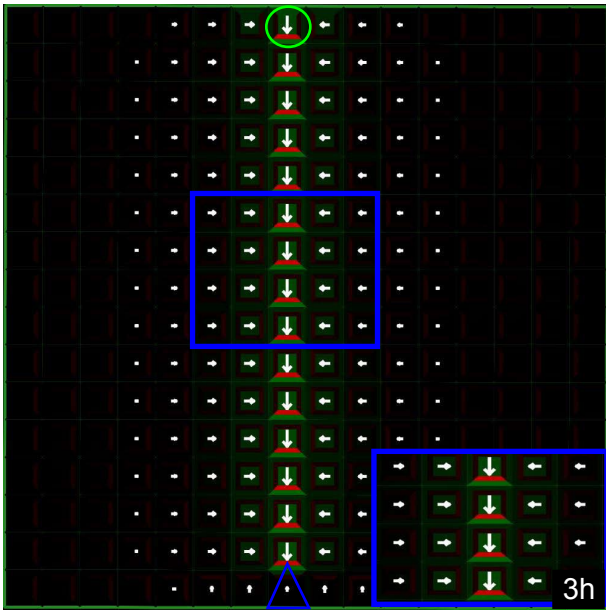


**Supplementary Figure 10. Model sensitivity with respect to altered boundary conditions.**

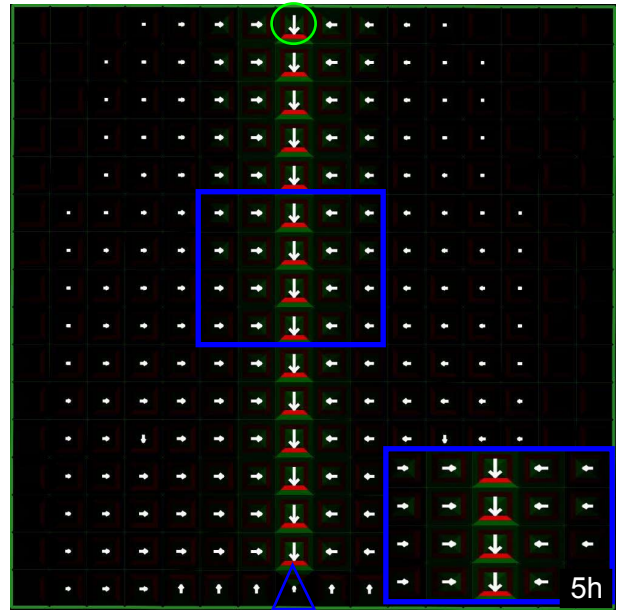
**(A)** Model simulation of auxin canalization on regular grid with an auxin source that was placed against the boundary. The strength of auxin source was set at  $0.001 \mu\text{M} \mu\text{m}^{-2} \text{s}^{-1}$ . Auxin canalization was observed in this ERP model simulation (A). Interestingly, the predicted auxin channel was not stringent to tissue boundary compared with the observations from predictions of classical canalization models suggesting that the ERP model faithfully and robustly reproduces auxin canalization patterns. **(B)** Auxin canalization on the regular grid predicted by the ERP mechanism with randomly chosen spot of the auxin biosynthesis. **(C)** The ERP model provides the robust sink finder mechanism for auxin canalization. An auxin sink was set at the random position on the cellular grid and two, equivalent in strength auxin sources ( $0.001 \mu\text{M} \mu\text{m}^{-2} \text{s}^{-1}$ ) were introduced at the same time on the grid tissue layout. The shortest path from each auxin source to an auxin sink was robustly found in the ERP model simulation (C). **(D)** The widening of auxin channel in the ERP model simulation. The single-cell auxin source located in the center of the top cell layer of a grid tissue layout was extended to the two adjacent cells which resulted in the formation of broad auxin channel (D).

For symbols and color code, see Figures 2E and Supplementary Figure 1N.

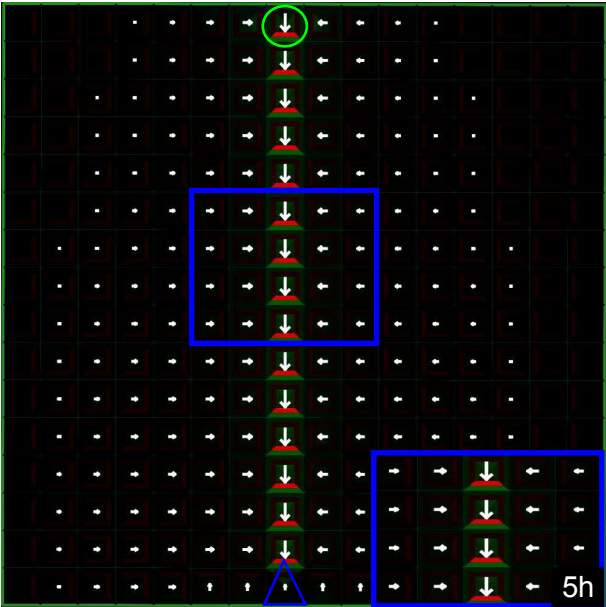
A



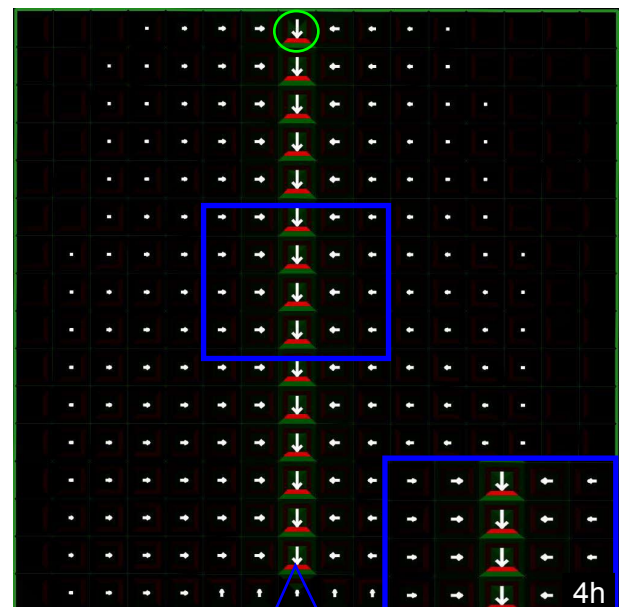
B



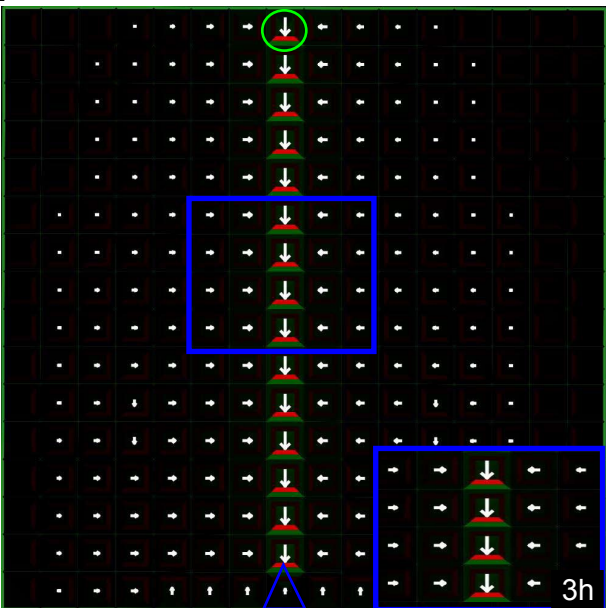
C



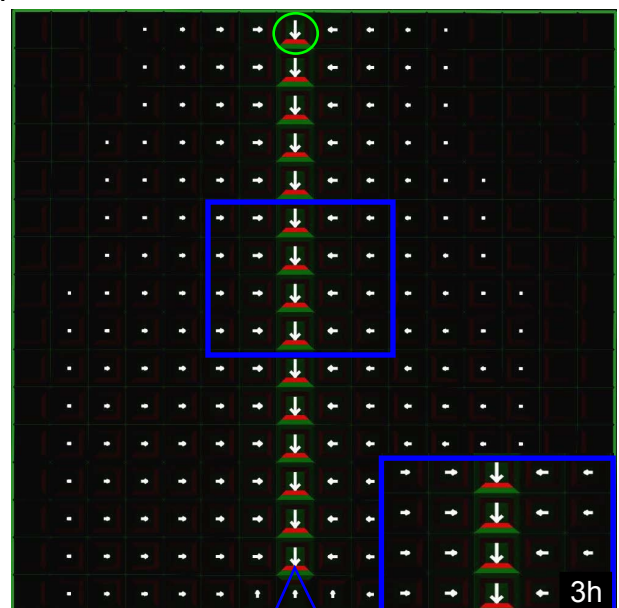
D



E



F



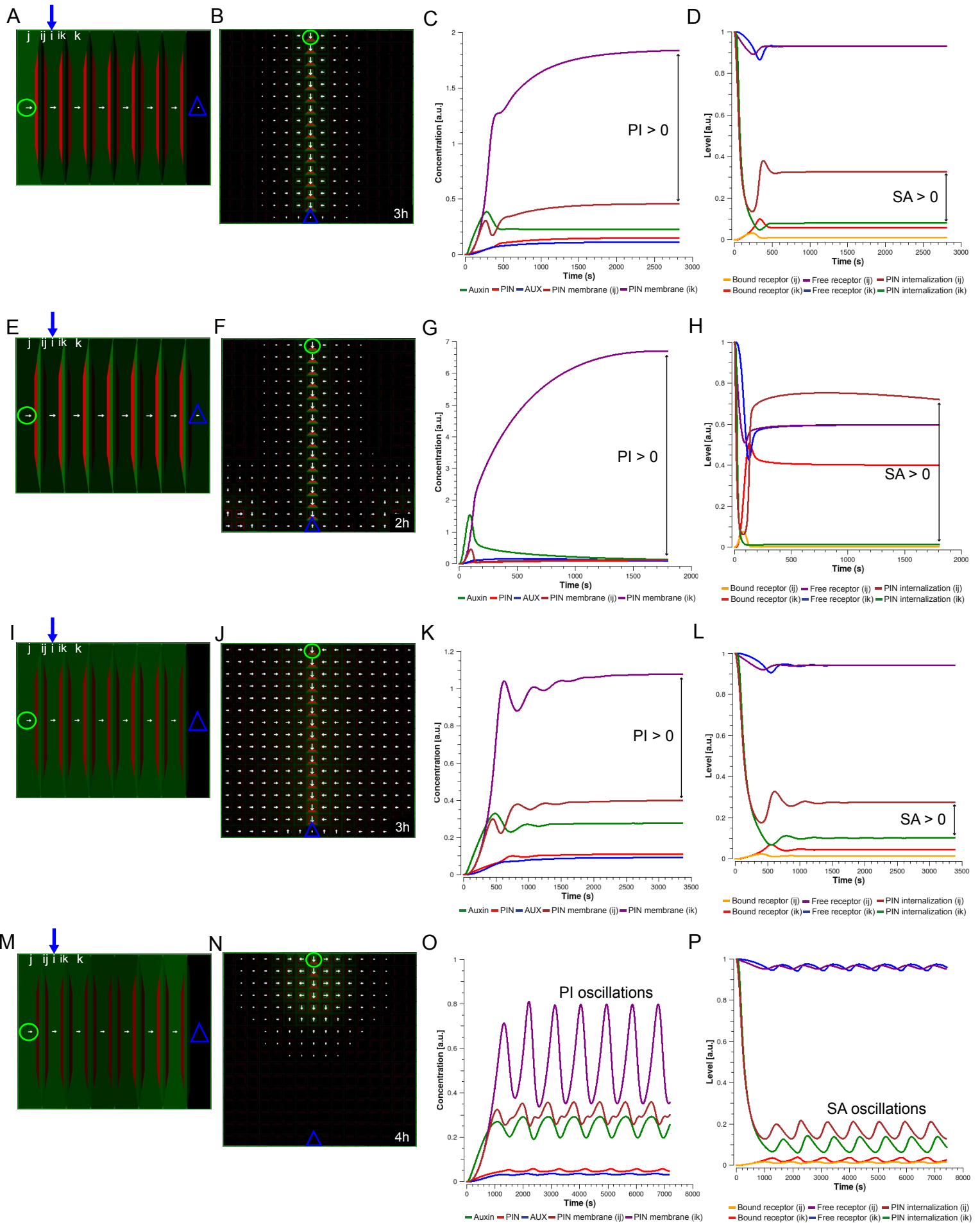
**Supplementary Figure 11. The ERP model with intracellular auxin diffusion.**

(A) Model simulations on the file of cells (A) and on the cellular grid (B) showed PIN polarization and canalization of auxin flow from an auxin source towards a distal auxin sink. Each cell is represented by a rectangular square with the mean auxin concentration in the cytoplasm (A) (the model inset was the same as simulation presented in Figure 3A and 3B). (B) The square box representing one cell was divided in four identical intracellular compartments and each component associated with the one side of the cell and the cell center. Here our model additionally integrated an intracellular auxin diffusion between these intracellular compartments that was described by Fick's law:

$$J_{1 \rightarrow 2} = -D \cdot \frac{c_1 - c_2}{L}$$

where  $J_{1 \rightarrow 2}$  is the net flux from intracellular compartment 1 to intracellular compartment 2,  $c_j$  is the concentration of intracellular auxin in compartment  $j$  for  $j=1, 2$ , and  $D$  is the diffusion coefficient of auxin in the cell, and  $L$  is a distance between the compartments. (B) The diffusion coefficient  $D$  was set at  $10 \mu\text{m}^2\text{s}^{-1}$ , (C)  $D = 50 \mu\text{m}^2\text{s}^{-1}$ , (D)  $D = 100 \mu\text{m}^2\text{s}^{-1}$ , (E)  $D = 300 \mu\text{m}^2\text{s}^{-1}$ , (F)  $D = 600 \mu\text{m}^2\text{s}^{-1}$ . These model simulations that include intracellular auxin diffusion were performed for a wide range of diffusion rates (B-F) and were yielded qualitatively similar predictions as the control simulations with no intracellular auxin diffusion (A).

Polarization Index (PI) and Signaling Asymmetry (SA) are introduced in Figure 2. For symbols and color code, see Figures 2E and Supplementary Figure 1N.



### Supplementary Figure 12. Auxin concentration is a main polarizing signal.

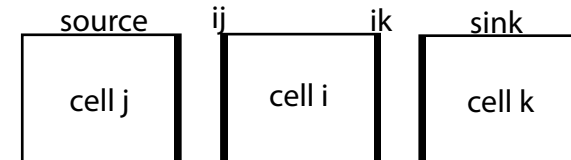
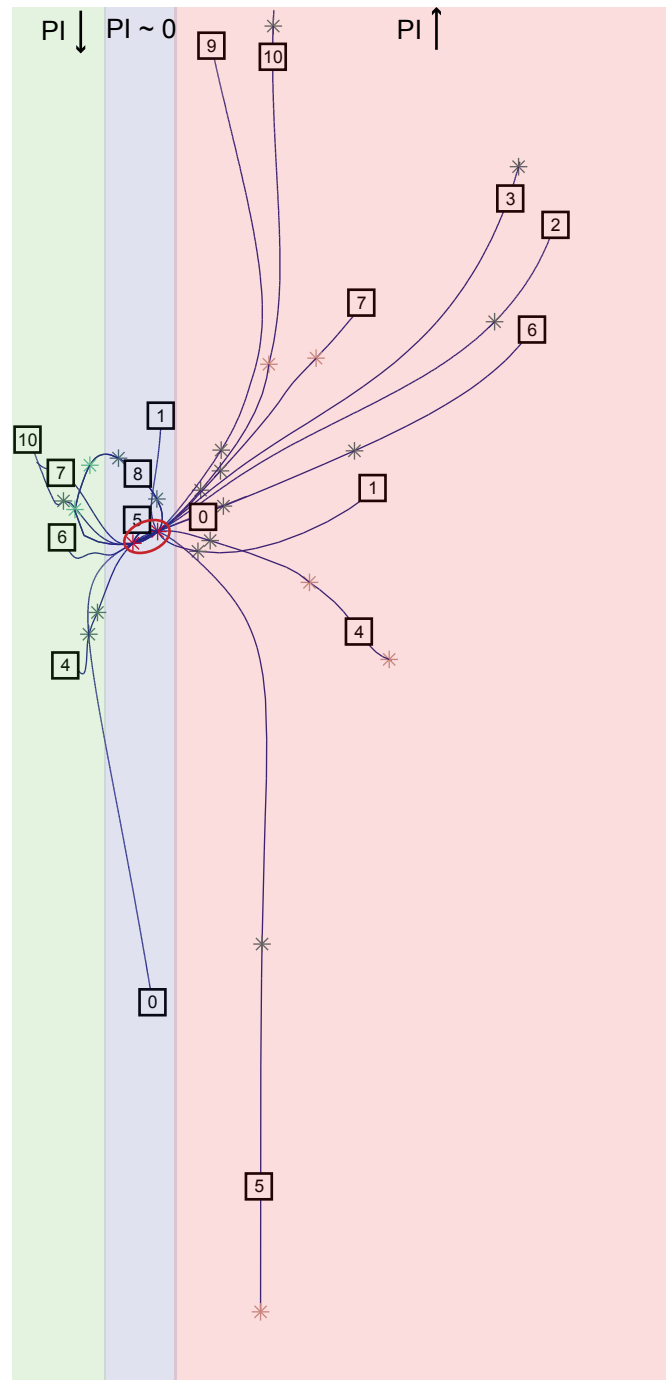
(A-D) ‘WT’ control simulation - Model simulations on the file of cells (A) and on the cellular grid (B) predicted PIN polarization and canalization of auxin flow from an auxin source towards a distal auxin sink. The auxin source was set to  $0.001 \mu\text{M} \mu\text{m}^{-2} \text{s}^{-1}$  (virtually the same as control simulation presented in Supplementary Figure 1A-D). (E-H). Model simulations on the file of cells (E) and on the cellular grid (F) with auxin source set to  $0.01 \mu\text{M} \mu\text{m}^{-2} \text{s}^{-1}$  and a distal auxin sink are presented. The auxin concentration threshold sufficient causing increase of the PI was reached nearly two times faster (G) compared to that presented in control simulation (C). Notably, the model predicted a steep difference in extracellular auxin signaling on both sides of *i*-th cell that was associated with the high positive value of SA (H). The PIN levels on *ik*-th membrane were a 7-fold higher than those on *ij*-th membrane (high PI) (G). (I-L) Model simulations on the file of cells (I) and on the cellular grid (J) with auxin source set to  $0.0005 \mu\text{M} \mu\text{m}^{-2} \text{s}^{-1}$  and a distal auxin sink are presented. The establishment of PIN polarization was delayed (K) in comparison with control simulation (C), by about 100s. This is presumably due to a longer time of auxin accumulation in the cell (K). Interestingly, in the presence of this weak auxin source, our model predicted fluctuations (oscillations) in the steady-state values of chemicals, that were damped over time resulting with stable PIN polarization pattern (K, L). Note that PI and SA – measures of PIN polarization and auxin signaling were also oscillating (M-P) Model simulations on the file of cells (M) and on the cellular grid (N) with an auxin source set to  $0.0001 \mu\text{M} \mu\text{m}^{-2} \text{s}^{-1}$  and a distal auxin sink are presented. In this model simulation, the establishment of PIN polarization was considerably delayed by about 1000 s (O) if compared to predictions from control simulation (C). Also here oscillations of values of PI and SA were observed and those corresponded to similar fluctuations in chemical levels (O, P). In summary, our model predicted unstable PIN polarity resulting in the lack of vascular connection (M, N).

We demonstrated that hot spots of auxin production (auxin sources) mediate the stability of PIN polarization patterns and thus provide means for auxin-regulated processes such as vascular formation/connection (Figures 3, 4, 5, 6A-E) and vascular repulsion (Figure 6I-M).

Polarization Index (PI) and Signaling Asymmetry (SA) are introduced in Figure 2. For symbols and color code, see Figures 2E and Supplementary Figure 1N.

Log(auxin source)

- 0 *auxin source*
- 1  $\rho_{IAAH}$
- 2  $\rho_{AUX}$
- 3  $\rho_{PIN}$
- 4  $k_t$
- 5  $D_a$
- 6  $\delta_{PIN}$
- 7  $\delta_{AUX}$
- 8  $D_c$
- 9  $R_T$
- 10  $K_D$



- \* Andronov-Hopf bifurcation (H)
- \* Zero-Hopf bifurcation (ZH)
- \* Generalized Hopf bifurcation (GH)
- \* Double Hopf (HH) bifurcation
- Oscillations of PIN polarization

Log(PIN membrane (ij))

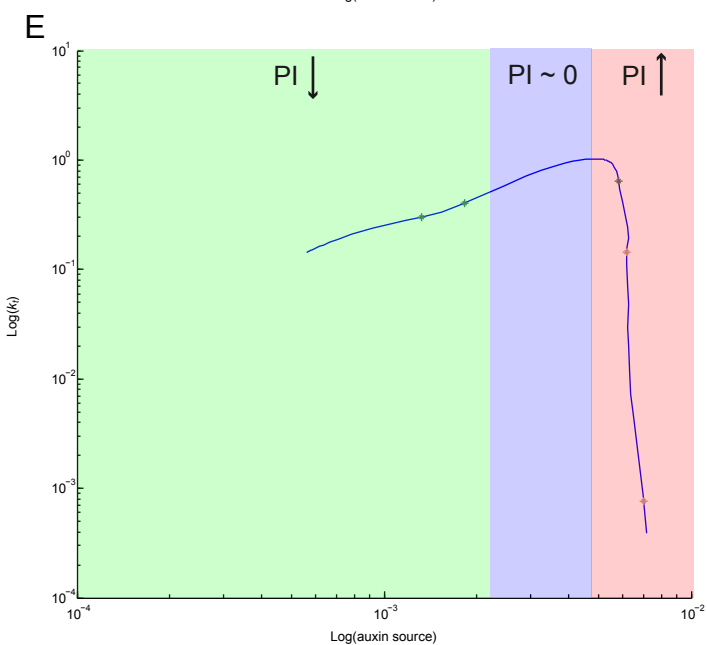
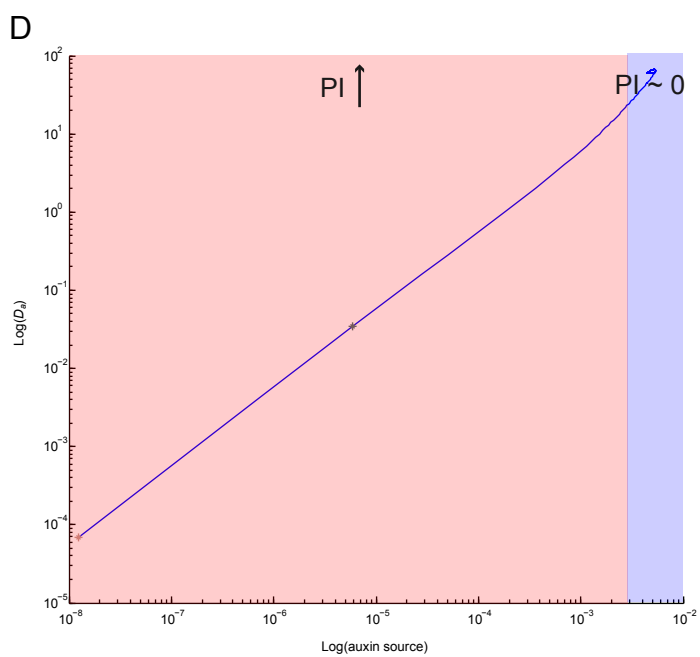
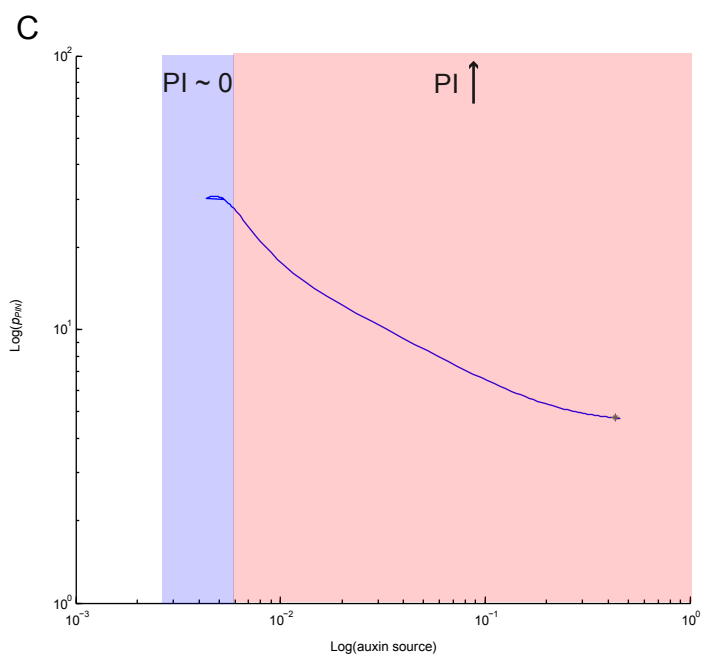
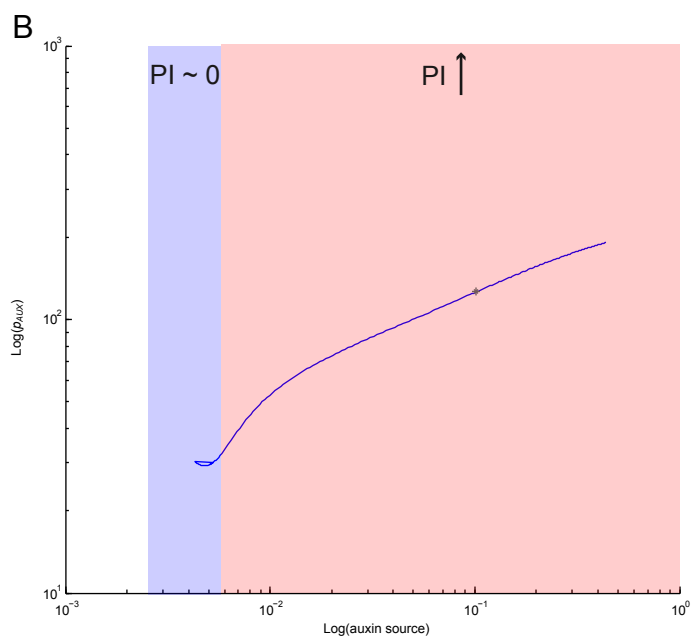
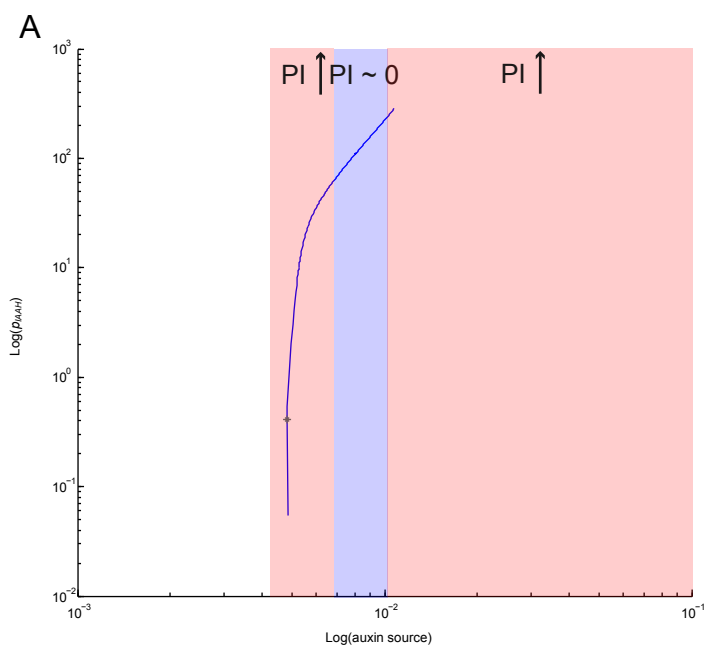
Log(PIN membrane (ik))

**Supplementary Figure 13. The evolution of stationary equilibrium under variation of model parameters.**

A bifurcation diagram represents the family of stationary solutions for varying source strength (0). Two Hopf-points (H) were detected using numerical continuation of the equilibrium. These points indicate the appearance of supercritical Andronov-Hopf bifurcation with stable limit cycle (first Lapunov coefficients were negative, a pair of purely imaginary eigenvalues). The curve connecting H points corresponds to the parameter regime for which oscillations of PIN polarization occur. The equilibrium curves (1-10) describe the families of stationary solutions for the variation of auxin source strength and one additional model parameter. Note that several additional bifurcations were detected including Generalized Hopf (GH), Zero-Hopf (ZH) (one zero eigenvalue) and Hopf-Hopf (HH) bifurcations. The schematic colorized planes describe three different model behaviors (green, blue, red) which are associated with:

- “Up-the-gradient” PIN polarization (green plane) associated with decreasing Polarization Index (PI)
- Unstable PIN polarization or no PIN polarization (blue plane) when PI is crossing zero.
- “With-the-gradient” PIN polarization (red plane) associated with increasing value of PI.

Each of these model behaviors correspond to different phenomena occurring during canalization of auxin flow in our model simulations that includes vein connection ( $PI > 0$ ), vein repulsion ( $PI \sim 0$ ) and PIN polarization towards an auxin source ( $PI < 0$ ). Polarization Index (PI) is described in Figure 2.

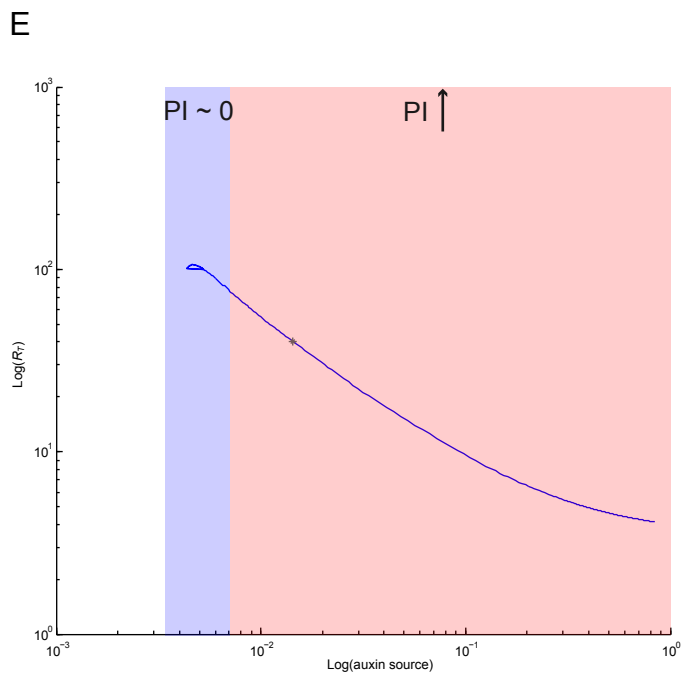
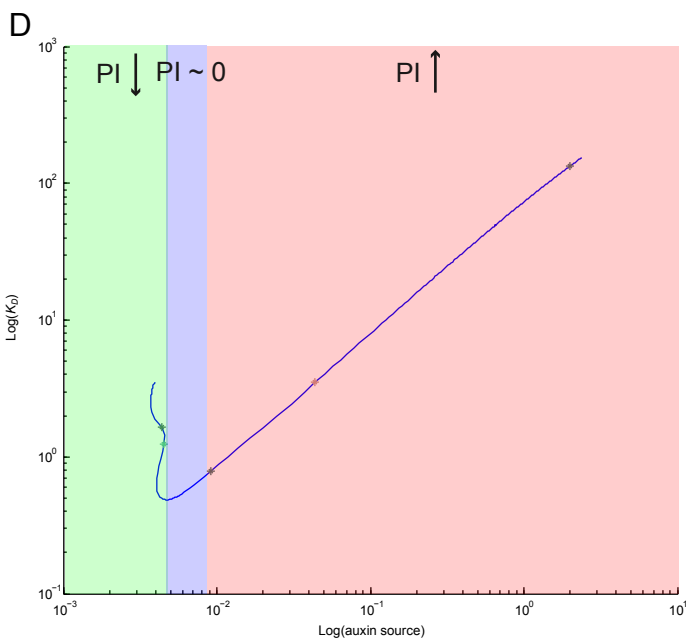
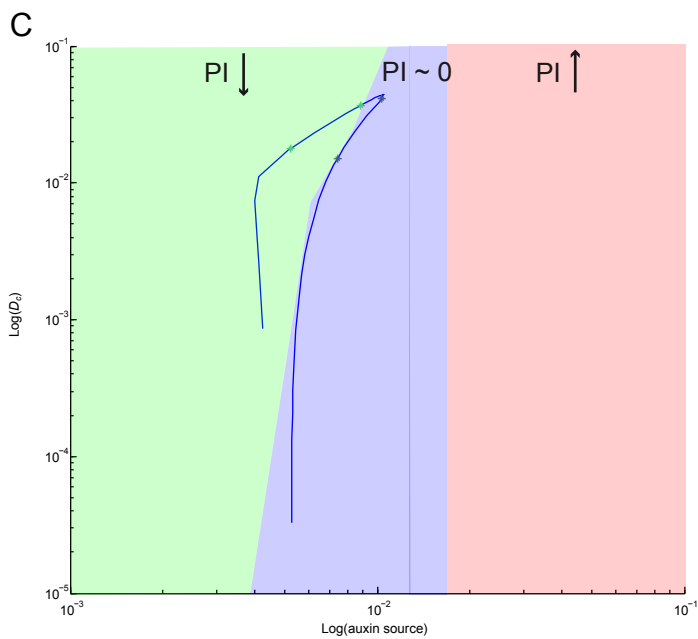
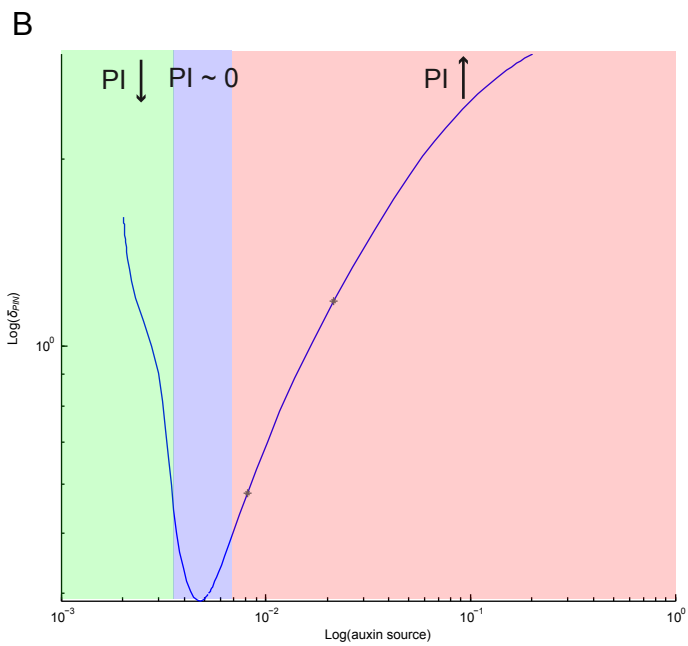
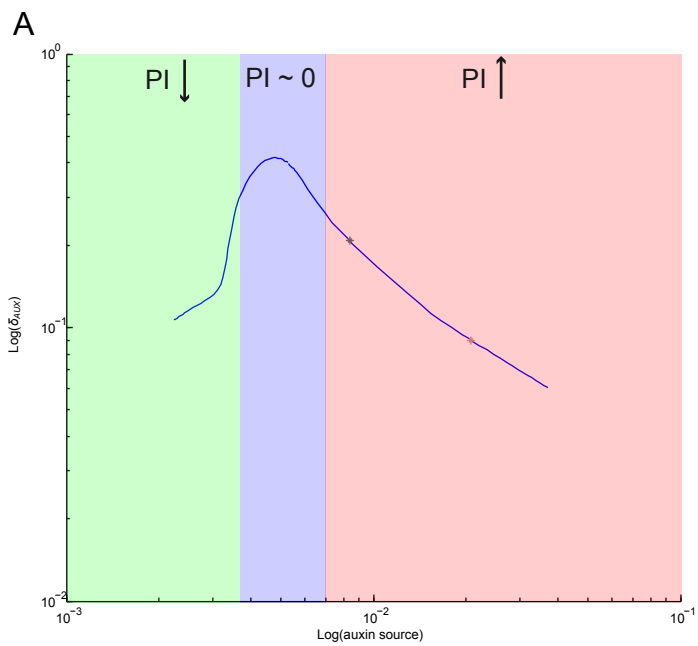


- \* Andronov-Hopf bifurcation (H)
- \* Zero-Hopf bifurcation (ZH)
- \* Generalized Hopf bifurcation (GH)
- \* Double Hopf (HH) bifurcation

**Supplementary Figure 14. Two-dimensional bifurcation diagrams for equilibrium curves (1-5) presented in Supplementary Figure 13.**

Analysis of model sensitivity and model behaviors associated with Polarization index (PI) are presented for the subsequent variation in strength of auxin source and one additional parameter: **(A)** passive auxin influx into cell ( $p_{IAAH}$ ), **(B)** efficiency of AUX/LAX- dependent transport ( $p_{AUX}$ ), **(C)** efficiency of PIN-dependent transport ( $p_{PIN}$ ), **(D)** auxin diffusion in the cell wall ( $D_a$ ), **(E)** saturation of polar auxin transport ( $k_t$ ).

Polarization Index (PI) is described in Figure 2. The sign of PI corresponds to different model behavior (Supplementary Figure 13).

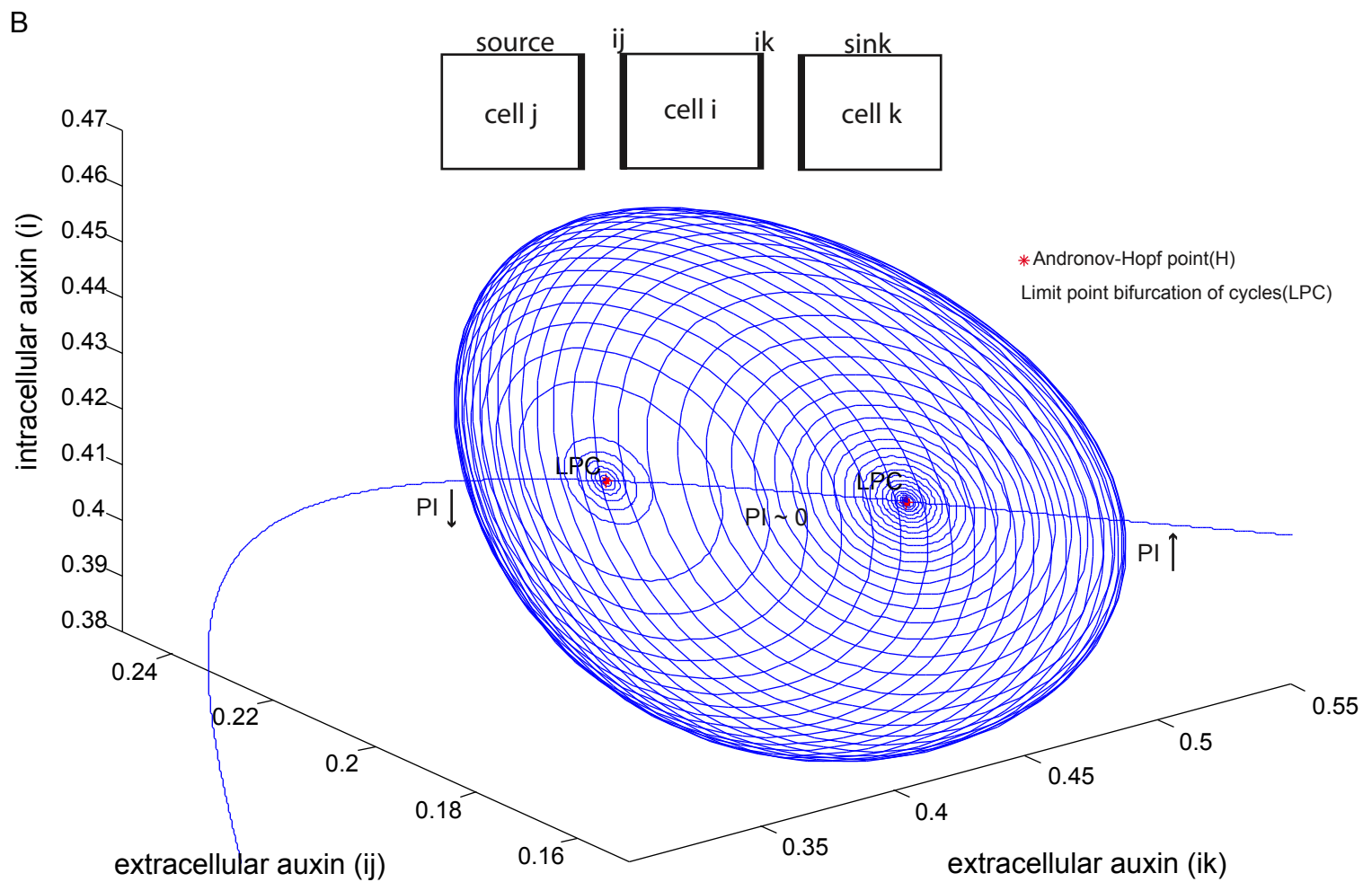
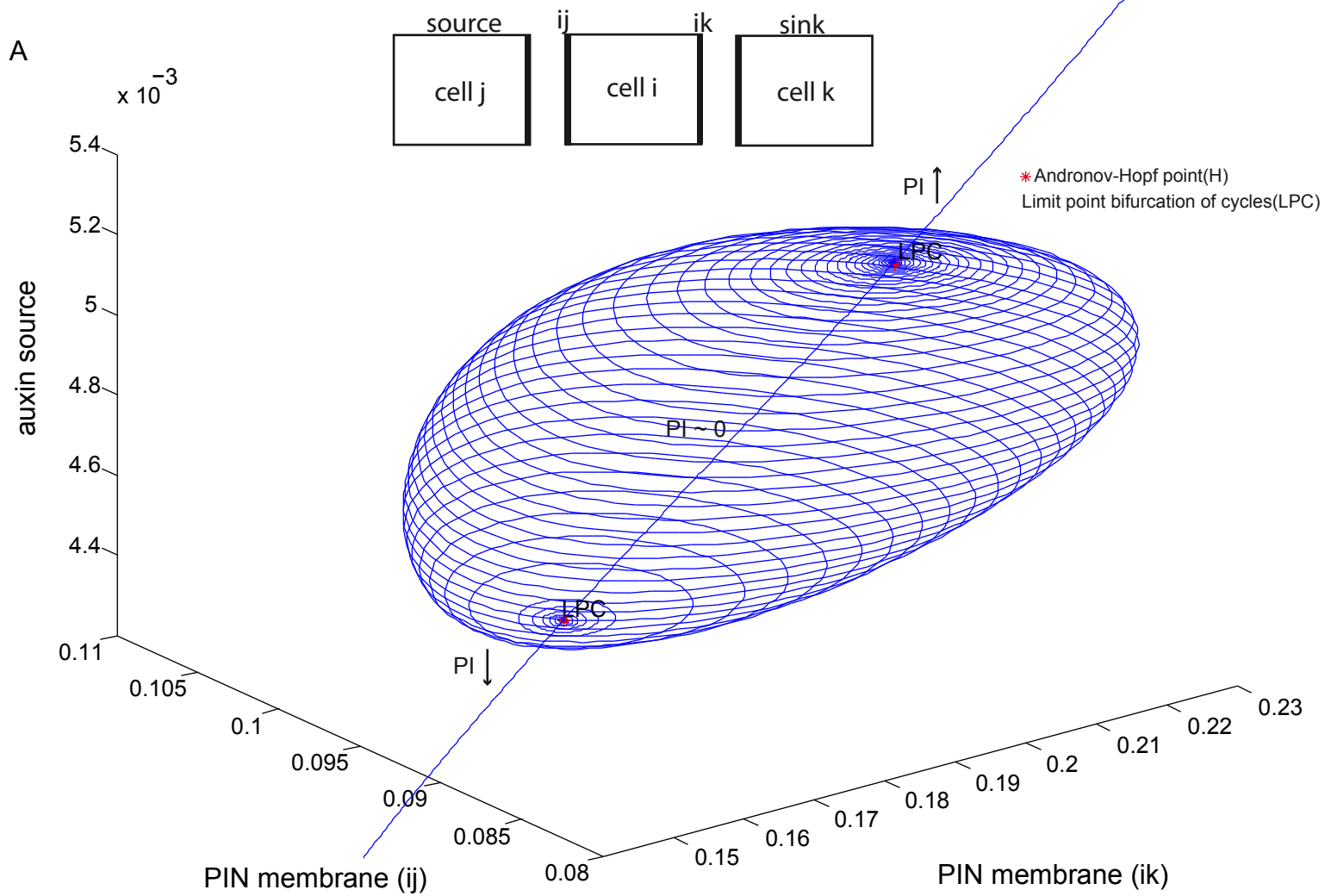


- \* Andronov-Hopf bifurcation (H)
- \* Zero-Hopf bifurcation (ZH)
- \* Generalized Hopf bifurcation (GH)
- \* Double Hopf (HH) bifurcation

**Supplementary Figure 15. Two-dimensional bifurcation diagrams for equilibrium curves (6-10) presented in Supplementary Figure 13.**

Analysis of model sensitivity and model behaviors associated with Polarization index (PI) are presented for the subsequent variation in strength of auxin source and one additional parameter: **(A)** degradation of auxin influx carriers ( $\delta_{AUX}$ ), **(B)** degradation of auxin efflux carriers ( $\delta_{PIN}$ ), **(C)** diffusion of auxin-bound receptors in the cell wall ( $D_c$ ), **(D)** receptor dissociation constant ( $K_D$ ), **(E)** Amount of extracellular auxin receptors in the intercellular pools ( $R_T$ ).

Polarization Index (PI) is described in Figure 2. The sign of PI corresponds to different model behavior (Supplementary Figure 13).



**Supplementary Figure 16. The periodic orbits of PIN and auxin levels correspond to stable limit cycle emerging from Hopf bifurcation.**

(A) Stable limit cycle (LPC) connects two Hopf points (H). The variation of auxin source strength yielded the appearance of either oscillatory ( $PI \sim 0$ ) or stable PIN polarization in the model ( $PI \neq 0$ ). (B) Phase portrait showing the borders between either oscillating ( $PI \sim 0$ ) or stable ( $PI \neq 0$ ) auxin levels, inside and outside of the cell.

Polarization Index (PI) is described in Figure 2. The sign of PI corresponds to different model behavior (Supplementary Figure 13).

## Model description

### Auxin transport

According to the classical chemiosmotic hypothesis proposed by Raven [1] and Goldsmith [2], in the presence of high cytoplasmic pH (7.2-7.6), auxin is almost completely deprotonated and requires polar transport mediated by PINs to move across the plasma membrane (with permeability  $p_{PIN}$ ) and consequently to leave the cell. In the apoplast at acidic pH (5.5), fractions of protonated and ionic auxin can either enter the cell via passive diffusion (with permeability  $p_{IAAH}$ ) and is enhanced by the activity of influx carriers (AUX/LAX) (with permeability  $p_{AUX}$ ). The model explicitly includes the movement of auxin within the apoplast [3] determined by diffusion coefficient  $D_a$ . The auxin movement between cells and within cell wall is given by:

$$\begin{aligned}
 \frac{dIAA_i}{dt} = & \frac{1}{V_i} \cdot \left[ p_{IAAH} \cdot \sum_{j \in N_i} l_{ij} \cdot (f_{in}^+(IAA_{ij}) - f_{out}^+(IAA_i)) \right] \\
 + & \frac{1}{V_i} \cdot \left[ p_{PIN} \cdot \sum_{j \in N_i} PIN_{ij} \cdot (f_{in}^-(IAA_{ij}) - f_{out}^-(IAA_i)) \right] \\
 + & \frac{1}{V_i} \cdot \left[ p_{AUX} \cdot \sum_{j \in N_i} AUX_{ij} \cdot (f_{out}^-(IAA_{ij}) - f_{in}^-(IAA_i)) \right]
 \end{aligned} \tag{1}$$

$$\begin{aligned}
 \frac{dIAA_{ij}}{dt} = & \frac{1}{V_{ij}} \cdot \left[ D_a \cdot \left\{ \frac{a_{ijj}}{d_{ijj}} \cdot (IAA_{ji} - IAA_{ij}) + \frac{a_{ijk}}{d_{ijk}} \cdot (IAA_{ik} - IAA_{ij}) + \frac{a_{ijil}}{d_{ijil}} \cdot (IAA_{il} - IAA_{ij}) \right\} \right] \\
 + & \frac{1}{V_{ij}} \cdot \left[ p_{IAAH} \cdot l_{ij} \cdot (f_{out}^+(IAA_i) - f_{in}^+(IAA_{ij})) \right] \\
 + & \frac{1}{V_{ij}} \cdot \left[ p_{PIN} \cdot PIN_{ij} \cdot (f_{out}^-(IAA_i) - f_{in}^-(IAA_{ij})) \right] \\
 + & \frac{1}{V_{ij}} \cdot \left[ p_{AUX} \cdot AUX_{ij} \cdot (f_{in}^-(IAA_i) - f_{out}^-(IAA_{ij})) \right]
 \end{aligned} \tag{2}$$

with

$$\begin{aligned}
f_{in}^+(IAA_{ij}) &= \frac{IAA_{ij}}{1+10^{pH_{wall}-pK}}, & f_{out}^+(IAA_i) &= \frac{IAA_i}{1+10^{pH_{cell}-pK}}, \\
f_{in}^-(IAA_{ij}) &= \frac{\Phi_{influx}}{1+10^{-pH_{wall}+pK}} \cdot \frac{IAA_{ij}}{k_t + IAA_{ij}}, & f_{in}^-(IAA_i) &= \frac{\Phi_{influx}}{1+10^{-pH_{cell}+pK}} \cdot \frac{IAA_i}{k_t + IAA_i}, \\
f_{out}^-(IAA_{ij}) &= \frac{\Phi_{efflux}}{1+10^{-pH_{wall}+pK}} \cdot \frac{IAA_{ij}}{k_t + IAA_{ij}}, & f_{out}^-(IAA_i) &= \frac{\Phi_{efflux}}{1+10^{-pH_{cell}+pK}} \cdot \frac{IAA_i}{k_t + IAA_i}
\end{aligned} \tag{3}$$

where  $IAA_i$  is the mean auxin concentration in the  $i$ -th cell and  $IAA_{ij}$ ,  $IAA_{ji}$ ,  $IAA_{ik}$ ,  $IAA_{il}$  are the mean auxin concentrations in adjacent wall compartments (Figure 1, main text),  $V_i$  and  $V_{ij}$  are the dimensions of the cell and wall compartment, respectively.  $N_i$  denotes the number of direct neighbors of cell  $i$ . The  $PIN_{ij}$  and  $AUX_{ij}$  variables determine the average level of PINs and AUX/LAXs carriers at the  $i$ -th plasma membrane facing cell  $j$ . The parameter  $k_t$  defines the saturation constant of polar auxin transport. The parameter  $D_a$  describes auxin diffusion between the neighboring wall compartments.  $p_{IAAH}$ ,  $p_{PIN}$ ,  $p_{AUX}$  are the membrane permeabilities for passive diffusion and carrier mediated transport, respectively. The pH differs between cytoplasm and extracellular space ( $pH_{cell}$ ,  $pH_{wall}$ ) leading to different auxin fractions inside/outside of the cell:  $f_{in}^+(IAA_{ij})$ ,  $f_{in}^-(IAA_{ij})$ ,  $f_{in}^-(IAA_i)$ ,  $f_{out}^+(IAA_i)$ ,  $f_{out}^-(IAA_{ij})$ ,  $f_{out}^-(IAA_i)$  (Figure 1 – main text). Each wall compartment ( $ij$ ) is considered to have three neighbors, left and right neighbors ( $il$ ,  $ik$ ) connected to the same cell  $i$  and one neighbor ( $ji$ ) “connected” to the neighboring cell  $j$ . The crossing area between neighboring cytoplasm and membrane/wall compartments (for passive transport) is denoted as  $l_{ij}$ , crossing areas between neighboring wall compartments is  $a_{iji}$ ,  $a_{ijk}$ ,  $a_{ijl}$  and distances between neighboring wall compartments used in the diffusion terms are given by  $d_{iji}$ ,  $d_{ijk}$ ,  $d_{ijl}$ . For simplicity we used the constant value of  $a = 0.25 \mu\text{m}$  corresponding to cell wall thickness of 500 nm. In addition, the model assumes that the active auxin transport mediated by PINs and AUX/LAXs proteins

depends on the electrochemical gradient between cytoplasm and the apoplast. The  $\Phi_{influx}$  and  $\Phi_{efflux}$  parameters (eq. 3) describe the membrane potential:

$$\Phi_{influx} = \Phi_{efflux} \cdot e^{\frac{zVF}{RT}} = \frac{zVF}{RT} \cdot \frac{e^{\frac{zVF}{RT}}}{e^{\frac{zVF}{RT}} - 1}, \quad (4)$$

where  $V = -100 \text{ mV}$ ,  $F = 9.6 \times 10^4 \text{ mol}^{-1}$ ,  $R = 8.3 \text{ Jmol}^{-1}\text{K}^{-1}$ ,  $T = 300\text{K}$ .

### Auxin carrier production and breakdown

We model the expression of AUX/LAX and PIN proteins in the cell as follows:

$$\frac{dPIN_i}{dt} = \alpha_{PIN} \cdot h(IAA_i) - \delta_{PIN} \cdot PIN_i \quad (5)$$

$$\frac{dAUX_i}{dt} = \alpha_{AUX} \cdot h(IAA_i) - \delta_{AUX} \cdot AUX_i \quad (6)$$

$$h(IAA_i) = \frac{IAA_i}{k_m + IAA_i} \quad (7)$$

where  $PIN_i$  and  $AUX_i$  are the total intracellular concentrations of PIN and AUX/LAX in cell  $i$ ,  $\alpha_{PIN}$  and  $\alpha_{AUX}$  define the rates of auxin-induced PIN and AUX/LAX synthesis [4]-[6] and  $\delta_{PIN}$  and  $\delta_{AUX}$  determine decay rates of PIN and AUX/LAX proteins.  $IAA_i$  expresses the mean auxin concentration in the  $i$ -th cell and  $k_m$  is a Michaelis–Menten constant for auxin-dependent carrier production ( $h(IAA_i)$ , Figure 1B - main text).

### Auxin carrier recycling

Auxin carriers recycle between endosomes and plasma membrane [7],[8] with the base rates  $a_{exo}$ ,  $k_{exo}$  and  $a_{endo}$ ,  $k_{endo}$  for AUX/LAX and PIN exocytosis (trafficking from endosomes to the plasma membrane) and their internalization (trafficking from plasma membrane to the endosomes), respectively. AUX/LAX transporters are distributed evenly on the cell membrane and show non-polar subcellular localization.

The AUX/LAX carriers are allocated in the plasma membrane in each time step as follows:

$$\frac{dAUX_{ij}}{dt} = a_{exo} \cdot AUX_i - a_{endo} \cdot AUX_{ij} \quad (8)$$

where  $AUX_{ij}$  represents the average amount of AUX/LAX proteins at the plasma membrane, and  $AUX_i$  is a total intracellular level of AUX/LAX in cell  $i$  and  $a_{exo}$  and  $a_{endo}$  are the rates of AUX/LAX exocytosis and internalization, respectively.

The corresponding change in intracellular AUX/LAX levels in  $ith$  cell is described as follows:

$$\frac{dAUX_i}{dt} = \sum_{j \in N_i} (a_{endo} \cdot AUX_{ij} - a_{exo} \cdot AUX_i) \quad (9)$$

The polar, subcellular localization of PIN auxin efflux facilitators in the model is determined by differential PIN retention at a given cell side [9] as a result of an auxin-dependent inhibition of PIN internalization [10] and an intracellular competition of cell membranes for auxin efflux transporters (Figure 1C, main text).

PIN allocation in the plasma membrane changes according to the following formula:

$$\frac{dPIN_{ij}}{dt} = k_{exo} \cdot PIN_i - PIN_{ij} \cdot (k_{endo} + kh_{ij}) \quad (10)$$

where  $PIN_{ij}$  are the PIN level on  $ij$ -th plasma membrane, and  $PIN_i$  is the total intracellular PIN level in  $i$ -th cell. The parameter  $k_{exo}$  determines the rate of PIN exocytosis, and  $k_{endo}$  is a base rate for PIN endocytosis whereas  $kh_{ij}$  determines the auxin-dependent effect on PIN internalization.

The corresponding change in intracellular PIN level in  $ith$  cell is given by:

$$\frac{dPIN_i}{dt} = \sum_{j \in N_i} (PIN_{ij} \cdot (k_{endo} + kh_{ij}) - k_{exo} \cdot PIN_i) \quad (11)$$

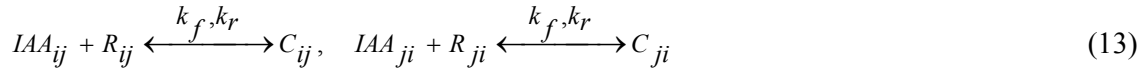
### Auxin effect on PIN internalization

We assumed in our model that two neighboring cells share the intercellular pool of auxin receptors which we denote as  $2R_T$ . These extracellular receptors bind to auxin to form an active auxin-receptor complex (recruited receptor) whereas remaining free receptors from intercellular pool freely diffuse from one side of the cell to the closest side of adjacent cell.

Because the amount of auxin receptors remains is conserved in the extracellular space between two neighboring cells, the mass conservation law is written as:

$$2R_T = R_{ij} + R_{ji} + C_{ij} + C_{ji} \quad (12)$$

where  $R_{ij}$  and  $R_{ji}$  are unbound/free solution receptors in the adjacent wall compartments, respectively and  $C_{ij}$  and  $C_{ji}$  are the active auxin-receptor complexes. The kinetics of the reversible auxin-receptor binding is given by:



where  $k_f$  and  $k_r$  are forward and backward rates of receptor cycling between active and inactive states, respectively. Then a dissociation constant of auxin-receptor complex ( $K_D$ ) is determined as:

$$K_D = \frac{k_r}{k_f} \quad (14)$$

Next the relative changes in the amount of bound and unbound receptors are governed by following ODE system:

$$\frac{dC_{ij}}{dt} = IAA_{ij} \cdot R_{ij} - K_D \cdot C_{ij} + D_c \cdot (C_{ji} - C_{ij}) \quad (15)$$

$$\frac{dC_{ji}}{dt} = IAA_{ji} \cdot R_{ji} - K_D \cdot C_{ji} - D_c \cdot (C_{ji} - C_{ij}) \quad (16)$$

$$\frac{dR_{ij}}{dt} = -IAA_{ij} \cdot R_{ij} + K_D \cdot C_{ij} + D_R \cdot (R_{ji} - R_{ij}) \quad (17)$$

$$\frac{dR_{ji}}{dt} = -IAA_{ji} \cdot R_{ji} + K_D \cdot C_{ji} - D_R \cdot (R_{ji} - R_{ij}) \quad (18)$$

where  $D_R$  is a free-receptor diffusion coefficient and  $D_C$  denotes the diffusion of the auxin-receptor complex. For simplicity we assume that auxin-receptor complexes and free receptors in  $ij$ -th and  $ji$ -th discrete wall compartments are practically in dynamic equilibrium (quasi-steady state) due to the fast kinetic reactions. In our model we considered the intercellular pools of extracellular receptor per each pair of neighboring cells such that the total amount of receptors in each intercellular pool is conserved. Therefore, the transversal diffusion of receptors can be negligible. To express that one puts the right side of equations (15)-(17) to zero whereas equation (18) can be replaced by equation (12). By solving the linear system of equations (12), (15)-(17) for  $C_{ij}$ ,  $C_{ji}$ ,  $R_{ij}$  and  $R_{ji}$ , one obtains the following relations:

$$C_{ij} = \frac{2 \cdot R_T \cdot \left( \sqrt{\alpha \cdot \beta} \cdot (IAA_{ij} + IAA_{ji}) + IAA_{ij} \cdot (\alpha \cdot IAA_{ji} + K_D) \right)}{K_D \cdot (2 \cdot K_D + IAA_{ij} + IAA_{ji}) + 2 \cdot \sqrt{\alpha \cdot \beta} \cdot (IAA_{ij} + IAA_{ji} + 2 \cdot K_D) + \alpha \cdot (2 \cdot IAA_{ij} \cdot IAA_{ji} + IAA_{ij} \cdot K_D + IAA_{ji} \cdot K_D)} \quad (19)$$

$$C_{ji} = \frac{2 \cdot R_T \cdot \left( \sqrt{\alpha \cdot \beta} \cdot (IAA_{ij} + IAA_{ji}) + IAA_{ji} \cdot (\alpha \cdot IAA_{ij} + K_D) \right)}{K_D \cdot (2 \cdot K_D + IAA_{ij} + IAA_{ji}) + 2 \cdot \sqrt{\alpha \cdot \beta} \cdot (IAA_{ij} + IAA_{ji} + 2 \cdot K_D) + \alpha \cdot (2 \cdot IAA_{ij} \cdot IAA_{ji} + IAA_{ij} \cdot K_D + IAA_{ji} \cdot K_D)} \quad (20)$$

$$R_{ij} = \frac{2 \cdot R_T \cdot K_D (K_D + 2 \cdot \sqrt{\alpha \cdot \beta} + \alpha \cdot IAA_{ji})}{K_D \cdot (2 \cdot K_D + IAA_{ij} + IAA_{ji}) + 2 \cdot \sqrt{\alpha \cdot \beta} \cdot (IAA_{ij} + IAA_{ji} + 2 \cdot K_D) + \alpha \cdot (2 \cdot IAA_{ij} \cdot IAA_{ji} + IAA_{ij} \cdot K_D + IAA_{ji} \cdot K_D)} \quad (21)$$

$$R_{ji} = \frac{2 \cdot R_T \cdot K_D (K_D + 2 \cdot \sqrt{\alpha \cdot \beta} + \alpha \cdot IAA_{ij})}{K_D \cdot (2 \cdot K_D + IAA_{ij} + IAA_{ji}) + 2 \cdot \sqrt{\alpha \cdot \beta} \cdot (IAA_{ij} + IAA_{ji} + 2 \cdot K_D) + \alpha \cdot (2 \cdot IAA_{ij} \cdot IAA_{ji} + IAA_{ij} \cdot K_D + IAA_{ji} \cdot K_D)} \quad (22)$$

where  $\alpha = \frac{D_C}{D_R}$ , and  $\beta = D_C \cdot D_R$ .

We assumed that the active auxin-receptor complexes are recruited with the highest probability to the nearest cell. Because recruited receptors transfer a signal to the plasma membrane they could be temporally immobilized at the cell surface (represented by discrete wall compartment) presumably due to its interaction with plasma membrane or its conformational changes. Therefore, the diffusion of free receptor in the apoplast becomes much larger than the diffusion of auxin-bound receptors ( $D_C \ll D_R$ ) which then implicates  $\alpha \sim 0$  and  $\beta \sim 0$  for finite values of  $D_R$  and  $D_C$ . In this case of  $D_C = 0$  and  $D_R \rightarrow \infty$  the equations (19)-(22) simplify to:

$$C_{ij} = \frac{2 \cdot R_T \cdot IAA_{ij}}{(2 \cdot K_D + IAA_{ij} + IAA_{ji})} \quad (23)$$

$$C_{ji} = \frac{2 \cdot R_T \cdot IAA_{ji}}{(2 \cdot K_D + IAA_{ij} + IAA_{ji})} \quad (24)$$

$$R_{ij} = R_{ji} = \frac{2 \cdot R_T \cdot K_D}{(2 \cdot K_D + IAA_{ij} + IAA_{ji})} \quad (25)$$

In our model we assume that the recruited receptors signal on PIN internalization. Taking into account equations (23)-(25) one derives the formula that describes the auxin-dependent inhibition of PIN internalization at the ( $ij$ ) side of the  $i$ -th cell:

$$kh_{ij} = \frac{\mu}{1 + C_{ij}} \quad (26)$$

where  $kh_{ij}$  expresses the effective rate of PIN endocytosis ( $\mu$ ) repressed by the amount of active signalling components at  $ij$ th side of the cell as presented in Figures 1D and 2A in the main text.

## Tissue layout

Two representations of a longitudinal section of the shoot apical meristem, including a two-dimensional grid and a cellular template with irregular cell topology, were used to simulate auxin transport during auxin canalization, vein loop formation, and tissue wounding. Depending on the specific case simulated, a single cell is either a square (grid representation) or an arbitrary polygon (longitudinal meristem section). Each cell was surrounded by wall compartments that included plasma membranes and the apoplast (extracellular space). A cell volume of  $100 \mu\text{m}^2$  and a wall length of  $10 \mu\text{m}$  in the two-dimensional were adopted in the grid tissue layout. The intracellular gradients in the grid tissue layout (Supplementary Figure 11) were modeled as follows:

The single cell box was divided in four identical triangular compartments each associated with the one side of the cell and the cell center. In this case, intracellular auxin freely diffuses within intracellular compartments following Fick's law:

$$J_{1 \rightarrow 2} = -D \cdot \frac{c_1 - c_2}{L} \quad (27)$$

where  $J_{1 \rightarrow 2}$  is the net flux from compartment 1 to compartment 2,  $c_j$  is the concentration of intracellular auxin in compartment  $j$  for  $j=1,2$ , and  $D$  is the diffusion coefficient of auxin in the cell, and  $L$  is a distance between compartments.

In the cellular templates, the cell volume and cell wall length varied, but were, on average, approximately  $98 \mu\text{m}^2$  and  $9 \mu\text{m}$ , respectively. For simplicity, cell wall thickness was set at  $0.5 \mu\text{m}$ .

## Boundary conditions

In the computer simulations of auxin canalization and tissue wounding (Figures 3, 4, and 7), the auxin source was represented by a cell that produced auxin at a rate of  $0.0015 \mu\text{M} \mu\text{m}^{-2} \text{s}^{-1}$ . The auxin sink was placed at the bottom-most part of the tissue (grid and cellular

tissue layouts) and to the right-most cell in simulations on the file of cells and corresponded to the site of the tissue where auxin was evacuated from the system (sink preserves near zero auxin concentration). For the remaining tissue borders in all model simulations, zero-flux boundary conditions were used. Virtual wounding (Figure 7) was represented by cell ablation (simply by removing cells from the tissue layout). For the simulations of vein loop patterns (Figure 5), the primary source was as above (Figures 3 and 4), and the secondary auxin sources were sites of enhanced auxin production at the rate of  $0.001 \mu\text{M} \mu\text{m}^{-2} \text{s}^{-1}$  (each source). In competitive canalization simulations (Figure 6), the pea stem decapitation corresponded to a strong reduction of strength of the primary auxin source by 10-fold but not its complete removal which would result in the suppression of stable PIN polarization pattern (Supplementary Figure 12). Most of the auxin biosynthesis is indeed coming from the decapitated region, however also the vascular tissue is the site of local auxin biosynthesis. Therefore we reduced the auxin level, which is likely to reflect *in planta* situation. The weak and strong auxin sources were represented by auxin-producing cells at rates of  $0.0002 \mu\text{M} \mu\text{m}^{-2} \text{s}^{-1}$  and  $0.002 \mu\text{M} \mu\text{m}^{-2} \text{s}^{-1}$ , respectively.

### **Cell expansion and cell division**

Cellular growth was described by cell expansion and was regulated by auxin in a concentration-dependent manner [14] and subsequent cell division. The tissue dynamics encompassed threshold of cell size above which cells start to divide. The arbitrary division threshold was set at  $1000 \mu\text{m}^2$ . For simplicity in the model, the pro-vascular cells undergo the auxin-dependent differentiation to mature cells. Once those cells reached maturity they lose their capability to divide [15]. We assumed that high auxin concentrations in the tissue promote vascular differentiation [15]. Simulations of growing tissue (Figure 4C-E) were carried out over 3 CPU time days, which corresponds to 259,200 simulation steps.

## **Numerical and simulation methods**

The dynamic cell-based simulations of auxin transport were done by numerical computations of coupled ODE systems, with an adaptive-size, fifth-order Runge-Kutta method with monitoring of local truncation error to ensure accuracy and adjustment of the step size. A time step was adjusted in each iteration to minimize local calculation errors. If the local truncation error was small enough, the method gave the output for the defined time interval and then proceeded to the next time step. A time interval of 1 s was used, but other values were also tested without significant changes in the qualitative results of the simulations. For the sensitivity and bifurcation analysis of the stationary solutions (Supplementary Figures 13-16), we used MATCONT - graphical Matlab package for numerical bifurcation analysis [16].

## **Parameters**

The general parameters for tissue layout and model simulations are shown in Supplementary Table 1. The parameters for auxin transport dynamics are presented in Supplementary Table 2, and were mainly derived from the literature [2], [3], [11]-[13]. The quantitative parameters for PIN and AUX/LAX recycling, production and degradation remain to a large extent unknown and were chosen to assert that auxin carriers recycling is a much faster process than an auxin carrier expression. They are presented in Supplementary Table 3.

## **Model sensitivity analysis**

We analyzed the importance of each component of the ERP model for general model behavior, sensitivity and robustness. Our model analysis was divided in four parts; each part treats about one structural component of the ERP model. For instance, we investigated the altered dynamics of extracellular receptor-based auxin signalling mechanism by modifying diffusion rates of bound and unbound receptors, the amount of receptors in the intercellular pools and specificity of auxin binding (receptor recruitment) (Supplementary Figures 1-3). We

concluded that the competitive utilization of auxin receptors in the apoplast determined by their respective motility is the actual trigger for initiation of PIN polarization. Therefore, we found that auxin-mediated carrier expression plays a crucial role in generating realistic PIN polarization patterns during vascularization and tissue regeneration (Supplementary Figures 4 and 5). Also the *in silico* interference with the main components of polar auxin transport system that includes PIN and AUX/LAX transporters led to the surprising observations (Supplementary Figures 6 and 7). In particular, the contribution of AUX/LAX-dependent transport to PIN polarization maintenance has been revealed (Supplementary Figure 7). Also the general role of polar auxin transport in buffering auxin diffusion in the apoplast to maintain cell polarities has been suggested (Supplementary Figures 8 and 9). Then we tested the robustness of the ERP model with respect to the auxin source/sink translocation and presence of intracellular diffusion-driven auxin gradients (Supplementary Figures 10 and 11). We also found that auxin biosynthesis play a crucial role in stabilizing PIN polarization and polar auxin transport in the tissue (Supplementary Figure 12) and their spatio-temporal regulation may be linked to phenomena such as vascular attraction/repulsion and competitive canalization of auxin flow in shoot branching. To investigate model behavior, we analyzed the sensitivity and robustness of stationary solutions with respect to perturbations in model parameters (Supplementary Figures 13-16). We identified the parameter regimes for which our model exhibits particular type of behavior (Supplementary Figures 13-16).

## Supplementary Tables

**Supplementary Table 1. General parameters for tissue layout and model simulations**

Parameter	Cell file	Grid layout	Cellular layout	Cellular growth	Units
Cell area ( $V_i$ )	100	100	98*	variable	$\mu\text{m}^2$
Wall area ( $V_{ij}$ )	$0.1 \times V_i$	$0.1 \times V_i$	$0.1 \times V_i^*$	variable	$\mu\text{m}^2$
Wall length ( $l_{ij}$ )	10	10	9.8*	variable	$\mu\text{m}$
Wall thickness term ( $a_{ij}/d_{ij}$ )	0.025	0.025	0.025	0.025	$\mu\text{m}$
Time step	1	1	1	1	s
Growth step	-	-	-	1	min
Cell expansion rate	-	-	-	0.01	-
Cell division threshold	-	-	-	1000	$\mu\text{m}^2$

\* Mean cell and wall volumes and mean wall length for cellular tissue layout

**Supplementary Table 2. Auxin transport parameters**

Parameter	Fig. 2,3,4,5,6,7 and Supp Fig 2,4,5,10,12	Supp Fig 1	Supp Fig 3	Supp Fig 6	Supp Fig 7	Supp Fig 8	Supp Fig 9	Supp Fig 11	Units
Apoplastic diffusion ( $D_a$ )	100	100	100, 10	100	100	100, 10	500, 20	100	$\mu\text{m}^2 \text{s}^{-1}$
Free receptor diffusion ( $D_R$ )	1	1, 0.1, 10, 100	1	1	1	1	1	1	$\mu\text{m}^2 \text{s}^{-1}$
Auxin-receptor complex diffusion ( $D_C$ )	0	0, 0.001, 0.1, 1	0	0	0	0	0	0	$\mu\text{m}^2 \text{s}^{-1}$
IAAH permeability ( $p_{IAAH}$ )	10	10	10	10	100, 10	10	50, 10	10	$\mu\text{m} \text{s}^{-1}$
PIN permeability ( $p_{PIN}$ )	30	30	30	300, 30, 1	30	30	150, 30	30	$\mu\text{m} \text{s}^{-1}$
AUX/LAX permeability ( $p_{AUX}$ )	30	30	30	30	300, 30, 1	30	150, 30	30	$\mu\text{m} \text{s}^{-1}$
pH in wall ( $pH_{wall}$ )	5.5	5.5	5.5	5.5	5.5	5.5	5.5	5.5	-
pH in cell ( $pH_{cell}$ )	7.6	7.6	7.6	7.6	7.6	7.6	7.6	7.6	-
Dissociation constant ( $pK$ )	5	5	5	5	5	5	5	5	-
Saturation constant for auxin transport ( $k_t$ )	1	1	1	1	1	10, 1	1	1	$\mu\text{M}$
Intracellular auxin diffusion ( $D$ )	-	-	-	-	-	-	-	600, 300, 100, 50, 10	$\mu\text{m}^2 \text{s}^{-1}$

**Supplementary Table 3. PIN and AUX/LAX dynamics**

Parameter	Fig.2,3,4,5,6,7 and Supp Fig 1,6,7,8,9,10,11,12	Supp Fig 2	Supp Fig 3	Supp Fig 4, 5	Units
PIN exocytosis base rate ( $k_{exo}$ )	1	1	1	1	$s^{-1}$
PIN internalization base rate ( $k_{endo}$ )	0.001	0.001	0.001	0.001	$s^{-1}$
Effective PIN internalization ( $\mu$ )	1	1, 0.1	1	1	$s^{-1}$
AUX/LAX exocytosis base rate ( $a_{exo}$ )	1	1	1	1	$s^{-1}$
AUX/LAX internalization base rate ( $a_{endo}$ )	0.1	0.1	0.1	0.1	$s^{-1}$
PIN production rate ( $\alpha_{PIN}$ )	1	1	1	1, 0.1, 0.01, 0	$s^{-1}$
PIN degradation rate ( $\delta_{PIN}$ )	0.03	0.03	0.03	0.03, 0.001, 0	$s^{-1}$
AUX/LAX production rate ( $\alpha_{AUX}$ )	1	1	1	1, 0.1, 0.01, 0	$s^{-1}$
AUX/LAX degradation rate ( $\delta_{AUX}$ )	0.05	0.05	0.05	0.05, 0.001, 0	$s^{-1}$
Saturation of auxin-induced PIN and AUX/LAX production ( $k_m$ )	100	100	100	100	$\mu M$
Receptor dissociation constant ( $K_D$ )	1	1	10, 1, 0.1	1	$\mu M$
The number of extracellular auxin receptors ( $R_T$ )	100	10000, 100, 1	100	100	-

## **Supplementary Movies**

### **Supplementary Movie 1**

The file contains Supplementary Movie 1 displaying the PIN-dependent auxin canalization on grid layout (simulation of Fig. 3A-C). Color coding schemes for auxin concentrations and PIN levels that were used in the model simulations as described in Fig. 3I. Auxin concentrations can vary from 0 (black) to 10 (bright green). PIN levels at the plasma membrane may change from 0 (black) to 10 (bright red). White arrows point in the direction of the preferential PIN polarity, and arrow size indicates the relative strength of PIN expression in the cell.

### **Supplementary Movie 2**

The file contains Supplementary Movie 2 showing the PIN-dependent auxin canalization on cellular layout (simulation of Fig. 3D, G, H). Color coding schemes for auxin concentrations and PIN levels that were used in the model simulations as described in Fig. 3I. Auxin concentrations can vary from 0 (black) to 10 (bright green). PIN levels at the plasma membrane may change from 0 (black) to 10 (bright red). White arrows point in the direction of the preferential PIN polarity, and arrow size indicates the relative strength of PIN expression in the cell.

### **Supplementary Movie 3**

The file contains Supplementary Movie 3 showing PIN polarity and auxin distribution associated with auxin canalization during dynamic cellular growth over 3 CPU days (simulation of Fig. 4C-E). Color coding schemes for auxin concentrations and PIN levels that were used in the model simulations as described in Fig. 3I. Auxin concentrations can vary

from 0 (black) to 10 (bright green). PIN levels at the plasma membrane may change from 0 (black) to 10 (bright red). White arrows point in the direction of the preferential PIN polarity, and arrow size indicates the relative strength of PIN expression in the cell.

#### **Supplementary Movie 4**

The file contains Supplementary Movie 4 displaying the formation of vein loop pattern (simulation of Fig. 5C-H). Auxin concentrations can vary from 0 (black) to 10 (bright green). PIN levels at the plasma membrane may change from 0 (black) to 10 (bright red). White arrows point in the direction of the preferential PIN polarity, and arrow size indicates the relative strength of PIN expression in the cell.

#### **Supplementary Movie 5**

The file contains Supplementary Movie 5 addressing competitive canalization and lateral bud release (simulation of Fig. 6A-E). Auxin concentrations can vary from 0 (black) to 10 (bright green). PIN levels at the plasma membrane may change from 0 (black) to 10 (bright red). White arrows point in the direction of the preferential PIN polarity, and arrow size indicates the relative strength of PIN expression in the cell.

#### **Supplementary Movie 6**

The file contains Supplementary Movie 6 showing competitive canalization and apical dominance (simulation of Fig. 6I-M). Auxin concentrations can vary from 0 (black) to 10 (bright green). PIN levels at the plasma membrane may change from 0 (black) to 10 (bright red). White arrows point in the direction of the preferential PIN polarity, and arrow size indicates the relative strength of PIN expression in the cell.

### **Supplementary Movie 7**

The file contains Supplementary Movie 7 illustrating the vascular tissue regeneration after wounding (simulation of Fig. 7). Color coding schemes for auxin concentrations and PIN levels that were used in the model simulations as described in Fig. 3I. Auxin concentrations can vary from 0 (black) to 10 (bright green). PIN levels at the plasma membrane may change from 0 (black) to 10 (bright red). White arrows point in the direction of the preferential PIN polarity, and arrow size indicates the relative strength of PIN expression in the cell.

## Additional references

1. Raven JA (1975) Transport of Indoleacetic-Acid in Plant-Cells in Relation to Ph and Electrical Potential Gradients, and Its Significance for Polar Iaa Transport. *New Phytologist* **74**: 163-172.
2. Goldsmith, M. H. M., Goldsmith, T. H. & Martin, M. H. Mathematical analysis of the chemosmotic polar diffusion of auxin through plant tissues. *PNAS*. **78**: 976-980 (1981).
3. Mitchison, G.J. The dynamics of auxin transport. *Proceedings of the Royal Society B: Biological Sciences* **209**: 489-511 (1980a).
4. Heisler, M. G. *et al.* Patterns of auxin transport and gene expression during primordium development revealed by live imaging of the *Arabidopsis* inflorescence meristem. *Curr. Biol.* **15**: 1899-1911 (2005).
5. Scarpella, E., Marcos, D., Friml, J. & Berleth, T. Control of leaf vascular patterning by polar auxin transport. *Genes Dev.* **20**: 1015-1027 (2006).
6. Vieten A., Vanneste S., Wisniewska J., Benkova E., Benjamins R., Beeckman T., Luschnig C., Friml J. Functional redundancy of PIN proteins is accompanied by auxin-dependent cross-regulation of PIN expression. *Development* **132**: 4521-4531 (2005).
7. Geldner, N., Xu, J., Uemura, T., Chory, J., Ueda, T., Nakano, A., Scheres, B. and Friml, J. Generation of cell polarity in plants links endocytosis, auxin distribution and cell fate decisions.. *Nature* **456**: 962-966 (2008).
8. Steinmann T, Geldner N, Grebe M, Mangold S, Jackson CL, et al. (1999) Coordinated polar localization of auxin efflux carrier PIN1 by GNOM ARF GEF. *Science* **286**: 316-318.
9. Dhonukshe, P., Tanaka, H., Goh, T., Ebine, K., Mähönen, AP., Prasad, K., Blilou, I., Geldner, N., Xu, J., Uemura, T., Chory, J., Ueda, T., Nakano, A., Scheres, B. and Friml, J. Generation of cell polarity in plants links endocytosis, auxin distribution and cell fate decisions. *Nature*

- 456:** 962-966 (2008).
10. Paciorek, T., Zazimalová, E., Ruthard, N., Petrasek, J., Stierhof, J.D., Kleine-Vehn, J., Morris, D.A., Emans, N., Jurgens, G., Geldner, N., Friml, J. Auxin inhibits endocytosis and promotes its own efflux from cells. *Nature* **435**: 1251-1256 (2005).
  11. Kramer, E.M. How far can a molecule of weak acid travel in the apoplast or xylem? *Plant Physiology* **141**: 1233-1236 (2006).
  12. Swarup, R *et al.* Root gravitropism requires lateral root cap and epidermal cells for transport and response to a mobile auxin signal. *Nature Cell Biol.* **7**: 1057-1065 (2005).
  13. Kramer, E. M., Frazer, N. L. and Baskin, T. I. Measurement of diffusion within the cell wall in living roots of *Arabidopsis thaliana* *J. Exp. Bot.* **58**: 3005-3015 (2007).
  14. Chen J-G, Ullah H, Young JC, Sussman MR, Jones AM (2001) ABP1 is required for organized cell elongation and division in *Arabidopsis* embryogenesis. *Genes Dev* **15**: 902-911.
  15. Ye Z-H (2002) Vascular tissue differentiation and pattern formation in plants. *Annu Rev Plant Biol* **53**: 183-202.
  16. Dhooge A., Govaerts W. and Kuznetsov Yu.A. (2003) MatCont: A MATLAB package for numerical bifurcation analysis of ODEs. *ACM TOMS* **29**:141-164.
  17. Tromas, A., et al. (2010) AUXIN BINDING PROTEIN 1: functional and evolutionary aspects. *Trends Plant Sci* **15**: 436-446.

## Pseudo c++ source code for the ERP model

```
/*
 * The Virtual Leaf is free software: you can redistribute it and/or
modify
 * it under the terms of the GNU General Public License as published by
 * the Free Software Foundation, either version 3 of the License, or
 * (at your option) any later version.
 *
 * The Virtual Leaf is distributed in the hope that it will be useful,
 * but WITHOUT ANY WARRANTY; without even the implied warranty of
 * MERCHANTABILITY or FITNESS FOR A PARTICULAR PURPOSE. See the
 * GNU General Public License for more details.
 *
 * You should have received a copy of the GNU General Public License
 * along with the Virtual Leaf. If not, see
<http://www.gnu.org/licenses/>.
 *
*/
// Pseudo code (C++) for the ERP model definition in Virtual Leaf
framework
//-----//
// Defines maximum number of chemicals in the model
//const int Cell::nchem = 5;

// class Parameter is a container for all model parameters (Virtual Leaf
framework)
// Parameter *par;

// class Wall defines wall interface implementation in Virtual Leaf
framework
// Wall *w;

// class Cell defines cell interface implementation in Virtual Leaf
framework
// Cell *c;

// w->C1() and w->C2() are wall object functions that return neighboring
cell objects (C1, C2)

// c->Chemical(i) gives i-th chemical in the cell

// w->Apoplast(i) gives i-th chemical in the wall

// w->Transporter1(i) gives i-th auxin transporter on the cell membrane
of Cell C1

// w->Transporter2(i) gives i-th auxin transporter on the cell membrane
of Cell C2

// Copyright 2010 Krzysztof Wabnik
// krwab@psb.vib-ugent.be
```

```

//-----//

// Fractions of auxin

double f_AH_cell = 1 / (1 + pow(10, (par->pH_cyto - par->pK)));
double f_AH_wall = 1 / (1 + pow(10, (par->pH_wall - par->pK)));
double f_A_cell = 1 / (1 + pow(10, (-par->pH_cyto + par->pK)));
double f_A_wall = 1 / (1 + pow(10, (-par->pH_wall + par->pK)));

// Interface class for auxin transport
class AuxinTransport : public TransportFunction {

public:
    virtual void operator()(Wall *w, double *dchem_c1, double *dchem_c2,
double *dap) {

// passive auxin diffusion: cell interface -> wall interface (cells C1
and C2 are neighbors)

        // Cell C1
        dchem_c1[0] += par->piaah * (w->Length() / w->C1()->Area()) *
(f_AH_wall * w->Apoplast(0) - f_AH_cell * w->C1()->Chemical(0));

        // Cell C2
        dchem_c2[0] += par->piaah * (w->Length() / w->C2()->Area()) *
(f_AH_wall * w->Apoplast(1) - f_AH_cell * w->C2()->Chemical(0));

// passive auxin diffusion: wall interface -> cell interface

        // Wall compartment 1
        dap[0] += par->piaah * (w->Length() / w->Area()) * (f_AH_cell * w-
>C1()->Chemical(0) - f_AH_wall * w->Apoplast(0));

        // Wall compartment 2
        dap[1] += par->piaah * (w->Length() / w->Area()) * (f_AH_cell * w-
>C2()->Chemical(0) - f_AH_wall * w->Apoplast(1));

// Auxin diffusion in the apoplast

        dap[0] += par->Da * (par->aijji / par->dijji) * (1 / w->Area()) * (w-
>Apoplast(1) - w->Apoplast(0));
        dap[1] += par->Da * (par->aijji / par->dijji) * (1 / w->Area()) * (w-
>Apoplast(0) - w->Apoplast(1));

```

```

// Transversal auxin diffusion in the apoplast
int ind1=0.;
int ind2=0.;
double trans_c1= w->C1()->GiveTrans(w, ind1); // total auxin influx
from neighboring wall compartments surrounding cell C1
double trans_c2= w->C2()->GiveTrans(w, ind2); // total auxin influx
from neighboring wall compartments surrounding cell C2

dap[0] += par->Da * (par->aijji / par->dijji) * (1 / w->Area()) *
(trans_c1 - ind1 * w->Apoplast(0));
dap[1] += par->Da * (par->aijji / par->dijji) * (1 / w->Area()) *
(trans_c2 - ind2 * w->Apoplast(1));

// Active auxin transport: cell interface -> wall interface (PINs)

// Cell C1
dchem_c1[0]-= par->p_pin * (1 / w->C1()->Area()) * (f_A_cell * par-
>Nefflux * w->Transporters1(0) * w->C1()->Chemical(0) / (par->kt + w-
>C1()->Chemical(0)));
dchem_c1[0]+= par->p_pin * (1 / w->C1()->Area()) * (f_A_wall * par-
>Ninflux * w->Transporters1(0) * w->Apoplast(0) / (par->kt + w-
>Apoplast(0)));

// Cell C2
dchem_c2[0]-= par->p_pin * (1 / w->C2()->Area()) * (f_A_cell * par-
>Nefflux * w->Transporters2(0) * w->C2()->Chemical(0) / (par->kt + w-
>C2()->Chemical(0)));

dchem_c2[0]+= par->p_pin * (1 / w->C2()->Area()) * (f_A_wall * par-
>Ninflux * w->Transporters2(0) * w->Apoplast(1) / (par->kt + w-
>Apoplast(1)));
// Active auxin transport: wall interface -> cell interface (PINs)
dap[0] += par->p_pin * (1 / w->Area()) * (f_A_cell * par->Nefflux *
w->Transporters1(0) * w->C1()->Chemical(0) / (par->kt + w->C1()-
>Chemical(0)));
dap[0] -= par->p_pin * (1/w->Area()) * (f_A_wall * par->Ninflux * w-
>Transporters1(0) * w->Apoplast(0) / (par->kt + w->Apoplast(0)));
dap[1] += par->p_pin * (1/w->Area()) * (f_A_cell * par->Nefflux * w-
>Transporters2(0) * w->C2()->Chemical(0) / (par->kt + w->C2()-
>Chemical(0)));
dap[1] -= par->p_pin * (1/w->Area()) * (f_A_wall * par->Ninflux * w-
>Transporters2(0) * w->Apoplast(1) / (par->kt + w->Apoplast(1)));

// Active auxin transport: cell interface -> wall interface (AUX\LAXs)

// Cell C1
dchem_c1[0]+= par->p_aux * (1 / w->C1()->Area()) * (f_A_wall * par-
>Nefflux * w->Transporters1(1) * w->Apoplast(0) / (par->kt + w-
>Apoplast(0)));
dchem_c1[0]-= par->p_aux * (1 / w->C1()->Area()) * (f_A_cell * par-
>Ninflux * w->Transporters1(1) * w->C1()->Chemical(0) / (par->kt + w-
>C1()->Chemical(0)));

```

```

// Cell C2
dchem_c2[0] += par->p_aux * (1 / w->C2()->Area()) * (f_A_wall * par-
>Nefflux * w->Transporters2(1) * w->Apoplast(1) / (par->kt + w-
>Apoplast(1)));
dchem_c2[0] -= par->p_aux * (1 / w->C2()->Area()) * (f_A_cell * par-
>Ninflux * w->Transporters2(1) * w->C2()->Chemical(0) / (par->kt + w-
>C2()->Chemical(0)));

// Active auxin transport: wall interface -> cell interface (AUX\LAXs)

dap[0] -= par->p_aux * (1 / w->Area()) * (f_A_wall * par->Nefflux *
w->Transporters1(1) * w->Apoplast(0) / (par->kt + w->Apoplast(0)));
dap[0] += par->p_aux * (1 / w->Area()) * (f_A_cell * par->Ninflux *
w->Transporters1(1) * w->C1()->Chemical(0) / (par->kt + w->C1()-
>Chemical(0)));
dap[1] -= par->p_aux * (1 / w->Area()) * (f_A_wall * par->Nefflux *
w->Transporters2(1) * w->Apoplast(1) / (par->kt + w->Apoplast(1)));
dap[1] += par->p_aux * (1 / w->Area()) * (f_A_cell * par->Ninflux *
w->Transporters2(1) * w->C2()->Chemical(0) / (par->kt + w->C2()-
>Chemical(0)));

// Source and Sink definition

// Sources an Sinks

if (w->C2()->Boundary() == Cell::SOURCE) { // Cell C1 is source
double aux_flux = par->auxin_source * w->Length() ;
dchem_c2[0] += aux_flux;
}

if (w->C1()->Boundary() == Cell::SOURCE) { // Cell C2 is source
double aux_flux = par->auxin_source * w->Length() ;
dchem_c1[0] += aux_flux;
}

if (w->C2()->Boundary() == Cell::SINK) { // Cell C1 is sink
dchem_c2[0] -= par->auxin_sink * w->C2()->Chemical(0);
}

if (w->C1()->Boundary() == Cell::SINK) { // Cell C2 is sink
dchem_c1[0] -= par->auxin_sink * w->C1()->Chemical(0);
}

// Ablated Cells

if (w->C1()->Boundary() == Cell::DEAD){
dchem_c1[0] -= w->C1()->Chemical(0);
dchem_c1[1] -= w->C1()->Chemical(1);
}

```

```

    }

    if (w->C2()->Boundary() == Cell::DEAD){

        dchem_c2[0] -= w->C2()->Chemical(0);
        dchem_c2[1] -= w->C2()->Chemical(1);

    }

};
};

// Interface class for membrane dynamics
class Carriers : public WallReaction {

public:
    virtual void operator()(Wall *w, double *dw1, double *dw2) {

// PIN internalization rates
        double khij=0.;
        double khji=0.;

        double U1=0; double U2=0; double D=0;

// Calculate steady-state bound receptors levels in the apoplast

        if ((w->Apoplast(0) > 0) || (w->Apoplast(1) > 0)) {

            double ratio_a = w->Apoplast(0) ;

            double ratio_b = w->Apoplast(1) ;

            U1= par->Dc * par->Dr * (ratio_a + ratio_b) + ratio_a * (par->Dc *
ratio_b + par->Dr * par->Kd);
            U2= par->Dc * par->Dr * (ratio_a + ratio_b) + ratio_b * (par->Dc *
ratio_a + par->Dr * par->Kd);

            D=2 * (par->Dr * par->Kd * (par->Kd + 0.5 * ratio_a + 0.5 *
ratio_b) + par->Dc * par->Dr * (ratio_a + ratio_b + 2 * par->Kd) + par-
>Dc * (ratio_a * ratio_b + 0.5 * ratio_a * par->kR + 0.5 * ratio_b * par-
>Kd));

// PIN internalization rates
            khij = 1 + 2 * par->RT * (U1 / D);

            khji = 1 + 2 * par->RT * (U2 / D);

```

```

    }
    else {
        khij = 1;

        khji = 1;
    }

    if ((w->C1()->Boundary() != Cell::DEAD) && (w->C2()->Boundary() !=
Cell::DEAD)) {

// PIN at the plasma membrane (due to recycling)

        double dPin1=0.; double dPin2=0.;

        dPin1 = par->k_exo * w->C1()->Chemical(2) - w->Transporters1(0) *
(par->k_endo + (par->mi / khij));

        dPin2 = par->k_exo * w->C2()->Chemical(2) - w->Transporters2(0) *
(par->k_endo + (par->mi / khji));

// AUX/LAX at the plasma membrane (due to recycling)

        double dAux_Lax_1=0.; double dAux_Lax_2=0.;

        dAux_Lax_1 = par->a_exo * w->C1()->Chemical(3) - par->a_endo * w-
>Transporters1(1);

        dAux_Lax_2 = par->a_exo * w->C2()->Chemical(3) - par->a_endo * w-
>Transporters2(1);

        dw1[0] = dPin1;
        dw2[0] = dPin2;
        dw1[1] = dAux_Lax_1;
        dw2[1] = dAux_Lax_2;
    }

// Ablated Cells
    if (w->C1()->Boundary() == Cell::DEAD){

        dw1[0] -= w->Transporters1(0); // PINS
        dw1[1] -= w->Transporters1(1); // AUX/LAX

    }

    if (w->C2()->Boundary() == Cell::DEAD){

        dw2[0] -=w->Transporters2(0); // PINS

```

```

        dw2[1] -= w->Transporters2(1); // AUX/LAX

    }

}
};

// custom functions that gives intracellular PIN and AUX/LAX levels
inline double complex_PIN(Cell &here, Cell &nb, Wall &w) { return
here.Chemical(2) ;}

inline double complex_AUX(Cell &here, Cell &nb, Wall &w) { return
here.Chemical(3) ;}

// custom functions that calculate PIN internalization rates khij and
khji
inline double inhibit_khij(Cell &here, Cell &nb, Wall &w) {

    double U1=0; double U2=0; double D=0; double khij;

// Calculate steady-state bound receptors levels in the apoplast

    if ((w.Apoplast(0) > 0) || (w.Apoplast(1) > 0)) {

        double ratio_a = w.Apoplast(0) ;

        double ratio_b = w.Apoplast(1) ;

        U= par->Dc * par->Dr * (ratio_a + ratio_b) + ratio_a * (par->Dc *
ratio_b + par->Dr * par->Kd);

        D=2 * (par->Dr * par->Kd * (par->Kd + 0.5 * ratio_a + 0.5 *
ratio_b) + par->Dc * par->Dr * (ratio_a + ratio_b + 2 * par->Kd) + par-
>Dc * (ratio_a * ratio_b + 0.5 * ratio_a * par->kR + 0.5 * ratio_b * par-
>Kd));

        // PIN internalization rates
        khij = 1 + 2 * par.inhibition_effect * (U / D);
    }
    else {
        khij = 1;
    }

    return w.Transporters1(0) * (par->k_endo + (par->mi / khij)) ;
}
inline double inhibit_khji(Cell &here, Cell &nb, Wall &w) {

    double U1=0; double U2=0; double D=0; double khji;

// Calculate steady-state bound receptors levels in the apoplast

    if ((w.Apoplast(0) > 0) || (w.Apoplast(1) > 0)) {

```

```

double ratio_a = w.Apoplast(0) ;

double ratio_b = w.Apoplast(1) ;

U= par->Dc * par->Dr * (ratio_a + ratio_b) + ratio_b * (par->Dc *
ratio_a + par->Dr * par->Kd);

D=2 * (par->Dr * par->Kd * (par->Kd + 0.5 * ratio_a + 0.5 *
ratio_b) + par->Dc * par->Dr * (ratio_a + ratio_b + 2 * par->Kd) + par-
>Dc * (ratio_a * ratio_b + 0.5 * ratio_a * par->kR + 0.5 * ratio_b * par-
>Kd));

// PIN internalization rates
khji = 1 + 2 * par.inhibition_effect * (U / D);

}
else {
khji = 1;
}

return w.Transporters1(0) * (par->k_endo + (par->mi / khji)) ;

}

```

```

// Interface class for intracellular dynamics
class AuxinAndDifferentiation : public CellReaction {

public:
virtual void operator()(Cell *c, double *dchem) {

double dPidt = 0.;
double dAUX = 0.;

double sum_Aux = c->SumTransporters( 2 ); // sum total levels of
AUX/LAX (intracellular and plasma membrane)

// Note: ReduceCellAndWalls is template c++ function implemented in Cell
class within Virtual Leaf framework. Its source code is upon request.

/* template<class P, class Op> P ReduceCellAndWalls(Op f, Op f1) {
P sum = 0;
for (list<Wall *>::const_iterator w=walls.begin();
w!=walls.end();
w++) {
sum += (*w)->c1 == this ?
f( *((*w)->c1), *((*w)->c2), **w ) :
f1( *((*w)->c2), *((*w)->c1), **w );
}
}

```

```

        }
        return sum;
    }
*/

// PIN recycling
dPidt = -par->k_exo * c->ReduceCellAndWalls<double>( complex_PIN ) +
c->ReduceCellAndWalls<double>( inhibit_khij, inhibit_khji);

// auxin-dependent PIN expression
dPidt += par->alpha_pin * c->Chemical(0) / (par->km + c-
>Chemical(0)) - c->Chemical(2) * par->delta_pin;

// AUX/LAX recycling
dAUX = -par->a_exo * c->ReduceCellAndWalls<double>( complex_AUX ) +
par->a_endo * sum_Aux;

// auxin-dependent AUX/LAX expression
dAUX += par->alpha_aux * c->Chemical(0) / (par->km + c->Chemical(0))
- c->Chemical(3) * par->delta_aux;

// Ablated cells
if (c->Boundary() == Cell::DEAD){

    dchem[2] -= c->Chemical(2);
    dchem[3] -= c->Chemical(3);

}
if (c->Boundary() != Cell::DEAD) {
dchem[2] = dPidt;
dchem[3] = dAUX;
}
}

};

// Example of interface classes for tissue growth rules
class CellHouseKeeping {
public:
    void operator() (Cell &c) const {

```

```

// Check if cell should divide - it reaches certain threshold
    c.CheckForDivision(); // see below

// Example of growth rules in Virtual Leaf (VL) framework expand if auxin
concentration is low, not provascular cells
    if (c.Chemical(0) < par->threshold_growth ) {
        c.EnlargeTargetArea(par->cell_expansion_rate);
// EnlargeTargetArea is Cell object function implemented in Virtual Leaf
framework. The code is upon request.
/* This function is based on modification of cellular pott models (CPM)
applied to model plant morphogenesis:
For more informations on see:

    "Simulation of Biological Cell Sorting Using a Two-Dimensional Extended
Potts Model," Francois Graner and James A. Glazier, Physical Review
Letters 69, 2013-2016 (1992).

    Roeland M.H. Merks, Alfons G. Hoekstra, Jaap A. Kaandorp, Peter M.A.
Sloot, and Paulien Hogeweg, 2006.
Problem-Solving Environments for Biological Morphogenesis. Computation in
Science and Engineering, 8(1), 61-72.

Book chapter
Ariel Balter, Roeland M.H. Merks, Nikodem J. Poplawski, Maciej Swat and
James A. Glazier. 2008.
The Glazier-Graner-Hogeweg Model: Extensions, Future Directions, and
Opportunities for Further Study.
In: Katarzyna A. Rejniak, Alexander Anderson and Mark Chaplain (eds).
Single Cell Based Models in Biology and Medicine. Birkhäuser-Verlag,
Basel, Boston and Berlin. Series "Mathematics and Biosciences in
Interaction." Chapter (ii).3. pp. 137-150.

    */
    }

}
};

// Example of Color coding rules for Cell class
void Cell::SetColor(QColor &color1,QColor &color2) {

// Green: Auxin in the cell
double tr = Chemical(0);
double h1 = 0; double s1 = 0; double v1 = 0;
double h2 = 0; double s2 = 0; double v2 = 0;

h1=120;
s1=255;
v1= 255*(tr/(1+tr));

    color1.setHsv( h1,s1,v1);
    color2.setHsv( h1,s1,v1);

```

```

}

// Check if divide
void Cell::CheckForDivision(void) {

    if (Area() > par.cell_division_threshold ) {

        Divide();
// Divide function are implemented in Cell class within VL framework. The
// code is upon request. The algorithm is searching for the shortest
// distance between two subsequent cell wall to establish axis of cell
// division.
// Area gives cell area of cell polygon
//http://mathworld.wolfram.com/PolygonArea.html

    }

}

// Example: Adjust chemicals in daughter cells
void Cell::OnDivide(ParentInfo &parent_info, Cell &daughter) {

    //cerr << "Calling Cell::OnDivide()" << endl;

    // Auxin distributes between parent and daughter according to area
    double area = Area(), daughter_area = daughter.Area();
    double tot_area = area + daughter_area;
    chem[0]*=(area/tot_area);
    daughter.chem[0]*=(daughter_area/tot_area);

    // For lack of detailed data, or a better rule, we assume
    that new cells are initially apolar
    // after division
    // So the PIN and AUX/LAX are redistributed according to the
    original polarization over the walls

    // parent_info contains info about the parent
    // redistribute the PIN and AUX/LAX in the endosome according to
    area

    chem[1] = parent_info.PINendosome*(area/tot_area);
    daughter.chem[1] =
parent_info.PINendosome*(daughter_area/tot_area);
    chem[2] = parent_info.PINendosome*(area/tot_area);
    daughter.chem[2] =
parent_info.PINendosome*(daughter_area/tot_area);

```

```
for (list<Wall *>::const_iterator w=walls.begin();
     w!=walls.end();
     w++) {

    // reset transporter value
    (*w)->setTransporter(this, 1, 0.);
    (*w)->setTransporter(this, 0, 0.);

}

for (list<Wall *>::const_iterator w=daughter.walls.begin();
     w!=daughter.walls.end();
     w++) {
    // reset transporter value
    (*w)->setTransporter(&daughter, 1, 0.);
    (*w)->setTransporter(&daughter, 0, 0.);

}

}
```